UNIVERSITY OF CALIFORNIA SAN DIEGO

Non-Volatile Marine and Non-Refractory Continental Sources of Particle-Phase Amine During the North Atlantic Aerosols and Marine Ecosystems Study (NAAMES)

A Thesis submitted in partial satisfaction of the requirements
for the degree Master of Science

in

Earth Sciences

by

Veronica Zsazsa Berta

Committee in charge:

Professor Lynn Russell, Chair
Professor Jennifer Haase
Professor Dan Lubin

2022

The Thesis of Veronica Zsazsa Berta is approved, and it is acceptable in quality and form for publication on microfilm and electronically.

University of California San Diego

2022

TABLE OF CONTENTS

LIST OF FIGURES

LIST OF TABLES

ACKNOWLEDGEMENTS

First and foremost, I would like to thank my advisor, Professor Lynn Russell, whose undergraduate course sparked my initial interest in this research and whose mentorship was crucial for my subsequent graduate studies and undoubtedly, my future career. I greatly appreciate their words of encouragement and countless hours of edits, emails, phone calls, and zoom meetings for the thesis. I must also thank the members of the Russell Group who always keep me in high spirits throughout the course of my research. Lastly, I thank my friends and family for all of their continuous and never failing support. Especially to my parents, who have always encouraged a curious mind.

I would like to acknowledge those who collected and analyzed data during NAAMES including Eric Saltzman, Laura Rivellini, Bill Brooks, Tim Onasch, Leah Williams, Raghu Betha, Maryam Askari Lamjiri, Derek Coffman, and Lucia Upchurch for their contributions to collecting and reducing data. I would specifically like to recognize Savannah Lewis who analyzed measurements made using FTIR spectroscopy that were used to obtain the results presented in this thesis.

The thesis, in part, is currently being prepared for submission for publication of the material. Berta, Veronica Z.; Russell, Lynn M., Price, Derek J.; Chen, Chia-Li; Lee, Alex K.Y.; Quinn, Patricia K.; Bates, Timothy S.; Bell, Thomas G.; Behrenfeld, Mike J. The thesis author was the primary researcher and author of this material.

ABSTRACT OF THE THESIS

Non-Volatile Marine and Non-Refractory Continental Sources of Particle-Phase Amine During the North Atlantic Aerosols and Marine Ecosystems Study (NAAMES)

by

Veronica Zsazsa Berta

Master of Science in Earth Sciences

University of California San Diego, 2022

Professor Lynn M. Russell, Chair

Amines were measured by aerosol mass spectrometry (AMS) and Fourier Transform Infrared (FTIR) spectroscopy during the North Atlantic Aerosols and Marine Ecosystems Study (NAAMES) cruises. Both AMS non-refractory (NR) amine ion fragments comprising the AMS $C_xH_yN_z$ family and FTIR non-volatile (NV) amine measured as primary (C-NH2) amine groups typically had greater concentrations in continental air masses than marine air masses. Secondary continental sources of AMS NR amine fragments were identified by consistent correlations to AMS NR nitrate, AMS NR m/z 44, IC non-sea salt potassium, and radon for most air masses.

FTIR NV amine group mass concentrations for particles with diameters <1 μm showed large contributions from a primary marine source that was identified by significant correlations with measurements of wind speed, chlorophyll *a*, seawater dimethylsulfide (DMS), AMS NR chloride, and ion chromatography (IC) sea salt as well as FTIR NV alcohol groups in both marine and continental air masses. FTIR NV amine group mass concentrations in <0.18 μm and <0.5 μm particle samples in marine air masses likely have a biogenic secondary source associated with strong correlations to FTIR NV acid groups, which are not present for <1 μm particle samples. The average seasonal contribution of AMS NR amine fragments and FTIR NV amine groups ranged from 27% primary marine amine and 73% secondary continental amine during Early Spring to 53% primary amine and 47% secondary continental amine during Winter. These results demonstrate that AMS NR and FTIR NV amine measurements are complementary and can be used together to investigate the variety and sources of amines in the marine environment.

1. INTRODUCTION

Amines are a class of nitrogen-containing organic compounds that have been identified as playing important roles in atmospheric aerosols by reacting with acids (HNO_3, H_2SO_4, CH_4O_3S) to add organic mass and by acting as precursors that are oxidized by atmospheric radicals (O_3, OH, NO_3) to nucleate new particles [1-3]. New particle formation driven by amines can contribute to both the aerosol direct and indirect effects by increasing the number of particles as well as the number of cloud condensation nuclei (CCN) [4]. Amines may also affect CCN activity by enhancing particle hygroscopicity through the formation of aminium salts or suppressing particle hygroscopicity through photochemical reactions with OH [5]. The potential for climate impacts associated with amines depends strongly on the magnitude and type of amines in the atmosphere.

While continental sources of amine include animal husbandry, industrial emissions, and biomass burning [6], marine sources of aliphatic amines are likely underwater plant, algae, and kelp species, which are found in seawater and sediments [7-9]. These marine sources of amine have also been identified as both primary and secondary contributions to particles (Table 1). Marine amines are estimated to contribute 0.6 TgC/yr to aerosol, and the formation of amine salts have been estimated to comprise 21% of submicron marine secondary organic aerosol (SOA) mass [10]. Primary marine sources of amines have been identified, showing correlations to sea salt, wind speed, and alcohol groups [11-13]. Secondary marine sources of amine were identified for diethylamine, dimethylamine, and monomethylamine, which were correlated with primary productivity of phytoplankton [14, 15].

Fluxes of amine gases from the ocean to the atmosphere are controlled by biological activity because processes including osmoregulation, protein degradation, and subsequent microbial decomposition produce a methylated form of low-molecular-weight aliphatic amine

Table 1: Summary of recent measurements of amine concentrations in marine regions.

Sampling Site and Season	Relevant Findings	Reference
Southeast Pacific during October-November	FTIR primary amine groups. The average mass concentration (μg m^{-3}) for campaign: 0.015 ± 0.014; marine air masses: 0.0089 ± 0.0068; mixed air masses: 0.019 ± 0.015; continental air masses: 0.023 ± 0.023.	[16]
Gulf of Mexico during August- September	FTIR primary amine groups with contributions from oil combustion and wood smoke. The average mass concentration (μg m^{-3}) for campaign: 0.25 ± 0.26; air masses over the Gulf: 0.10 ± 0.07; southerly continental air masses: 0.48 ± 0.33; northerly continental air masses: 0.16 ± 0.13.	[17]
Western Atlantic during August	FTIR primary amine groups. 2% of OM in all ambient aerosols, 13% of OM in generated primary marine aerosols.	[18]
Tropical East Atlantic during November-January (May-June)	HPLC with ESI-IT-MS secondary marine aliphatic amines (pg m^{-3}) . MA: 2-520 (0-30); DMA: 100-1400 (130-360); DEA: 90-760 (5-110).	[15]
Gulf of Maine during June-August	FTIR primary amine groups below detection.	[19]
Eastern North Atlantic during high biological activity	IC secondary, marine dimethylammonium and diethylammonium salts (ng m^{-3}) in clean air masses: 4-13 and 7-24, respectively. Concentrations peaked in 0.25-0.5 μm size range. Monoalkylammonium, and trialkylammonium salt concentrations below detection.	[14]
Coastal Ireland during low (high) biological activity	IC secondary, marine dimethylammonium and diethylammonium salts (ng m^{-3}): <1-8 (2-24) and <1-12 (4-32), respectively. Monoalkylammonium and trialkylammonium salt concentrations below detection.	[14]
La Jolla in coastal California during August-October	FTIR primary amine groups average mass concentration 0.11 ± 0.09 μg m^{-3}. 1% of combustion (3.0 μg m^{-3}) were amines. 3% of marine (0.97 μg m^{-3}) were amines.	[20]
Western North Pacific during Aμgust-September	TOC/TON analyzer secondary, marine DEA: <0.1 to 0.8 ng m^{-3}.	[21]
Coastal Northern China during January-February (November-December)	UHPLC-MS amines (MA, DEA, DMA, PA, TMA, MEA, PYR, BA, DEA, MOR, AN, DPA, TEA, DBA, TPA) with averages ranging from 0.1 to 58.7 (0.1 to 86.3) ng m^{-3} from coal combustion activities, industrial emissions, vehicle exhaust, biomass burning, and agricultural and marine emissions.	[22]
Coastal Norway during September-November	GC-MS and LC-MS nitrosamines and alkyl amines (nM) in fog. MEA: BDL-7.1; MA: 0.4-8.9; DMA: 130.3-255; DEA: 1.7-5.8. NDEA, NMOR, NDBA, and NPIP, EA were below detection.	[23]
Tropical East Atlantic (2-year average)	IC secondary, aliphatic amines (ng m^{-3}) scavenged in the gas phase by the particle phase. DMA: 5.6; MA: 0.2; DEA: 3.9 .	[24]
Coastal California during July-August	IC and ICP-MS secondary, marine DMA: 2.3-70.3 ng m^{-3}.	[25]

Table 1: Summary of recent measurements of amine concentrations in marine regions, Continued.

Sampling Site and Season	Relevant Findings	Reference
East China Sea during June	IC secondary, marine aliphatic amines (nmol m^{-3}). DMA: 0.67 ± 0.21; TMA: 0.20 ± 0.11.	[26]
Coastal site near Yellow Sea during August	IC secondary, marine aliphatic amines (nmol m^{-3}). DMA: 0.62 ± 0.50; TMA: 0.15 ± 0.11.	[26]
Yellow Sea and Bohai Sea during [1]Aμgust-September [2]June-July [3]November	IC secondary, marine methylated amines (nmol m^{-3}). [1]DMA: 0.52 ± 0.28; TMA: 0.31 ± 0113. [2]DMA: 1.1 ± 0.47; TMA: 0.35 ± 0.13. [3]DMA: 0.41 ± 0.36; TMA: 0.53 ± 0.32.	[26]
High Arctic during July	Single particle laser ablation AMS TMA: 23% of particles 200-1000 nm in diameter.	[27]
Tropical East Atlantic during Winter and Spring	HPLC/ESI-IT-MS aliphatic amines. DMA and DEA: 270 pg m^{-3} (Spring) to 830 pg m^{-3} (Winter).	[28]
North Atlantic during September, May-June, March-April, November	FTIR primary amine groups. 5-8% of OM in atmospheric primary marine aerosols, 5-12% of OM in generated primary marine aerosols.	[29]
California coast during May	FTIR primary amine groups. 14% of OM in generated primary marine aerosols.	[30]
Huaniao Island during January	HPLC/fluorescence alkyl amines (ng m^{-3}). MA: 0.27-7.04 ; EA: 0.37-1.78; PA: 0.76-4.03 ; BA: BDL-0.15; PEN: 0.07–0.40, HEX: BDL; MEA: 0.84–5.62.	[31]

*Abbreviations: MA- monomethylamine, DMA- dimethylamine, DEA- diethylamine, TMA- trimethylamine, EA-ethylamine, TEA- triethylamine, PA- propylamine. DPA- dipropylamine, TPA- tripropylamine, BA-butylamine, DBA - dibutylamine, MEA- ethanolamine, MOR-morpholine, PYR- pyrrolidine, AN- aniline, PEN-pentylamine, HEX- hexylamine, PIP- piperidine, NDMA-nitrosodimethylamine, NDEA-nitrosodiethylamine; NBA-nitrosodibutylamine; NPIP- nitrosopiperidine, UHPLC: Ultra High Performance Liquid Chromatography, GC: Gas Chromatography, ESI-IT-MS: Electrospray Ionization Ion Trap Mass Spectrometer, ICP: Inductively Coupled Plasma, TOC/TON: Total Organic Carbon/Total Organic Nitrogen

that is concentrated in surface waters [8, 32]. This volatile form allows some amines to enter the atmosphere by air-sea exchange and then partition into the solid phase to form secondary marine aerosols (SMA) by a variety of reactions. These reactions may be accelerated by airborne oxidants and other pollutants (NO_x, O_3, SO_x) that are transported from continental sources or produced by ships locally.

Amines are also included in primary sea spray aerosols (SSA) as jet and film drops of seawater that are ejected into the atmosphere by bursting bubbles formed by breaking waves at the ocean surface. These aerosol types have been associated with biologically-derived marine organic compounds, since they frequently contain a consistent ratio of primary ($C\text{-}NH_2$) amine

groups to organic mass across multiple oceans including the Arctic, Atlantic, and Pacific [11]. Similar primary amine group contributions have been identified across four seasons in the North Atlantic in seawater, sea surface microlayer, generated primary particles, and atmospheric aerosol particles [12, 29].

Here we assess the sources and quantities of amine components sampled in atmospheric aerosol particles during the North Atlantic Aerosols and Marine Ecosystems Study (NAAMES). NAAMES provided unique sampling of the open ocean during distinct seasons that correspond to different periods of the phytoplankton annual biomass cycle. To obtain the most complete picture of open-ocean amines for the region, this study compares online measurements of AMS non-refractory (NR) amine fragments by High-Resolution Time-of-Flight Aerosol Mass Spectrometer (HR-ToF-AMS) to non-volatile (NV) primary amine groups by Fourier Transform Infrared Radiation (FTIR) Spectroscopy of size-resolved filters. Chemical and meteorological tracers are used to associate the amine components with both primary and secondary processes and marine or continental sources. Together, the AMS NR amine fragments and FTIR NV amine groups provide a more complete picture of the varied aspects of amine-containing aerosol particles in the North Atlantic.

2. METHODS AND MATERIALS

2.1. NAAMES Cruises

The North Atlantic Aerosols and Marine Ecosystems Study (NAAMES) was a multi-year campaign that explored the dynamics of ocean ecosystems, atmospheric aerosols, clouds, and climate. The measurements reported here were collected on the R/V Atlantis in the western subarctic Atlantic during four separate phases of the phytoplankton annual biomass cycle (Behrenfeld et al., 2019). The first cruise (NAAMES 1) took place during the winter transition in November-December (Winter) 2015. The second cruise (NAAMES 2) took place during the transition in the bloom climax in May-June (Late Spring) 2016. The third cruise (NAAMES 3) took place during the declining biomass in August-September (Autumn) 2017. The final cruise (NAAMES 4) took place during the early accumulation phase of the spring bloom in March-April (Early Spring) 2018. The first three NAAMES cruises departed from Woods Hole, Massachusetts, and the NAAMES 4 cruise sailed from San Juan, Puerto Rico. All four cruises returned to Woods Hole, Massachusetts.

2.2. Marine and Continental Air Mass Periods

Ambient measurements were categorized by air mass origins. Online measurements were considered to be associated with marine air masses if they met the criteria of Saliba et al. [33], namely (1) particle number concentrations <1,500 cm^{-3}, (2) HYSPLIT 48 hour back trajectories originating from the North or tropical Atlantic that did not pass over land during that time, (3) black carbon (BC) concentrations were <50 ng m^{-3}, (4) radon concentrations <500 mBq m^{-3}, and (5) relative wind direction was within ±90° of the bow of the ship (to avoid ship stack contamination). For the multi-hour filters collected, the classification scheme of Lewis et al. [29]

was used: marine filters were those for which 90% or more of the sampling time met these conditions; air masses were considered to have continental sources when the HYSPLIT 48 hour back trajectories originated from North America; mixed filters were those that did not meet either marine or continental criteria.

2.3. HR-ToF-AMS

A HR-ToF-AMS (Aerodyne Research Inc., Billerica, MA) was deployed to measure non-refractory (AMS NR) components of submicron (approximately 100-800 nm dry aerodynamic diameter) ambient particles [34] downstream of a 1 μm cyclone [35]. The instrument alternated periodically between different ion flight modes including a high-resolution W-mode (1-min), a high-sensitivity V-mode (2-min), and an additional single-particle event trigger (ET) mode (2-min). Particle measurements with the W-mode of the AMS instrument were collected for all particles (not separated by size) and were analyzed by the data analysis software packages SQUIRREL (SeQUential Igor data RetRiEvaL) version 1.24 and PIKA (Peak Integration by Key Analysis) version 1.63 on IGOR PRO 8 (Wavemetrics, Inc.). This mode was used instead of the V-mode to obtain better peak separation, which was necessary to identify contributions of amine-containing fragments from other fragments at similar masses. SQUIRREL was used to pre-process data by checking m/z calibration and baselines for each run. PIKA was then utilized for high-resolution analysis of individual ion fragments to be fitted for each mass-to-charge ratio (m/z). AMS NR amine fragments were calculated as the sum of $C_xH_yN_z$ ion fragments [36, 37].

The ET mode of the instrument extracted a mass spectrum for individual particles that had ion signals within a certain range of m/z values that exceeded a threshold established using particle-free air. Single particle analysis of ET mode measurements was previously completed for Winter and Late Spring [38]. This analysis was also performed for Autumn and Early Spring,

identifying 5-7 relatively similar clusters for each cruise. The AMS ET methods and results for Autumn and Early Spring are available in the supporting information sections 6.2 and 6.3. Amine fragment contributions were estimated using the unit-mass fragments associated with common amine ion fragments. The fraction of amine signal that was associated with the Autumn and Early Spring particle clusters was estimated to be 1.0-3.6% of the total ion signal and for 2.7-8.1% of the total organic signal. These contributions remained largely consistent across particle clusters, showing no notable differences between the particle clusters.

Positive Matrix Factorization (PMF) Evaluation Tool v3.06B of W-mode data was used for Autumn and Early Spring to compute factors of ion fragments with unique temporal correlations for high-resolution organic mass spectral data, as described in section 6.1. The analysis included selected high-resolution sulfate mass spectral signals that included SO^+, SO_2^+, SO_3^+, HSO^+, $H_2SO_4^+$, HSO_3^+, H_2SO^+, HSO_2^+, and $H_2SO_2^+$ ion fragments. Most of the factors identified typically included small amounts of amine; when a factor with higher amine was found, the variability of its mass concentration was largely noise, limiting further source appointment, given the magnitude of twice that of its mean (Table 9).

The HR-ToF-AMS used during NAAMES utilizes a multi-slit chopper that obtains efficient Particle Time-of Flight (ePToF) measurements rather than a single-slit chopper that obtains PToF measurements. ePToF ensures high signal-to-noise ratios in the raw spectral bins necessary for marine environments with low aerosol concentrations. ePToF measurements can be analyzed as size distributions of individual unit-mass resolution ion fragments but processing of high resolution mass spectra for separate size bins has not yet been implemented. Size distributions of cumulative and individual mass fragments for organic and sulfate had low signal-to-noise given the clean marine conditions and low concentrations of AMS NR components. Unit

mass resolution did not represent any of the selected amine fragments with sufficiently high signal-to-noise to determine an amine size distribution or size cuts (e.g. <0.5 μm), as the amine fragments comprised less than half of the unit mass resolution peaks in the m/z spectra (Table 11). Consequently size-resolved measurements of AMS NR amine fragments are not available.

2.4. FTIR Spectroscopy

During all four cruises, atmospheric particles were collected after size cuts on pre-scanned 37 mm Teflon filters (Pall Inc., 1 μm) for offline analysis by Fourier Transform Infrared (FTIR) spectroscopy (Tensor 27 spectrometer, Bruker, Billerica, MA) of the NV components that were retained on the filters [35]. Berner impactors with size cuts of 0.18 μm and 0.5 μm were operated at 30 L min^{-1}, and a 1 μm sharp cut cyclone was operated at 16.7 L min^{-1}. Sampling times for each filter spanned 12 to 23 hours. Quantification of NV organic amine group concentration was accomplished by identifying a primary amine ($C\text{-}NH_2$) peak at an absorption frequency of 1630 cm^{-1} in the FTIR spectrum. Note that the term 'primary' refers to the NH_2 group type that is bonded to the carbon not to the aerosol source type. Specifically, the FTIR absorbance at 1630 cm^{-1} is not sensitive to secondary ($C_2\text{-}NH$) or tertiary ($C_3\text{-}N$) groups in amines, and absorbance peaks for secondary and tertiary amines were not identified in the spectra [39]. The FTIR spectra were quantified by baselining, peak-fitting, and integrating peak areas using calibration standards and an automated algorithm [40]. Carboxylic acid, alkane, primary amine, and alcohol functional groups were estimated from fitting spectral peaks as described in detail by [29, 41].

2.5. Ion Chromatography

Inorganic ions including SO_4^{2-}, NO_3^-, NH_4^+, Na^+, $CH_4O_3S^-$ (MSA), Mg^{2+} K^+, Cl^-, Ca^{2+},

and Br^- were collected on a two stage multi-jet impactor with a 1.1 μm size cut filter at 30% RH and subsequently measured using ion chromatography (IC) [42, 43]. Sea salt concentrations were estimated as Na^+ (μg m^{-3}) ×1.47 + Cl^- (μg m^{-3}) [11, 30, 33, 44]. Non-sea salt (nss) potassium (K^+) concentrations were estimated as K^+ (μg m^{-3}) - Na^+ (μg m^{-3}) × (ratio of K to Na in seawater), where the latter ratio is constant across major water masses in the ocean [45].

2.6. Other Measurements

Seawater and atmospheric dimethylsulfide (DMS) concentrations were measured continuously during NAAMES [46]. A Single Particle Soot Photometer (SP2, DMT, Boulder, CO) measured the mass concentrations of refractory black carbon (BC) in particles with diameters of 60 to 700 nm. Other meteorological properties measured during NAAMES and used in our analysis include sea surface temperature (SST), solar radiation, wind speed, relative humidity, ambient temperature, ozone, and radon and these data were accessed from the SeaBASS archive [47].

3. RESULTS

Figure 1 shows AMS NR amine fragments and FTIR NV amine groups for all four NAAMES cruises. Concentrations of AMS NR amine fragments were higher during continental periods (with concentrations ranging from 18 to 54 ng m^{-3}) than during marine periods, when concentrations averaged below 33 ng m^{-3} (Table 2). The exception to this trend was the Early Spring cruise when concentrations were slightly higher at 33 ± 6 ng m^{-3} during marine periods than during continental periods (32 ± 11 ng m^{-3}), but largely similar for both marine and continental air masses (Table 2). Similar to AMS NR amine fragments, FTIR NV amine group concentrations were higher overall during continental periods, highlighting that continental transport is a significant source of amines in the North Atlantic. The average FTIR NV amine group concentration ranged from 7 to 18 ng m^{-3} during marine periods and from 16 to 33 ng m^{-3} during continental periods (including filters with amine below the detection limit).

For both marine and continental air masses, concentrations of AMS NR amine fragments were lowest in Winter, when AMS NR organic mass (OM) was also lowest and IC MSA concentrations were below detection. These low concentrations of 14 to 18 ng m^{-3} in Winter may indicate that biologically-derived amine makes up a significant fraction of non-refractory amine during other seasons, since primary production has previously been shown to influence amine concentrations in the North Atlantic [15]. The highest concentration of AMS NR amine fragments for marine periods was 33 ± 6 ng m^{-3} in Early Spring and for continental periods 54 ± 49 ng m^{-3} in Autumn. For marine air masses, FTIR NV amine groups were highest in Late Spring, but, for continental air masses, FTIR NV amine groups were highest in Winter. FTIR NV amine group concentrations were lowest for both marine and continental air masses in Early

Spring, when only two filters, both with FTIR NV amine groups below detection, met the marine criteria.

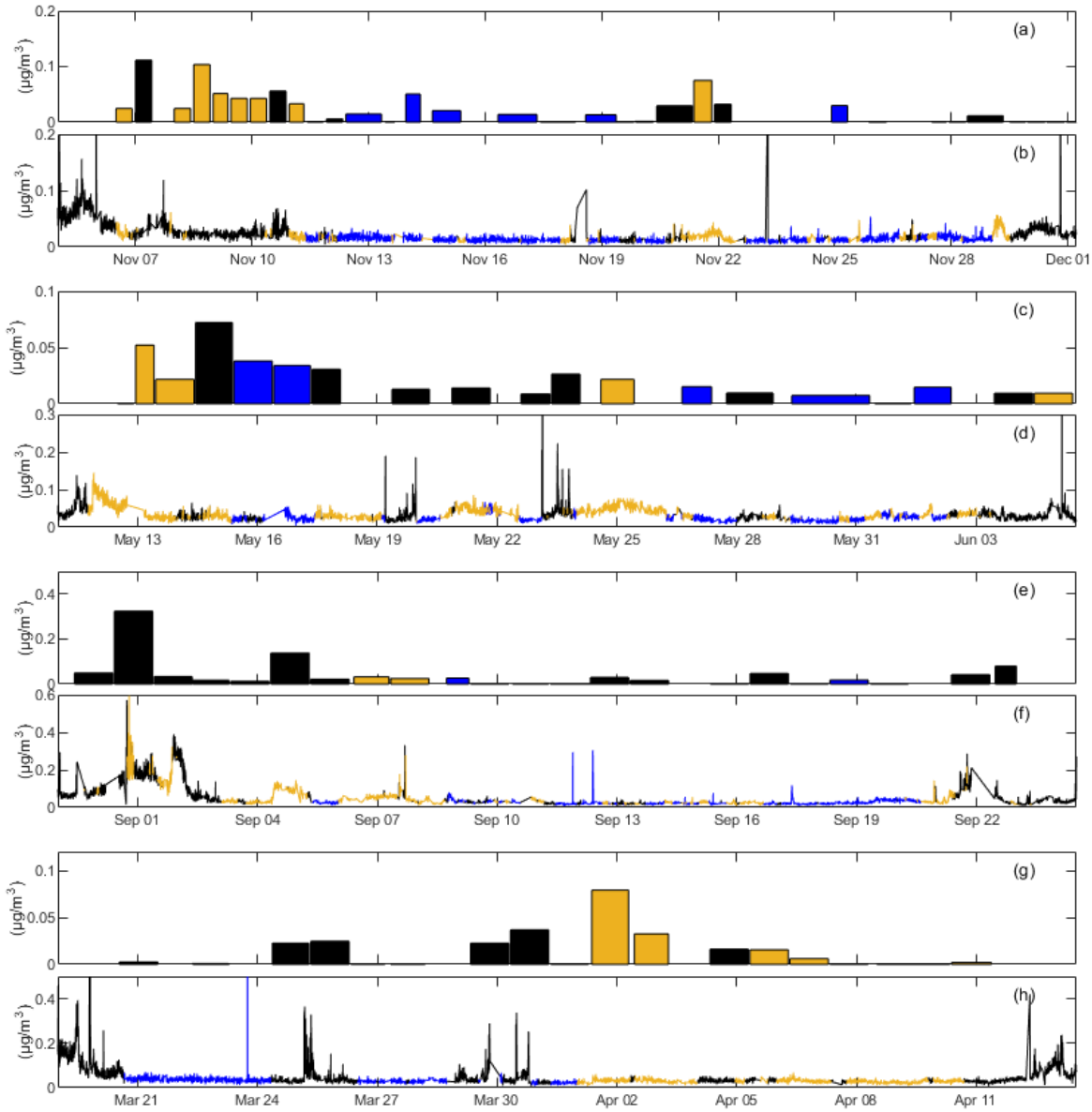

Figure 1: Time series of AMS NR amine fragments measured by the HR-ToF-AMS (b,d,f,h) and FTIR NV amine groups measured by FTIR spectroscopy in particles with diameters <1 μm (a,c,e,g) for all four cruises. From top to bottom: Winter (a,b), Late Spring (c,d), Autumn (e,f), Early Spring (g,h). Marker colors represent air mass type- blue: marine, yellow: continental, black: winds abaft or mixed.

Average concentrations of FTIR NV amine groups were lower than AMS NR amine fragments concentrations, except for continental periods in Winter. Two campaigns had positive correlations of FTIR NV amine groups with AMS NR amine fragments, with R = 0.45 in Winter

($p = 0.01$) and $R = 0.87$ in Autumn but not statistically significant ($p = 0.08$). The two Spring campaigns had negative correlations of FTIR NV amine groups and AMS NR amine fragments.

Table 2: Mean concentrations and standard deviations of amine, tracer, and environmental measurements during NAAMES for marine (first row) and continental (second row, in parentheses) periods. Seasonal mean concentrations and standard deviations are given in in square brackets, which were averaged over the sampling times of filters categorized as marine, continental, or mixed.

Season	Winter	Early Spring	Late Spring	Autumn
AMS NR Amine Fragments (ng/m^3)	14 ± 3 (18 ± 7) [18 ± 6]	33 ± 6 (32 ± 11) [31 ± 6]	23 ± 8 (37 ± 13) [33 ± 12]	26 ± 9 (54 ± 49) [30 ± 11]
FTIR NV Amine Groups (ng/m^3)*	10 ± 15 (33 ± 33) [20 ± 26]	BDL (16 ± 28) [12 ± 23]	18 ± 15 (21 ± 20) [17 ± 14]	7 ± 11 (28 ± 6) [16 ± 15]
Sum of AMS NR Amine Fragments & FTIR NV Amine Groups (ng/m^3)*	24 ± 15 (57 ± 31) [39 ± 27]	32 ± 7 (47 ± 30) [43 ± 25]	43 ± 14 (63 ± 15) [50 ± 16]	36 ± 16 (80 ± 10) [46 ± 21]
AMS NR OM (ng/m^3)	151 ± 47 (321 ± 309)	296 ± 107 (422 ± 227)	373 ± 269 (824 ± 658)	295 ± 150 (990 ± 1187)
FTIR NV OM (ng/m^3)	281 ± 198 (315 ± 220)	210 ± 156 (209 ± 327)	220 ± 165 (422 ± 420)	200 ± 175 (375 ± 431)
AMS NR Nitrate (ng/m^3)	6 ± 3 (12 ± 12)	9 ± 4 (15 ± 5)	10 ± 6 (45 ± 101)	8 ± 2 (14 ± 14)
AMS NR m/z 44 (ng/m^3)	56 ± 13 (91 ± 55)	137 ± 33 (192 ± 70)	123 ± 36 (224 ± 104)	147 ± 36 (319 ± 241)
Black Carbon (ng/m^3)	12 ± 14 (220 ± 354)	29 ± 5 (197 ± 62)	21 ± 16 (141 ± 240)	20 ± 17 (148 ± 147)
Ozone (ppb)	41 ± 2 (38 ±5)	33 ± 14 (47 ± 9)	38 ± 7 (39 ± 6)	29 ± 6 (31 ± 7)
Radon ($mBq\ m^{-3}$)	246 ± 109 (472 ± 366)	272 ± 130 (873 ± 333)	298 ± 80 (466 ± 289)	404 ± 202 (876 ± 612)
Wind Speed (m/s)	9.9 ± 3.9 (10.4 ± 3.9)	9.2 ± 3.2 (11.7 ± 4.6)	9.7 ± 5.1 (6.6 ± 3.2)	9.4 ± 4.1 (5.9 ± 3.1)
atm. DMS (ppt)	66 ± 21 (93 ± 51)	129 ± 71 (91 ± 78)	463 ± 293 (214 ± 186)	138 ± 233 (118 ± 87)
sw. DMS (nmol/L)	1.4 ± 0.6 (1.4 ± 0.7)	3.0 ± 1.1 (4.6 ± 3.2)	3.2 ± 2.5 (2.5 ± 2.5)	3.3 ± 0.7 (3.1 ± 1.4)
Temperature (ºC)	10.2 ± 5.8 (11.9 ± 6.5)	19.7 ± 4.3 (13.6 ± 4.5)	8.5 ± 4.3 (9.1 ± 3.8)	13.5 ± 3.4 (16.7 ± 3.1)
Chlorophyll *a* (ng/L)	457 ± 242 (713 ± 774)	643 ± 247 (578 ± 360)	1956 ± 1689 (1647 ± 1396)	379 ± 236 (284 ± 255)
SST (ºC)	13.2 ± 0.05 (13.8 ± 5.5)	21.6 ± 3.6 (16.0 ± 3.2)	10.1 ± 5.1 (10.5 ± 4.7)	14.5 ± 2.8 (17.8 ± 4.2)
IC MSA ($\mu g/m^3$)	-- --	-- (0.11 ± 0.19)	0.05 ± 0.05 (0.06 ± 0.03)	0.01 ± 0.01 (0.01 ± 0.00)
IC Sea Salt ($\mu g/m^3$)	1.01 ± 0.75 (1.45 ± 0.72)	-- (1.28 ± 0.51)	0.30 ± 0.30 (0.06 ± 0.04)	0.45 ± 0.30 (0.43 ± 0.55)
IC $nssK^+$ ($\mu g/m^3$)	0.01 ± 0.01 (0.02 ± 0.01)	-- (0.02 ± 0.02)	0.00 ± 0.00 (0.02 ± 0.01)	0.00 ± 0.00 (0.03 ± 0.02)

*The average included filters with amine concentration below detection.

that were not statistically significant (Fig.2). Consequently, combining the four cruises for both air mass types gives no correlation between FTIR NV amine groups and AMS NR amine fragments ($\rho = 0.02$, where a Spearman's rank correlation coefficient was used for the non-normal distribution of FTIR NV amine groups and AMS NR amine fragments). This result

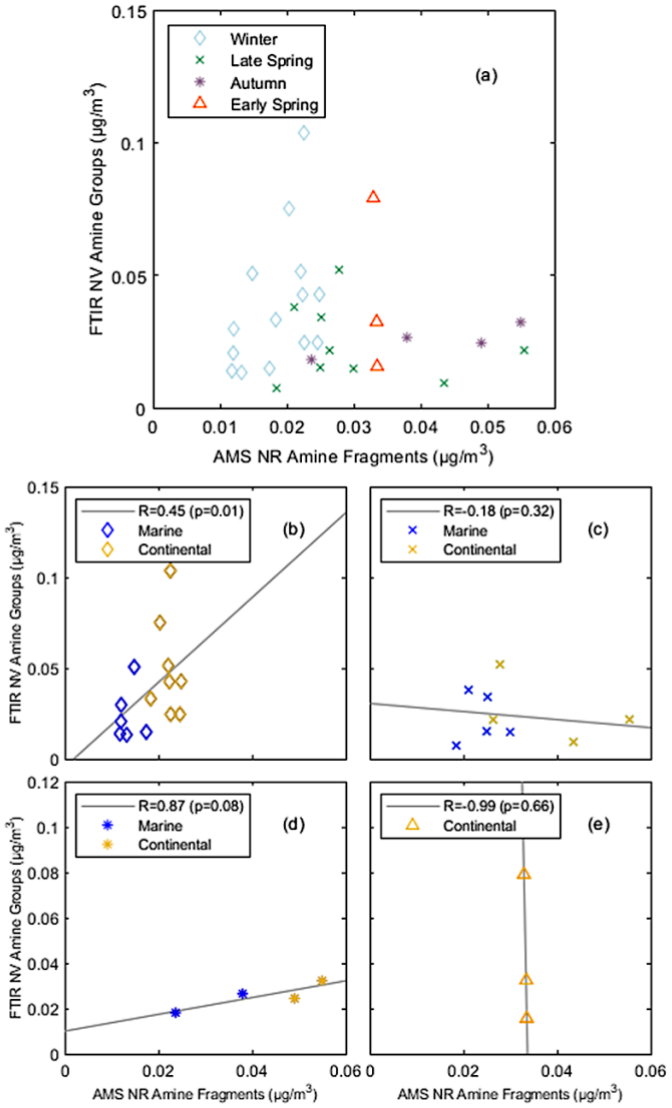

Figure 2: Scatter plot of (ADL) FTIR NV amine groups in particles with diameters <1 μm versus AMS NR amine fragments for (a) all cruises ($\rho = 0.02$, $p = 0.18$), (b) Winter, (c) Late Spring, (d) Autumn, and (e) Early Spring. Markers represent each cruise- open diamond: Winter, crosses: Late Spring, asterisk: Autumn, open triangle: Early Spring. Marker colors represent air mass type: blue: marine, yellow: continental. The solid grey lines are the lines of best fit obtained using an ordinary least squares regression. A two-tailed T test is used to estimate p-values.

suggests that FTIR and AMS are measuring different amine compounds, likely associated with different source types. In particular, AMS measures non-refractory components and FTIR measures non-volatile components (but some amine compounds are on refractory sea spray particles and some amines volatilize from filters). The inability of AMS to detect non-refractory components that are found mixed with sea spray particles is another reason that amine measured by FTIR and AMS are from different sources (Frossard et al., 2014b). The non-zero y-intercepts of AMS NR amine fragments to FTIR NV amine groups in Figures 2b-2e further support the interpretation that AMS and FTIR are measuring different amine compounds.

AMS NR amine fragments had moderate to strong correlations ($0.73 < R < 0.98$, Table 3) with AMS NR OM, suggesting that many of the organic sources included a consistent fraction of amines. The weak correlation for the marine period in Early Spring is likely evidence of the AMS not measuring components including amine on refractory sea salt particles [18]. FTIR NV amine groups had some weak correlations to AMS NR OM ($-0.66 < R < 0.54$, Table 4) but moderate to strong correlations to FTIR NV OM ($0.69 < R < 0.96$) in all seasons when filters were available (with the exception of Late Spring continental periods). Correlations of FTIR NV amine groups to AMS NR amine fragments in continental and marine air masses were variable across individual seasons.

Table 3: Pearson correlation (R) coefficient values between AMS NR amine fragments and various tracers for marine periods (columns 1-4) and continental periods (columns 5-8). Negative correlations are shaded blue and positive correlations are shaded red. The strength of each correlation determines the level of saturation for the corresponding shading- no correlation ($|R| < 0.25$)- gray, weak correlation ($0.25 \leq |R| < 0.50$)- light blue/red, moderate correlation ($0.50 \leq |R| < 0.80$)- medium blue/red, strong correlation ($0.80 \leq |R|$)- dark blue/red. Correlations that are statistically insignificant ($p \geq 0.05$) are indicated by *.

Air Masses	Marine				Continental			
Season	Winter	Early Spring	Late Spring	Autumn	Winter	Early Spring	Late Spring	Autumn
AMS NR OM	0.85	0.27	0.80	0.78	0.73	0.83	0.81	0.98
FTIR NV OM	-0.26	--	-0.07	0.88	-0.32	0.48	0.45	--
AMS NR Nitrate	0.59	-0.17	0.79	0.31	0.71	0.10	0.67*	0.84
AMS NR Sulfate	0.59	0.68	0.52	0.27	0.49	0.14	0.46	0.36
AMS NR Chloride	0.13	-0.09	-0.08	-0.07	0.06	-0.15	-0.07	-0.03
AMS NR m/z 44	0.77	0.18	0.85	0.55	0.85	0.62	0.89	0.94
Black Carbon	0.60*	-0.04*	0.61*	0.33	0.31	0.30	0.30	0.86
Ozone	0.11	-0.70	-0.25	-0.22	-0.26	0.02	0.42	0.41
Radon	0.37	-0.01	-0.17	0.03	0.66	0.18	0.55	0.55
Wind Speed	-0.18	-0.09	-0.53	0.03	0.00	-0.41	-0.13	-0.45
sw. DMS	0.08	-0.06	-0.09	0.05	0.07	0.05	-0.23	-0.08
atm. DMS	-0.20	0.50	-0.20	0.04	0.41	-0.34	-0.20	0.36
Solar Radiation	-0.03	0.00	0.16	0.08	-0.02	0.29	-0.05	0.33
Relative Humidity	-0.55	0.00	-0.08	-0.04	0.11	-0.26	0.04	-0.49
Temperature	-0.30	0.77	-0.17	0.34	0.21	0.26	0.41	0.59
Chlorophyll *a*	-0.09	0.09	0.09	-0.46	0.21	-0.07	-0.01	-0.26
SST	-0.15	0.80	-0.23	0.33	0.23	0.29	0.23	0.60
IC MSA	BDL	--	0.50*	0.90	BDL	0.25*	0.12*	-0.10
IC Sea Salt	0.59	--	-0.72	0.65	-0.84	0.15	-0.17*	-0.05*
IC nssK^+	0.78	--	0.27	0.83	0.79*	0.59	0.95	0.89

Table 4: Pearson correlation (R) coefficient values between FTIR NV amine groups (ADL & BDL) in particles with diameters <1 μm and various tracers for marine periods (columns 1-4) and continental periods (columns 5-8). Negative correlations are shaded blue and positive correlations are shaded red. The strength of each correlation determines the level of saturation for the corresponding shading- no correlation ($|R| < 0.25$)- gray, weak correlation ($0.25 \leq |R| < 0.50$)- light blue/red, moderate correlation ($0.50 \leq |R| < 0.80$)- medium blue/red, strong correlation ($0.80 \leq |R|$)- dark blue/red. Correlations that are statistically insignificant ($p \geq 0.05$) are indicated by *.

Air Masses	Marine				Continental			
Season	Winter	Early Spring	Late Spring	Autumn	Winter	Early Spring	Late Spring	Autumn
AMS NR OM	-0.13	--	0.26	-0.14	0.26	0.54	-0.66	--
FTIR NV OM	0.68	--	0.90	0.79	0.69	0.96*	0.09*	--
AMS NR Nitrate	-0.16*	--	0.19*	-0.23*	0.01*	0.13*	-0.59*	--
AMS NR Sulfate	-0.19	--	0.61	0.27	0.35	-0.34	-0.50	--
AMS NR Chloride	0.57*	--	0.73*	0.00*	0.67	0.76*	-0.43*	--
AMS NR m/z 44	-0.14	--	-0.63	-0.24	0.19	0.52	-0.72	--
Black Carbon	-0.16*	--	-0.84*	0.14*	0.61	0.04	-0.26*	--
Ozone	0.45	--	0.16	-0.20	0.17	0.28	0.31	--
Radon	-0.67	--	0.28	-0.23	-0.54	-0.01	-0.32	--
Wind Speed	-0.23	--	-0.16	0.04	0.49	0.52	0.02	--
sw. DMS	-0.30	--	0.85	-0.36	0.54	-0.26	--	--
atm. DMS	-0.50	--	0.46	-0.15	0.24	0.05	--	--
Solar Radiation	-0.43	--	0.17	-0.44	0.49	0.05	-0.94	--
Relative Humidity	-0.24	--	0.77	-0.01	-0.21	-0.45	-0.74	--
Temperature	-0.25	--	-0.66	0.32	0.08	-0.05	-0.14	--
Chlorophyll *a*	0.24	--	0.86	-0.33	-0.36	0.09	-0.26	--
SST	-0.34	--	-0.70	0.66	-0.31	0.17	0.02	--
IC MSA	--	--	0.74*	-0.44*	--	-0.34*	-0.75*	--
IC Sea Salt	0.23	--	0.33	0.64	--	0.78	-0.25	--
IC nssK^+	0.20*	--	0.35*	0.06*	--	0.72*	-0.31*	--

4. DISCUSSION

4.1. Marine Amine Sources

FTIR NV amine functional groups have been reported in atmospheric aerosol, generated primary marine aerosols, seawater, and the sea surface microlayer sampled in air masses that were considered clean marine in the North Atlantic, with their presence in both seawater and aerosols supporting that those amines are largely both primary and marine [11, 12]. FTIR NV amine groups indicate an association with sea spray [48] because of their positive ($0.49 < R < 0.52$, Figure 3h) correlations to wind speed during continental periods in Winter and Early Spring, which included the highest wind speeds during NAAMES. AMS NR amine fragments did not correlate positively to wind speed (Figure 4c,d), consistent with the expectation that primary amines would be mixed with refractory sea salt particles [16, 18].

Additional markers for a primary marine source include IC sea salt and AMS NR chloride. While AMS NR amine fragments correlated moderately ($0.59 < R < 0.65$, Figure 4e,f) with IC sea salt for marine air masses in Winter and Autumn, FTIR NV amine groups showed low to moderate correlations ($R = 0.33$-0.64, Figure 3e,f) to IC sea salt during the marine period in Late Spring and Autumn and even a strong correlation ($R = 0.78$) during the continental period in Early Spring. FTIR NV amine groups correlated moderately ($0.57 < R < 0.76$, Figure 3a,b) with AMS NR chloride during both continental periods (Winter and Early Spring) and two of the three marine periods (Winter and Autumn) for which measurements were available. Although these correlations of FTIR NV amine groups and AMS NR chloride are only significant ($p < 0.05$) for the continental Winter period, the consistency of their positive correlations contrast with the absence of correlation ($-0.15 < R < 0.13$, Table 3) between AMS NR chloride and AMS NR amine fragments during all four NAAMES cruises.

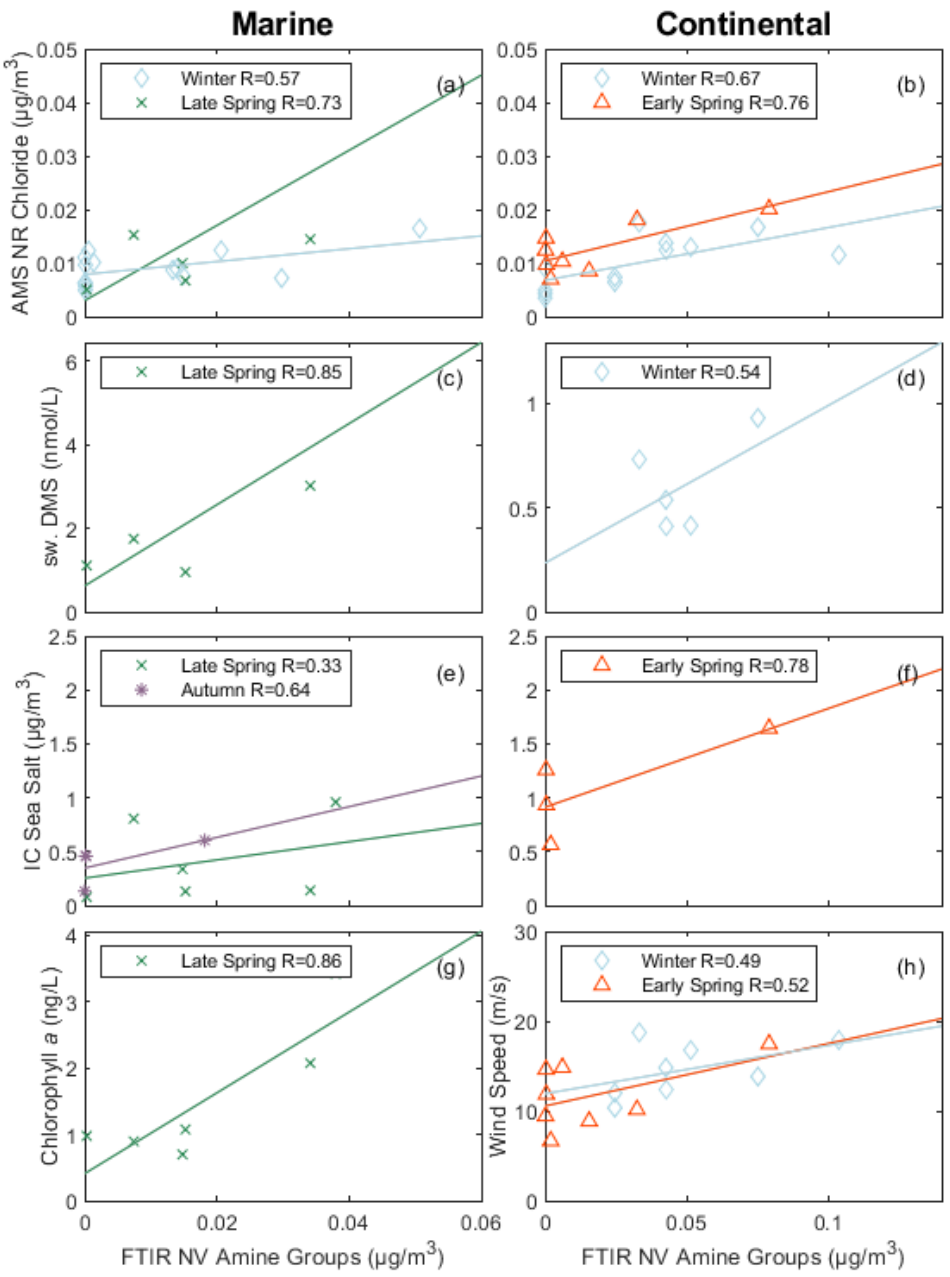

Figure 3: Scatter plot of marine tracers versus FTIR NV amine groups in particles with diameters <1 µm for marine periods (a,c,e,g) and continental periods (b,d,f,h). The panels include AMS NR chloride (a,b), seawater DMS (c,d), IC sea salt (e,f), chlorophyll a (g), wind speed (h). Markers represent each cruise- blue open diamond: Winter, green cross: Late Spring, purple asterisk: Autumn, red open triangle: Early Spring. All correlations shown are statistically significant ($p < 0.05$) with the exception of AMS NR chloride. The solid lines are the lines of best fit obtained using an ordinary least squares regression and a two-tailed T test is used to estimate p-values.

Chlorophyll *a* (chl *a*) is a common proxy for phytoplankton productivity that has previously been found to strongly correlate with organic mass in sea spray aerosols in coastal Atlantic regions [49], but during NAAMES there was no clear dependence for <1 µm OC

samples and a weak dependence for <1 μm OM cruise averages [33, 50]. Consistent with these prior open ocean results for OM during NAAMES, no positive correlations were found for AMS NR amine fragments and chl *a*, or for FTIR NV amine groups in most of the cruises. The exception was a strong (R = 0.85, Figure 3g) correlation for FTIR NV amine groups during the marine period in Late Spring, which is the climax of the annual phytoplankton bloom. This finding is analogous to that of Russell et al. [51] who attributed a weak, positive correlation of organic mass with chl *a* to particulate organic carbon (POC) in marine particles in bloom regions in the North Atlantic. The lack of correlations of organic mass and chl *a* is consistent with the less variable DOC pool as a carbon source for marine particles, as DOC typically does not correlate to chl *a* [52].

The production of methylated amines and sulfurs varies with individual metabolic processes and across different ocean phytoplankton species [53, 54]. Similar to methylated sulfurs, a significant portion of methylated amines are derived from phytoplankton and subsequent biological degradation [55]. While chlorophyll *a* is produced by various phytoplankton species for photosynthesis, dimethylsulfide (DMS) is primarily produced by coccolithophores [56]. Therefore, DMS may serve as an alternative tracer for ocean biological production in addition to chl *a*. FTIR NV amine groups correlated positively ($0.54 < R < 0.85$, Figure 3c,d) with seawater DMS during the marine period in Late Spring and the continental period in Winter. During these same periods, correlations of atmospheric DMS and FTIR NV amine groups were weakly positive ($0.26 < R < 0.46$) and lower than the correlations of FTIR NV amine groups to seawater DMS. The weaker correlation with atmospheric than seawater DMS may be explained by the photochemical reactions of atmospheric DMS leading to daytime concentration decreases that are lagged by the peaks in concentration of FTIR NV amine groups.

No correlations of seawater DMS to AMS NR amine fragments were observed. This is a distinct difference from FTIR NV amine groups that suggests the seawater DMS is more correlated to seawater organic components (DOC or POC) rather than secondary organic components, and that those seawater organic components are emitted on refractory sea spray particles that are not measured by AMS. Weak to moderate correlations (0.36 <R < 0.50, Figure 4a,b) of atmospheric DMS and AMS NR amine fragments were observed during continental periods in Winter and Autumn and during the marine period in Early Spring, consistent with a secondary contribution to the AMS NR amine fragments that is distributed on AMS NR particles rather than sea salt.

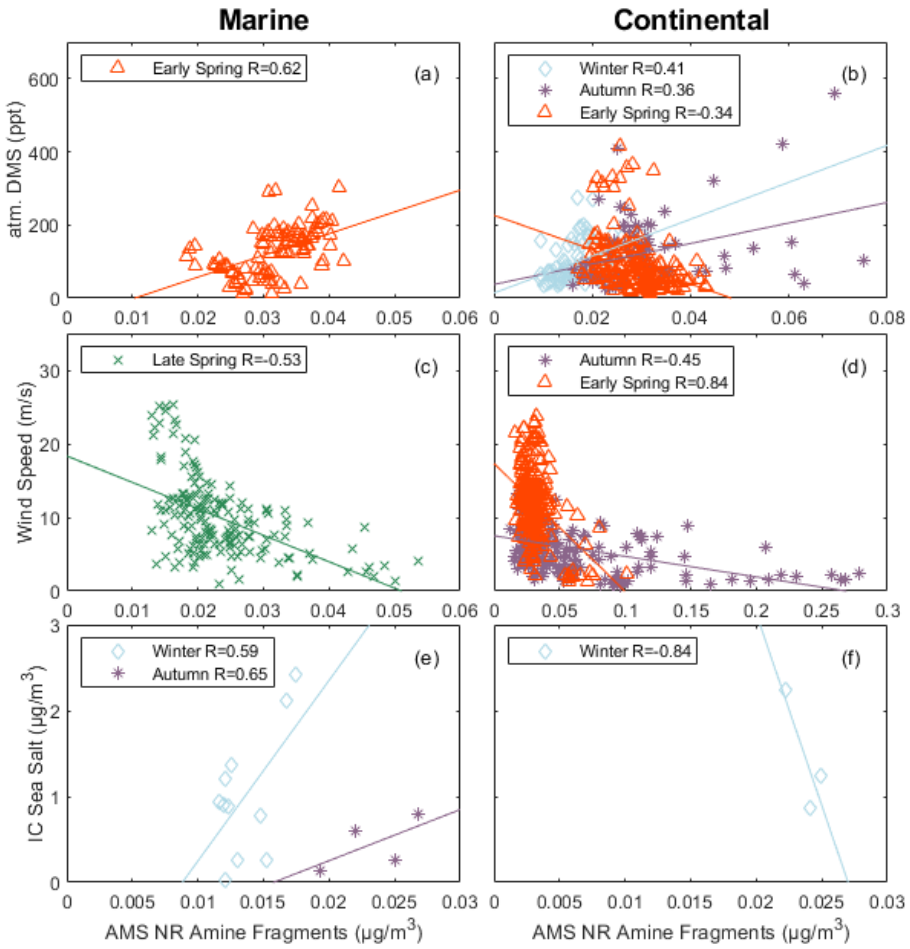

Figure 4: Scatter plot of marine tracers versus AMS NR amine fragments for marine periods (a,c,e) and continental periods (b,d,f). The panels include atmospheric DMS (a,b), wind speed (c,d), IC sea salt (e,f). Markers represent each cruise- blue open diamond: Winter, green cross: Late Spring, purple asterisk: Autumn, red open triangle: Early Spring. All correlations shown are statistically significant ($p < 0.05$). The solid lines are the lines of best fit obtained using an ordinary least squares regression and a two-tailed T test is used to estimate p-values.

Methanesulfonic acid (MSA), an oxidated derivative of DMS, can serve as a reliable indicator of secondary atmospheric processing, since its formation also lags atmospheric DMS concentrations [38]. MSA may also react with alkylamines in acid-base reactions, similar to nitric acid [57-60]. During marine periods, correlations between IC MSA and AMS NR amine fragments were moderate (R = 0.50) in Late Spring and strong (R = 0.90) in Autumn, indicating that AMS NR amine fragments during marine periods likely included a secondary marine source. IC MSA measurements were below detection during Winter and too few marine air masses were sampled in Early Spring to be able to identify a correlation with any IC inorganic ions. Submicron FTIR NV amine groups were also moderately correlated (R = 0.74) with IC MSA for marine air masses in Late Spring supporting a secondary contribution to the FTIR NV amine groups as well, but this result was not significant ($p \geq 0.05$). Additional evidence for secondary contributions of FTIR NV amine groups is considered for <0.5 μm particles in Section 4.3.

4.2. Continental Amine Sources

Anthropogenic nitrogen oxides (NOx) can undergo a variety of reactions that form nitrate-containing secondary organic aerosols. For example, heterogeneous hydrolysis of dinitrogen pentoxide (N_2O_5) can produce nitric acid (HNO_3) that may form aminium nitrate salts though acid-base reactions with amines [61, 62]. Aminium salts can also form by the displacement of ammonium by amine in ammonium nitrate. The volatility of these amine-containing compounds is lower than ammonium nitrate such that they are more likely to partition into the particle phase [63]. The moderate to strong ($0.67 < R < 0.84$, Figure 5b) correlations of AMS NR amine fragments and AMS NR nitrate for the Winter, Late Spring, and Autumn cruises during continental periods provide some evidence that the formation of particle-phase amine is associated with nitrate. To a lesser extent, AMS NR amine fragments and AMS NR nitrate also

correlated weakly to moderately (0.31 < R < 0.79, Figure 5a) during the marine periods for the Winter, Late Spring, and Autumn cruises. This suggests a secondary source for AMS NR amine fragments that is present during continental and marine periods. The steeper slopes of the linear fits for continental air masses (Y = 0.24-4.28, Table S17) compared to those of marine air masses (Y = 0.08-0.58, Table S17) suggest that these amines have continental sources that are present at low concentrations during the marine periods. No positive correlations (-0.59 < R < 0.19, p > 0.05) of FTIR NV amine groups and AMS NR nitrate were observed, suggesting that the

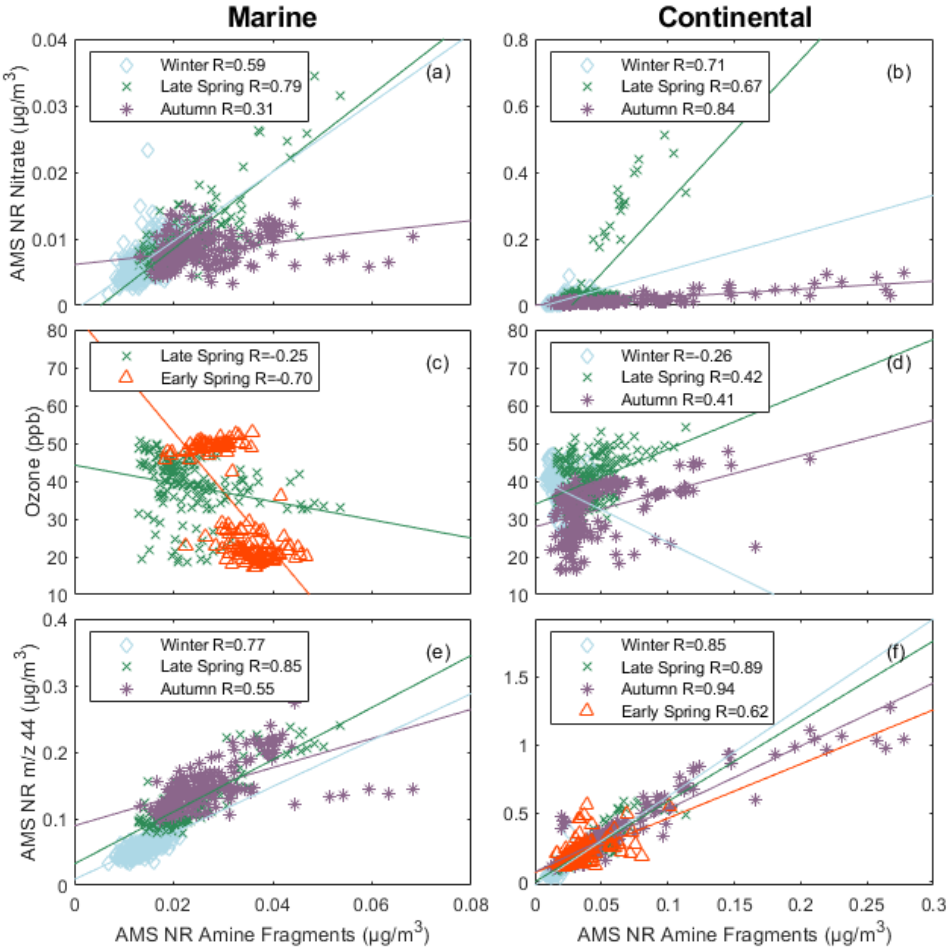

Figure 5: Scatter plot of secondary tracers versus AMS NR amine fragments for marine periods (a,c,e) and continental periods (b,d,f). The panels include submicron AMS NR nitrate (a,b), ozone (c,d), and AMS NR m/z 44 (e,f). Markers represent each cruise- blue open diamond: Winter, green cross: Late Spring, purple asterisk: Autumn, red open triangle: Early Spring. All correlations shown are statistically significant ($p < 0.05$) except for AMS NR nitrate during the Late Spring continental period ($p = 0.27$). The solid lines are the lines of best fit obtained using an ordinary least squares regression and a two-tailed T test is used to estimate p-values.

aminium salts may not have primary amine groups (NH_2) or may be too volatile to remain for filter analysis. Correlations for FTIR NV amine groups were not available for the continental periods in Autumn and the marine periods in Early Spring.

Figures 6a and 6b shows the weak to strong ($0.30 < R < 0.86$) correlations of AMS NR amine fragments to black carbon for continental air masses as well as for Autumn marine air masses. This correlation is consistent with the correlation to AMS NR nitrate, as AMS NR nitrate and black carbon are typically produced by combustion. BC is often an indicator of a primary combustion source, suggesting that AMS NR amine fragments may also include some primary sources of amines [22, 64]. BC and AMS NR nitrate could be emitted by ocean-going vessels locally or transported from continents. Two tracers for continental processes are radon (from rocks and soils) and non-sea salt potassium (from biomass burning).

Since radon is a decay product of rocks and soil, it is used as a naturally occurring tracer for continental air masses. The weak correlation ($R = 0.37$, Figure 6c) of AMS NR amine fragments to radon during the marine period in Winter and moderate ($0.55 < R < 0.66$, Figure 6d) correlations during the continental periods in Winter, Autumn, and Late Spring indicate that much of the AMS NR amine fragments are continental. In contrast, all but the Late Spring marine period showed no or negative correlations ($-0.67 < R < -0.01$, Table 4) of FTIR NV amine groups with radon, suggesting that FTIR NV amine groups are largely from marine sources.

Non-sea salt potassium ($nssK^+$) is a widely-used tracer for biomass burning, which also can produce a continental source of methylated amines [65]. Weak to strong correlations ($0.27 < R < 0.95$, Figure 6e,f) of AMS NR amine fragments to IC $nssK^+$ were found for all marine and continental periods when IC measurements of K^+ and sodium (Na^+) were available. The

correlations of AMS NR amine fragments and IC nssK^+ are significant for all marine and continental seasons except Winter, suggesting an important continental contribution to AMS NR amine fragments. No correlations of FTIR NV amine groups to IC nssK^+ were statistically significant (Table 4).

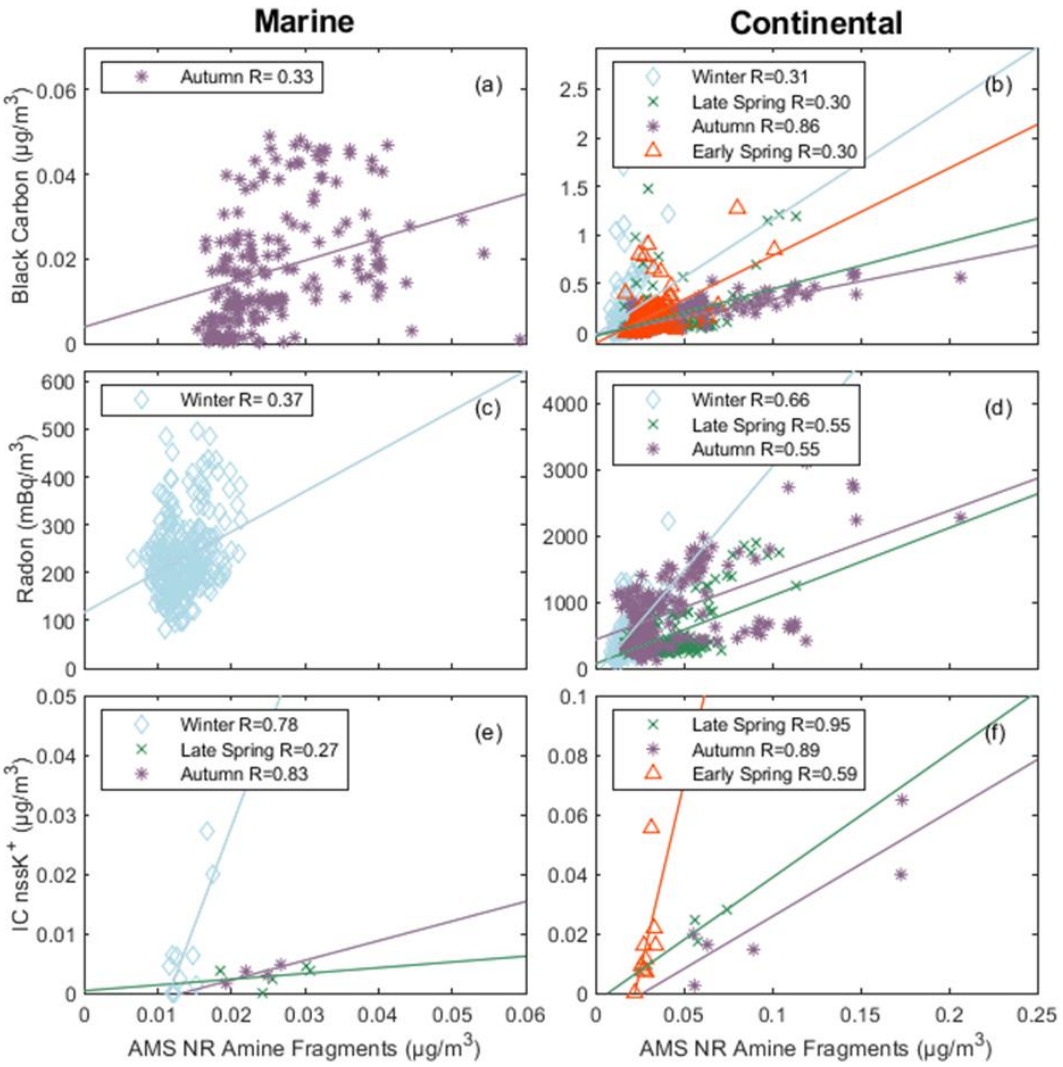

Figure 6: Scatter plot of non-marine tracers versus AMS NR amine fragments for marine periods (a,c,e) and continental periods (b,d,f). The panels include black carbon (a,b), radon (c,d), IC nssK^+ (e,f). Markers represent each cruise- blue open diamond: Winter, green cross: Late Spring, purple asterisk: Autumn, red open triangle: Early Spring. All correlations shown are statistically significant ($p < 0.05$). The solid lines are the lines of best fit obtained using an ordinary least squares regression and a two-tailed T test is used to estimate p-values.

During marine periods in Winter and continental periods in Autumn and Early Spring, correlations of AMS NR amine fragments to relative humidity revealed a negative, weak to

moderate correlation (-0.55 < R < -0.26). FTIR NV amine groups and relative humidity correlations were also negative (-0.74 < R < -0.45) during Autumn and Early Spring continental periods (Table 4). The partitioning of secondary amine between the particle and gas phase is a strong function of relative humidity [5], such that these results provide some support for secondary contributions to both AMS NR amine fragments and FTIR NV amine groups. There was also one positive correlation between relative humidity and FTIR NV amine groups, namely the marine period in Late Spring (R = 0.77, Table 4).

Ozone has also been used as a tracer for secondary processes when its availability has limited secondary aerosol formation [20, 66]. Some evidence for photochemical formation is observed by positive, weak correlations (0.41 < R < 0.42) during continental periods in Late Spring and Autumn (Figure 5d) but marine periods in Late and Early Spring and continental periods in Winter did not show positive correlations. The possible photochemical formation is supported by the weak correlations with solar radiation during continental periods in Autumn (R = 0.33) and Early Spring (R = 0.29). FTIR NV amine groups weakly correlated (0.28 < r < 0.48, Table 4) with ozone during periods when no positive correlations (-0.94 < R < 0.05) with solar radiation were observed, providing inconsistent support for a photochemical contribution to FTIR NV amine groups.

The AMS ion signal at m/z 44 (CO_2^+) is a measure of particle oxidation and a tracer for secondary processing [67]. Figures 5e and 5f display largely consistent trends between AMS NR amine fragments and AMS NR m/z 44. Moderate to strong (0.85 < R < 0.94) correlations of AMS NR m/z 44 and AMS NR amine fragments are present across all air masses and seasons, with the exception of marine periods in Early Spring. Murphy et al. [61] identified large signals of AMS NR m/z 44 in mass spectra of aminium nitrate salts produced by photooxidation,

providing further evidence of secondary formation of AMS NR amine fragments. AMS NR m/z 44 positively correlated (R = 0.52) with FTIR NV amine group mass concentrations for only the continental period in Early Spring, possibly because aminium nitrate salts are too volatile to be retained on filters for FTIR analysis.

The Early Spring cruise began in Puerto Rico rather than Massachusetts and sampled marine air masses at latitudes lower than the other cruises. Few sampled air masses in Early Spring met the criteria for "marine", in part because black carbon concentrations were high (29 ± 5 ng m^{-3}, Table 2) compared to other cruises. However, AMS NR amine fragments in Early Spring marine air masses did not correlate with continental tracers (black carbon, AMS NR nitrate, radon, or IC nssK^+). AMS NR amine fragments did correlate moderately with atmospheric DMS and ozone, which could be consistent with a secondary marine source that was not evident in the other cruises at higher latitudes. For marine air masses in Bermuda, near where marine air masses were sampled in Early Spring, anthropogenic activity is not a large contributor to organic nitrogen compounds, such as amine, despite being downwind of continental pollution sources [68]. It is also possible that the lack of correlation with the available tracers could be from sampling shorter durations of marine air masses during Early Spring, which limits the comparison of Early Spring marine periods to marine periods in other seasons.

4.3. Sources for <0.5 and <0.18 μm Amines

Submicron (<1 μm) sampling of marine aerosol over the open ocean and from bubble generators has suggested that alcohol functional groups serve as useful tracers for marine-derived saccharides, amino sugars, and carbohydrates [11, 29, 51, 69, 70]. Conversely, carboxylic acid groups serve as a tracer for photochemical reaction products of VOCs [11, 20, 51, 71, 72]. Figure 7 shows the correlations of FTIR NV amine groups to FTIR NV alcohol and FTIR NV acid

groups measured across all four cruises for three different size cut-offs (<1 μm, <0.5 μm, <0.18 μm).

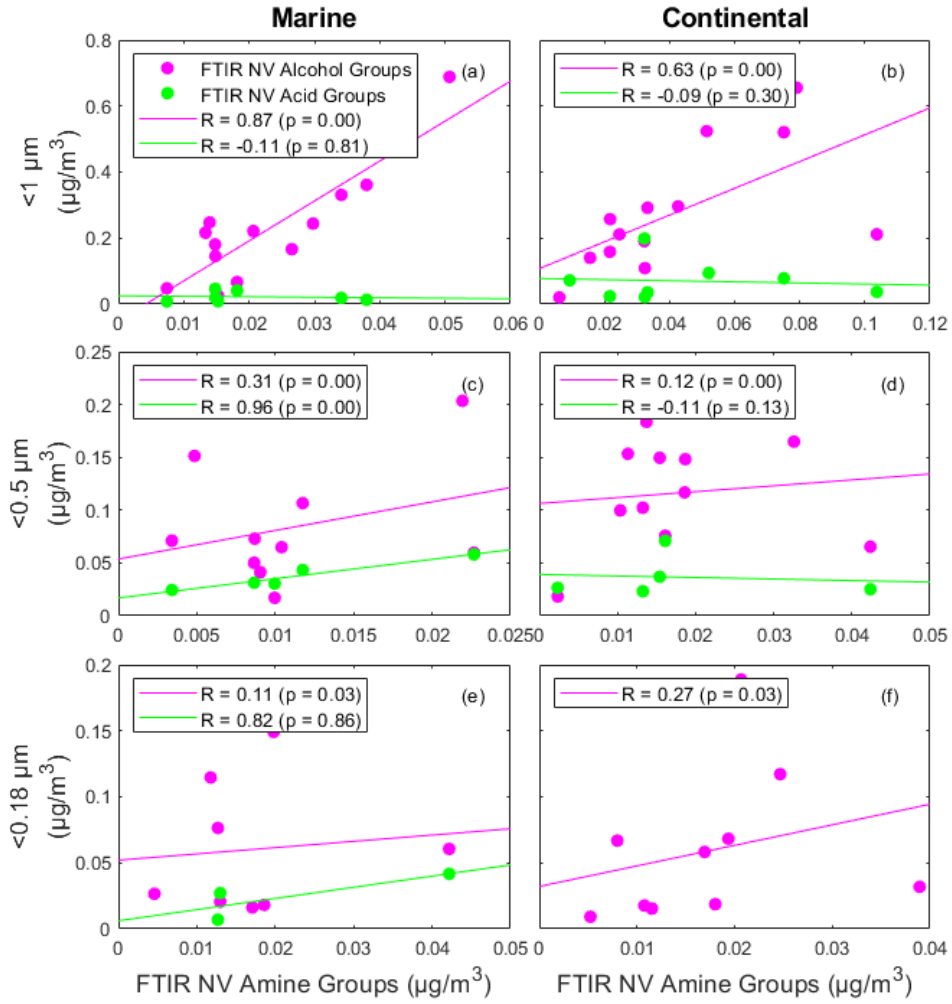

Figure 7: Scatter plot of FTIR primary (FTIR NV alcohol group: pink) and secondary (FTIR NV carboxylic acid group: green) tracers versus FTIR NV amine groups for marine filters (a,c,e) and continental filters (b,d,f) with functional group concentrations twice the standard deviation. The panels show the three filter size cutoffs: 1 μm (a,b), 0.5 μm (c,d), and 0.18 μm (e,f). The solid lines are the lines of best fit obtained using an ordinary least squares regression. All correlations with FTIR NV alcohol groups and only one correlation (<0.5 μm, marine) with FTIR NV acid groups were statistically significant ($p < 0.05$). A two-tailed T test is used to estimate p-values.

For <1 μm particle samples, there was a strong correlation (R = 0.87, Figure 7a) between FTIR NV alcohol and amine groups for marine periods and a moderate correlation (R = 0.63, Figure 7b) for continental periods, consistent with a primary source of FTIR NV amine groups. The difference between marine and continental air masses shows that the primary seawater amine source explains more variability for marine air masses than for continental air masses. The

correlation of FTIR NV alcohol and amine groups was weaker for marine filters for <0.5 μm and <0.18 μm particle samples, with R = 0.31 for <0.5 μm (Figure 7c) and R = 0.11 for <0.18 μm (Figure 7e). Similarly, there were lower correlations of FTIR NV alcohol and amine groups for continental filters with R = 0.12 for <0.5 μm (Figure 7d) and R = 0.27 for <0.18 μm (Figure 7f). These results show that non-volatile amine groups associated with sea spray are largely found in >0.5 μm particles, where their mass is sufficiently large to control the <1 μm mass variability. The weak correlations of FTIR NV alcohol and amine groups for <0.5 μm and <0.18 μm particle samples could result from non-marine sources such as combustion that have different ratios of FTIR NV alcohol and amine groups than those found in sea spray [20, 64, 73, 74]. The correlations may also be reduced by the higher volatility of combustion-derived aerosols that may be contributed by continental sources [75, 76].

In contrast to the weak correlations found for FTIR NV amine groups with FTIR NV alcohol groups for <0.5 μm and <0.18 μm particle samples, strong (0.82 < R < 0.96, Figure 7c,e) correlations of FTIR NV amine to acid groups were found for <0.5 μm and <0.18 μm during marine periods. No correlation of FTIR NV amine to acid groups was found for <1 μm samples. The correlations of FTIR NV acid to amine groups for <0.5 μm and <0.18 μm particle samples suggest that secondary amine groups contribute more to particles with diameters smaller than 0.5 μm, which is consistent with expectations for condensing gases having a proportionately larger impact on the mass composition of smaller particles [77, 78]. Secondary dimethyl- and diethylaminium salts produced by acid-base reactions with biogenic, gaseous amines have been shown to have mass concentration peaks in similar size ranges of 0.25-0.50 μm [14] and 0.14-0.42 μm [15]. The strong correlation between FTIR NV amine and acid groups for <0.5 μm and <0.18 μm particle samples indicate that a gas-to-particle reaction mechanism contributes to

primary (C-NH_2) amine groups in size ranges that are important for CCN. A secondary marine source of FTIR NV amine groups in aerosols with diameters of <0.18 μm and <0.5 μm is supported by weak to moderate correlations ($0.39 < R < 0.73$) of MSA and FTIR NV amine groups during marine periods in Late Spring for both size ranges. These correlations for marine periods in two seasons were the only statistically significant correlations among the four cruises that were available for MSA due to the limited number of marine filters. There was no significant correlation between FTIR NV acid and amine groups for any size of the continental FTIR filters. There were not enough continental filters with both FTIR NV amine and acid groups above detection to investigate correlations for continental <0.18 μm particle samples.

4.4. Combined AMS NR and FTIR NV Amine Contributions

In general, our results support the expectation that FTIR NV amine groups and AMS NR amine fragments do not measure the same chemical components. Specifically, FTIR measures NV amine groups with primary C-NH_2 that may or may not be refractory. The correlations summarized in Figure 8 show that, in marine air masses, most of the FTIR NV amine groups in <1 μm particles are primary and marine and that <0.5 μm and <0.18 μm diameter fractions are secondary and marine. In contrast, the AMS measures NR amine fragments with primary, secondary, and tertiary amine moieties that may be too volatile to be sampled on filters. The correlations summarized in Figure 8 show that AMS NR amine fragments are largely continental and secondary, although some contribution of primary emissions from combustion is also likely.

During marine periods in Late Spring, the variability of FTIR NV amine groups was largely explained by correlations with AMS NR chloride, IC sea salt, seawater DMS, and chl *a* all of which are consistent with primary marine sources. In contrast, the variability of AMS NR

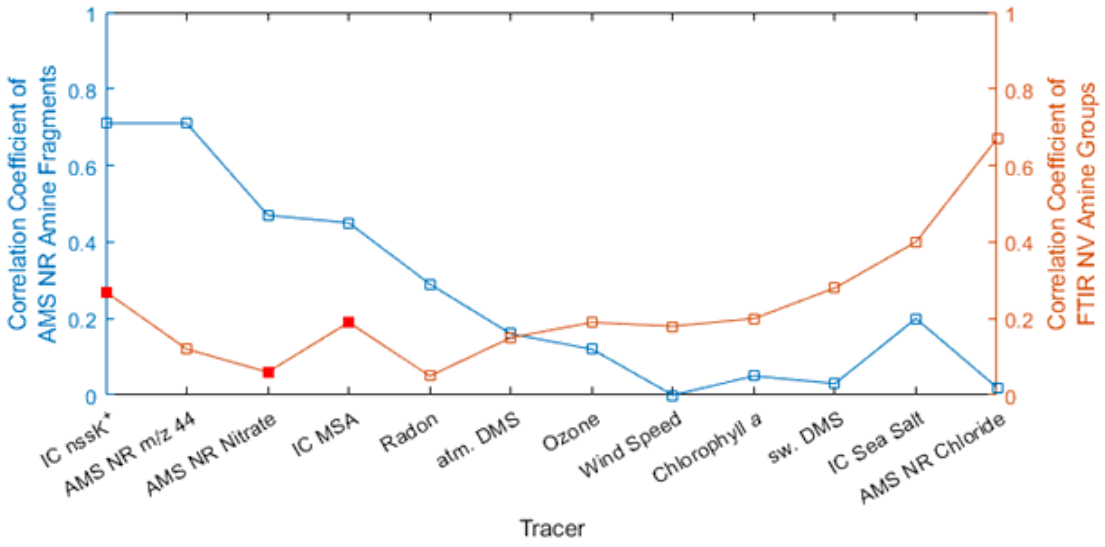

Figure 8: Plot of average Pearson correlation coefficients (R) of AMS NR amine fragments (blue) and FTIR NV amine groups in particles with diameters <1 μm (orange) with selected tracers. Negative correlations were averaged as 0 and only statistically significant ($p < 0.05$) correlations were included, except for markers shown as solid red (which were not significant).

amine fragments was largely explained by correlations with AMS NR nitrate, IC nssK^+, radon, and AMS NR m/z 44, all of which indicate continental secondary sources. Figure 9 shows similar correlations with AMS NR nitrate and IC sea salt in Autumn that exemplify the AMS NR amine fragments correlation to AMS NR nitrate concentrations and the FTIR NV amine groups correlation to IC sea salt. A diagram describing the sources and mechanisms of amine in marine environments is shown in Figure 10.

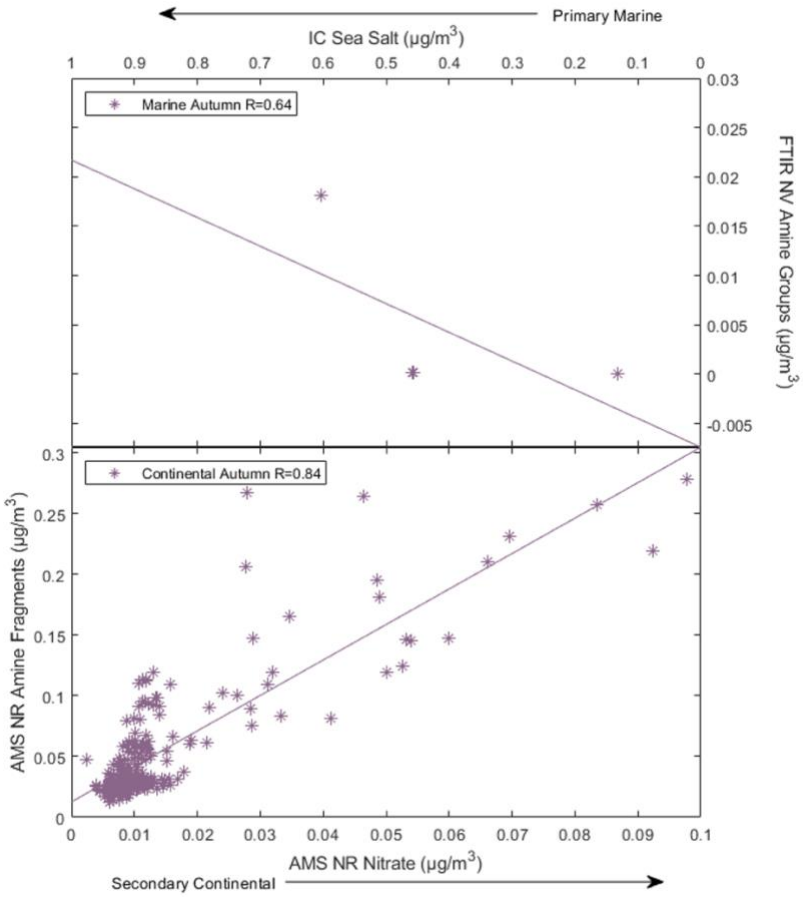

Figure 9: Scatter plot of (top) FTIR NV amine groups in particles with diameters <1 µm versus a primary marine tracer (IC sea salt) and (bottom) AMS NR amine fragments versus a secondary continental tracer (AMS NR nitrate) during the Autumn season. Both correlations are statistically significant ($p < 0.05$). The solid lines are the lines of best fit obtained using an ordinary least squares regression and a two-tailed T test is used to estimate p-values.

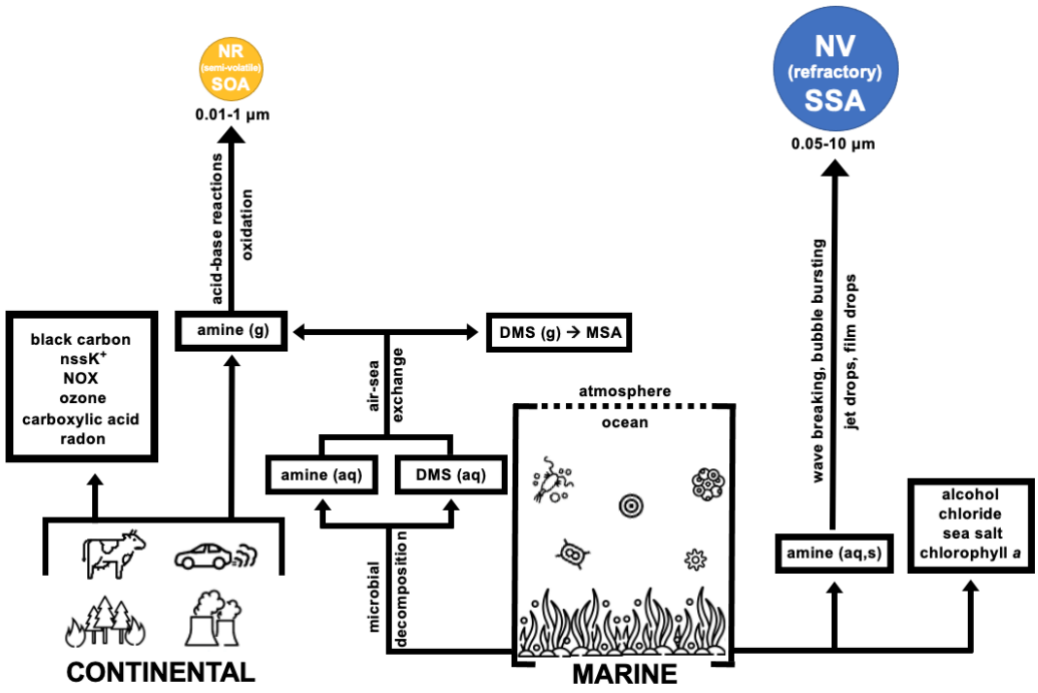

Figure 10: Schematic diagram of continental and marine sources of tracers and amine in non-refractory, semi-volatile secondary organic aerosols and non-volatile, refractory sea spray aerosols in marine environments.

The distinctly different sources of FTIR NV amine groups and AMS NR amine fragments suggest that combining the two measurements is likely to provide a better estimate of particle-phase amines in marine environments than either measurement separately. This approach is supported by the poor overall correlation of $\rho = 0.02$ (Figure 2a) of the two measurements. FTIR NV amine groups provide a good estimate of <1 µm marine primary amine group mass concentration; AMS NR amine fragments provide a good estimate of continental amine sources that are likely secondary. Results for individual seasons illustrate that the contributions of FTIR NV amine groups and AMS NR amine fragments vary by season (based on Table 2). For Winter, the primary marine FTIR NV amine group accounts for 53% compared to 47% secondary continental AMS NR amine fragments. For Late Spring and Autumn, primary marine FTIR NV amine group accounts for 34% compared to 66% secondary continental AMS NR amine fragments. And for Early Spring, primary marine FTIR NV amine group accounts for 27% compared to 73% secondary continental AMS NR amine fragments.

5. CONCLUSIONS

FTIR and AMS amine measurements were used to investigate the sources of submicron aerosol in the North Atlantic during different seasons. Marine and continental air masses were distinguished to separate the different conditions that were measured. Amine concentrations from AMS and FTIR were compared to chemical and meteorological tracers for identification of marine and continental sources and primary and secondary processes. FTIR and AMS measured greater amine concentrations for continental air masses than for marine air masses except for the Early Spring cruise, likely due to its lower latitudes and less pristine marine air masses. AMS NR amine fragments largely correlated with secondary tracers such as AMS NR nitrate, ozone, AMS NR m/z 44, and IC MSA but did not correlate positively with seawater DMS, AMS NR chloride, chlorophyll *a* or wind speed. Correlations with tracers for secondary particles were lower for <1 μm FTIR NV amine groups than for AMS NR amine fragments, but correlations of FTIR NV amine groups with primary marine tracers such as wind speed, IC sea salt, and seawater DMS, NR chloride, and chlorophyll *a* were higher than for AMS NR amine fragments.

FTIR NV amine groups measured during marine periods were found to have largely primary sources for <1 μm particles but secondary sources for <0.5 and <0.18 μm particles. Correlations with FTIR NV alcohol groups show the contribution of a primary source of non-volatile amine for aerosols with diameters <1 μm that had weaker correlations for <0.5 and <0.18 μm. Correlations between FTIR NV amine groups with both FTIR NV acid groups and IC MSA for particles <0.5 and <0.18 μm diameter revealed that secondary processes were a larger contributor for amine groups than in <1 μm particles.

Results presented herein are also consistent with the expectation that FTIR measures the refractory, amine-containing sea salt particles missed by AMS, and that AMS measures the semi-

volatile, amine-containing particles missed by FTIR spectroscopy. Therefore, these two techniques offer complementary analyses of amine in marine environments for <1 μm atmospheric particles. Combining them provides a rough source apportionment for marine periods, with primary marine amine accounting for 53% compared to 47% secondary continental amine in Winter, but primary marine amine accounting for only 27% compared to 73% secondary continental amine for Early Spring.

6. APPENDIX

6.1. PMF Analysis of AMS NR HR-Org and AMS NR HR-SO_4

Positive matrix factorization of high resolution (HR) organic (Org) and sulfate (SO_4) AMS data was performed using the PMF Evaluation Tool, PET [79]. Ion fragments with low signal-to-noise (SNR) were downweighted ($0.2 < SNR < 2$) by a factor of 2 or removed ($SNR < 0.2$). Ion fragments associated with m/z 44 (CO_2^+, CO^+, H_2O^+, HO^+, O^+) were also downweighted by a factor of 2. No data smoothing or spike removal was applied to the matrices.

Fit quality (Q/Q_{exp}) and uncentered correlations were used to identify the best number of factors. Q/Q_{exp} decreases with an increasing number of factors as each factor introduces an additional degree of freedom. Solutions with numbers of factors that resolve Q/Q_{exp} near a value of 1 is ideal such that an increased distance of Q/Q_{exp} from 1 is used as one of the criteria for rejecting a solution.

The 1 to 7 factor solutions and criteria of PMF analysis are summarized in Tables 5-8. Both “OminusC” and “Diff” data types were used for PMF analysis. The Diff data type is obtained by fitting the raw difference spectra while the OminusC data type is obtained by subtracting the “Open” ion sticks from the “Closed” ion sticks after peak fitting. The HR Diff Sticks data type was chosen due to its low absolute residual when compared to the HR OminusC Sticks data type. The OminusC data type had also produced solutions with high Q/Q_{exp} values, indicating that the errors associated with the input data have been underestimated.

The highest number of factors with no temporal nor spectral correlations was the final number of factors chosen as a solution for each period. A 3-factor solution with a Q/Q_{exp} value of 0.73 was chosen for marine periods during Autumn as the 4-factor solution produced an additional factor with a very similar spectrum ($R > 0.8$) to a factor identified in both the 3- & 4-

factor solutions. A 2-factor solution with a Q/Q_{exp} value of 2.41 was selected for continental periods during Autumn. A 2-factor solution with a Q/Q_{exp} value of 0.51 was selected for marine periods during Early Spring. A 2-factor solution with a Q/Q_{exp} value of 0.34 was selected for continental periods during Early Spring. Only 1 factor in the 3-factor solution made up less than 10% of the total mass for marine periods during Autumn. For all other time periods, each factor made up more than 10% of the total mass.

The 2-3 resulting factors included a combination of a low-volatility oxidized organic aerosol (LVOOA) factor, a Sulfate factor, and an Amine factor. The mass spectra and time series of each factor are shown in Figures 11-15, and Table 9 shows the average mass concentrations.

Table 5: Summary of solutions and criteria used for PMF analysis of AMS NR HR-Org and HR-SO_4 for marine air masses in Autumn. Criteria that are not applicable for one factor are indicated by N/A. Paired clusters that do not have uncentered correlation coefficients (UC) higher than 0.8 are indicated by None.

Criteria \ Factor number (p)		1	2	3	4	5	6	7
Diff	Q/Q_{exp}	1.00	0.79	0.73	0.71	0.69	0.66	0.65
	Absolute residual	40.0	19.8	19.2	14.3	12.1	12.6	13.3
	Temporal correlation factors strength (R > 0.8)	N/A	None	None	None	None	None	None
	Similarity of factor spectra (R > 0.8)	N/A	None	None	2 pairs	3 pairs	2 pairs	5 pairs
	Factors with less than 10% total mass	None	None	1 factor	1 factor	2 factors	3 factors	5 factors
OminusC	Q/Q_{exp}	2.39	2.15	2.12	2.11	2.11	2.09	2.09
	Absolute residual	46.0	28.0	33.6	32.8	29.5	28.6	28.0
	Temporal correlation factors strength (R >0.8)	N/A	None	None	None	None	1 pair	3 pairs
	Similarity of factor spectra (R > 0.8)	N/A	None	1 pair	1 pair	3 pairs	3 pairs	2 pairs
	Factors with less than 10% total mass	None	None	None	1 factor	1 factor	2 factors	2 factors

Table 6: Summary of solutions and criteria used for PMF analysis of AMS NR HR-Org and HR-SO_4 for continental air masses in Autumn. Criteria that are not applicable for one factor are indicated by N/A. Paired clusters that do not have uncentered correlation coefficients (UC) higher than 0.8 are indicated by None.

Criteria \ Factor number (p)		1	2	3	4	5	6	7
Diff	Q/Q_{exp}	2.74	2.14	2.05	1.93	1.88	1.82	1.79
	Absolute residual	30.8	16.9	14.5	12.7	8.92	10.3	8.67
	Temporal correlation factors strength (R > 0.8)	N/A	None	None	None	None	None	None
	Similarity of factor spectra (R > 0.8)	N/A	None	1 pair	1 pair	2 pair	6 pair	5 pair
	Factors with less than 10% total mass	None	None	None	1 factor	1 factor	3 factors	3 factors
OminusC	Q/Q_{exp}	3.37	2.82	2.71	2.58	2.55	2.53	2.51
	Absolute residual	81.9	97.9	70.6	71.4	69.8	63.9	64.0
	Temporal correlation factors strength (R >0.8)	N/A	None	None	None	None	2 pairs	1 pair
	Similarity of factor spectra (R > 0.8)	N/A	None	None	1 pair	1 pair	1 pair	3 pairs
	Factors with less than 10% total mass	None	None	1 factor	2 factors	3 factors	4 factors	5 factors

Table 7: Summary of solutions and criteria used for PMF analysis of AMS NR HR-Org and HR-SO_4 for marine air masses in Early Spring. Criteria that are not applicable for one factor are indicated by N/A. Paired clusters that do not have uncentered correlation coefficients (UC) higher than 0.8 are indicated by None.

Criteria \ Factor number (p)		1	2	3	4	5	6	7
Diff	Q/Q_{exp}	0.55	0.51	0.48	0.48	0.45	0.43	0.41
	Absolute residual	30.2	28.4	23.3	22.7	20.9	19.5	19.4
	Temporal correlation factors strength (R > 0.8)	N/A	None	None	None	None	None	None
	Similarity of factor spectra (R > 0.8)	N/A	None	1 pair	3 pairs	None	None	15 pairs
	Factors with less than 10% total mass	None	1 factor	1 factor	2 factors	2 factors	3 factors	4 factors
OminusC	Q/Q_{exp}	0.88	0.88	0.87	0.86	0.86	0.85	0.85
	Absolute residual	34.6	28.7	29.0	31.3	31.0	31.8	32.3
	Temporal correlation factors strength (R >0.8)	N/A	None	None	1 pair	None	None	None
	Similarity of factor spectra (R > 0.8)	N/A	None	1 pair	1 pair	1 pair	1 pair	2 pairs
	Factors with less than 10% total mass	None	None	None	None	1 factor	2 factors	2 factors

Table 8: Summary of solutions and criteria used for PMF analysis of AMS NR HR-Org and HR-SO_4 for continental air masses in Early Spring. Criteria that are not applicable for one factor are indicated by N/A. Paired clusters that do not have uncentered correlation coefficients (UC) higher than 0.8 are indicated by None.

Criteria \ Factor number (p)		1	2	3	4	5	6	7
Diff	Q/Q_{exp}	0.38	0.34	0.31	0.29	0.28	0.28	0.26
	Absolute residual	29.8	28.3	8.45	8.40	8.38	7.71	7.64
	Temporal correlation factors strength (R > 0.8)	N/A	None	None	None	None	None	None
	Similarity of factor spectra (R > 0.8)	N/A	None	1 pair	None	None	None	1 pair
	Factors with less than 10% total mass	None	1 factor	1 factor	2 factors	3 factors	3 factors	4 factors
OminusC	Q/Q_{exp}	0.88	0.88	0.87	0.86	0.86	0.85	0.85
	Absolute residual	30.3	11.8	9.55	10.4	10.4	10.5	10.8
	Temporal correlation factors strength (R >0.8)	N/A	None	None	None	None	None	None
	Similarity of factor spectra (R > 0.8)	N/A	None	1 pair	1 pair	1 pair	2 pairs	4 pairs
	Factors with less than 10% total mass	None	None	None	None	None	1 factor	2 factors

Table 9: Mean mass concentrations and standard deviations (ng m^{-3}) of each PMF factor resolved for marine and continental air masses in Autumn and Early Spring.

Air Mass/Season \ Factor	LVOOA	Sulfate	Amine
Marine Autumn	184 ± 216	281 ± 224	17 ± 34
Marine Early Spring	--	493 ± 314	39 ± 70
Continental Autumn	995 ± 1602	590 ± 400	--
Continental Early Spring	--	609 ± 376	51 ± 90

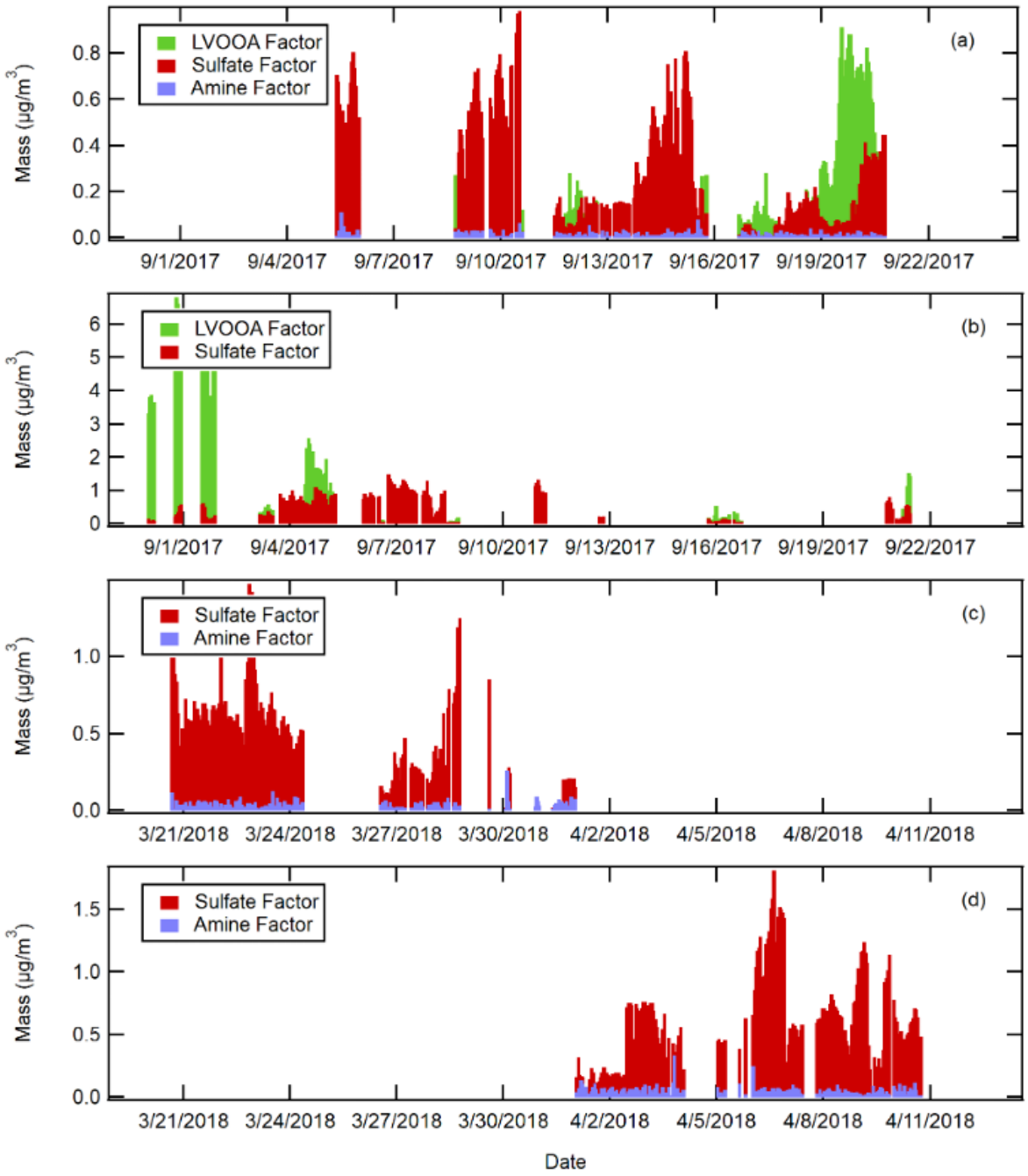

Figure 11: Time series (bottom right) of factors resolved from PMF analysis of AMS NR HR-Org and HR-SO_4 for (a) marine air masses in Autumn, (b) continental air masses in Autumn, (c) marine air masses in Early Spring, and (d) continental air masses in Early Spring.

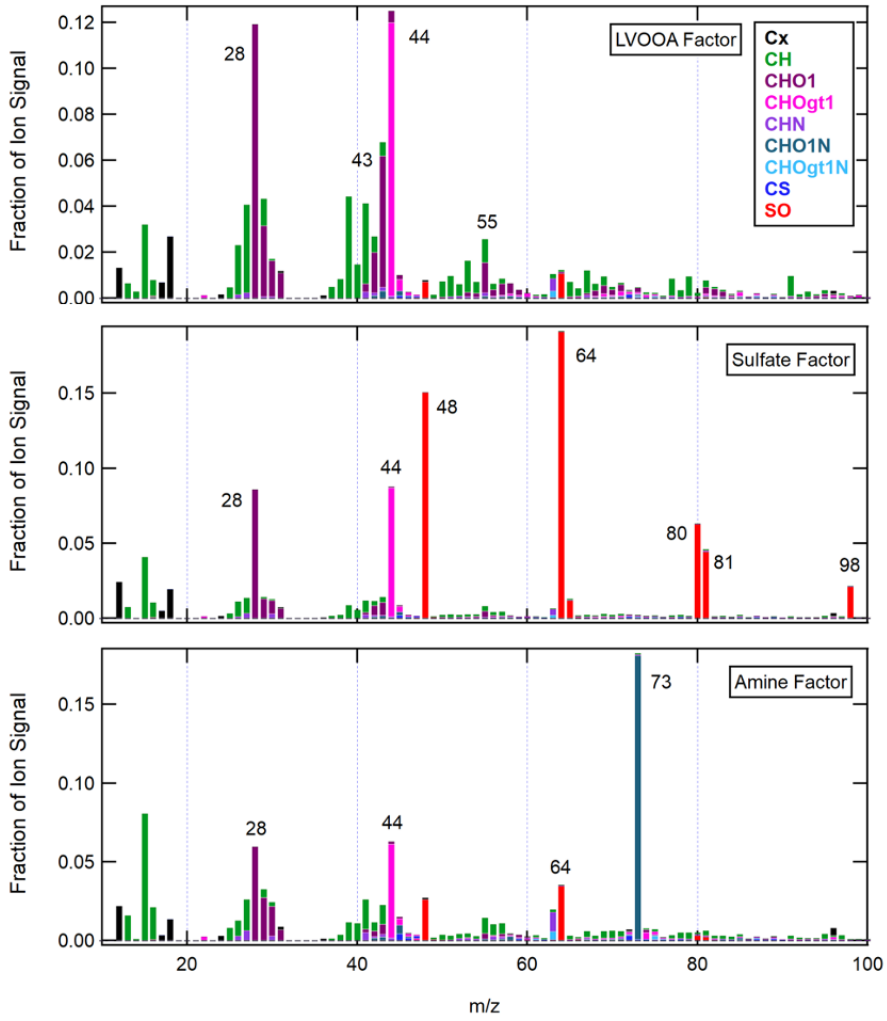

Figure 12: Mass spectra of factors resolved from PMF analysis of AMS NR HR-Org and HR-SO_4 for marine air masses in Autumn. The factors shown include the LVOOA factor (top), the Sulfate factor (middle), and the Amine factor (bottom).

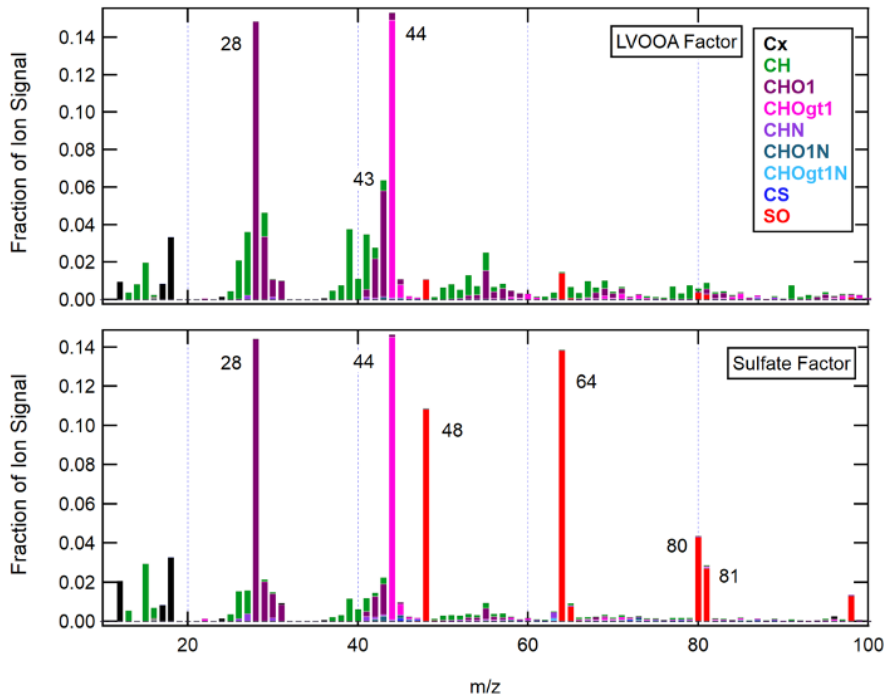

Figure 13: Mass spectra of factors resolved from PMF analysis of AMS NR HR-Org and HR-SO_4 for continental air masses in Autumn. The factors shown include the LVOOA factor (top) and the Sulfate factor (bottom).

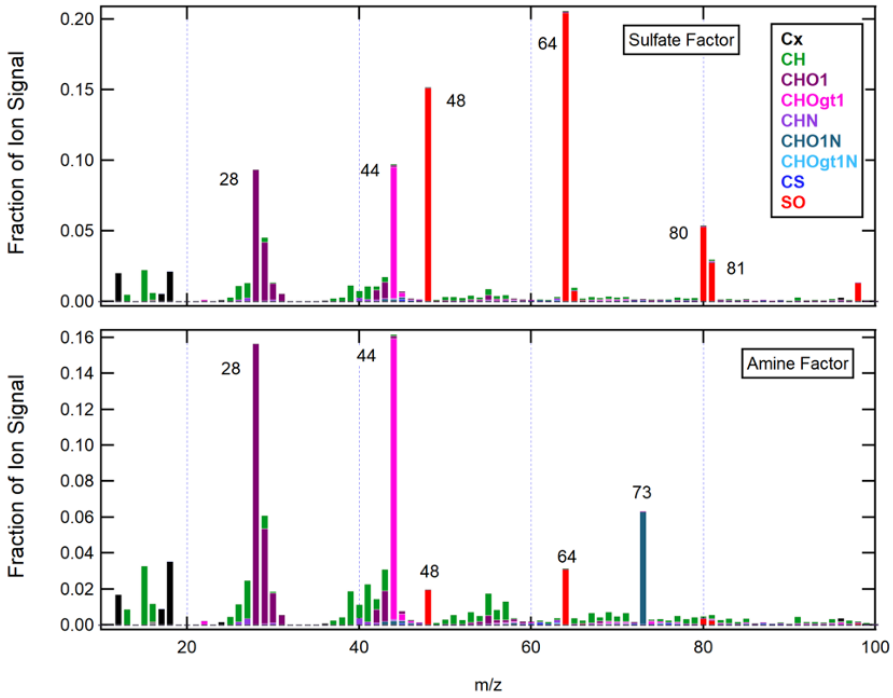

Figure 14: Mass spectra of factors resolved from PMF analysis of AMS NR HR-Org HR-SO_4 for marine air masses in Early Spring. The factors shown include the Sulfate factor (top) and the Amine factor (bottom).

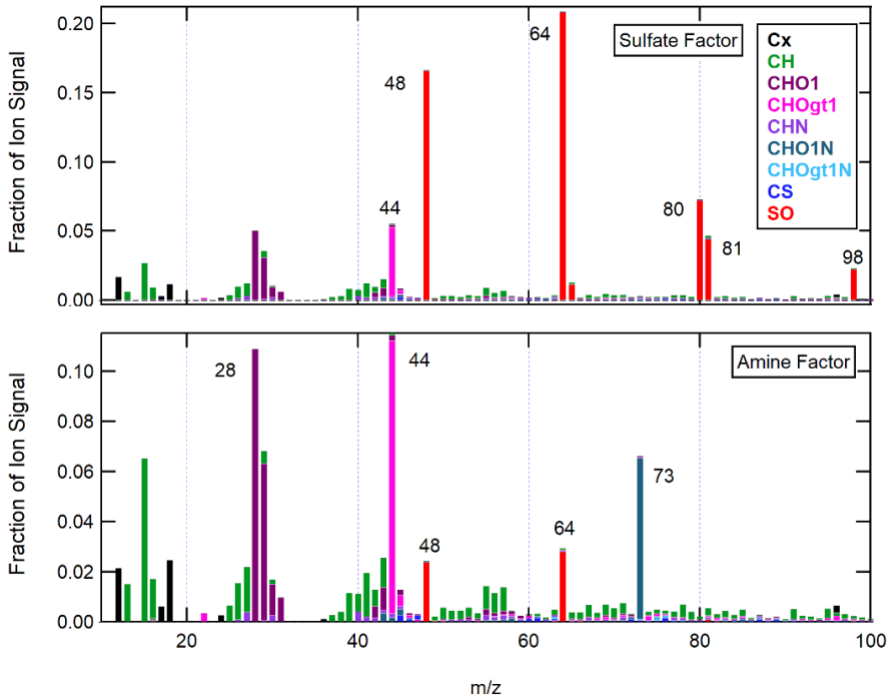

Figure 15: Mass spectra of factors resolved from PMF analysis of AMS NR HR-Org and HR-SO_4 for continental air masses in Early Spring. The factors shown include the Sulfate factor (top) and the Amine factor (bottom).

The mass spectrum of the LVOOA factor shows prominent peaks at m/z 28 (CO^+), m/z 43 ($C_2H_3O^+$) and m/z 44 (CO_2^+), which are attributed to oxidized organic fragments (CHO1 and CHOgt1 AMS families). A high ratio of m/z 44/43, also evident of SOA oxidation, is used to identify the LVOOA factor as well as comparisons to previously reported LVOOA factors [80-83]. This factor was present throughout Autumn but absent during Early Spring when there was also less continental transport of AMS NR amine fragments. During continental periods in Autumn, this factor had the highest mass concentration but also the most variability (995 ± 1602 ng m^{-3}).

The Sulfate factor was found within all air masses and seasons and contained sulfate peaks at m/z 48 (SO^+), m/z 64 ($SO2^+$), m/z 80 (SO_3^+), m/z 81 (HSO_3^+), m/z 96 (SO_4^+), and m/z 98 ($H_2SO_4^+$) as well as organic peaks that are characteristic of particle aging at m/z 28 (CO^+) and m/z 44 (CO_2^+) in its mass spectrum. Larger organic peaks were present in continental air masses

and during Autumn. Mass concentrations of the Sulfate factor were higher during continental periods than during marine periods and in Early Spring than in Autumn. The highest mass concentration of the Sulfate factor was observed during continental periods in Early Spring (609 ± 376 ng m^{-3}). With the exception of continental periods in Autumn, the Sulfate factor had the highest mass concentration among all the factors.

The final factor resolved during NAAMES was the Amine factor. This factor's mass spectrum consisted of both sulfate (m/z 48, m/z 64) and organic fragments, namely m/z 28 (CO^+) and m/z 44 (CO_2^+) which were of similar intensities. This factor is further characterized by a large, peak at m/z 73 ($C_3H_7NO^+$, $C_2H_5N_2O^+$), analogous to an oxidized amine ion fragment. This peak had the highest intensity for marine air masses in Autumn. Alternatively, oxidized organic peaks (m/z 28, m/z 44) had higher intensities during Early Spring. An unoxidized peak of a parent amine is seen at m/z 63 (C_4HN^+) for only marine air masses in Autumn [84]. Interestingly, this factor was not observed during continental periods in Autumn. The highest mass concentration observed for the Amine factor was during continental periods in Early Spring (51 ± 90 ng m^{-3}). Overall, the Amine factor accounted for the lowest observed mass concentrations among all factors.

It is likely that a lack of organic mass during Early Spring resulted in no LVOOA factor and a smaller organic ion signal for the Sulfate factor for both marine and continental air masses. The Amine factor was very noisy, exhibiting high variability in mass concentration (±34-90 ng m^{-3}) that was nearly twice that of its mean (±17-51 ng m^{-3}). The noisiness of the time series of the Amine factor meant that it did not yield any useful source information for AMS NR amine fragments.

6.2. AMS NR Single Particle Amine Fragments

AMS NR single particle amine fragments were estimated from the sum of 29 ions ($\Sigma CHN = CHN^+ + CH_3N^+ + CH_4N^+ + C_2H_3N^+ + C_2H_4N^+ + CHNO^+ + C_2H_5N^+ + C_2H_6N^+ + C_2H_4NO^+ C_3H_8N^+ + C_2H_5NO^+ + C_3H_9N^+ + CH_4N^+ + C_3H_6NO^+ + C_4H_{10}N^+ + C_2H_3NO_2^+ + C_2H_5N_2O^+ + C_3H_7NO^+ + C_4H_{11}N^+ + C_4H_6NO^+ + C_5H_{10}N^+ + C_4H_7NO^+ + C_5H_{11}N^+ + C_4H_8NO^+ + C_5H_{12}N^+ + C_4H_8N_2O^+ + C_5H_{10}NO^+ + C_6H_{14}N^+ + C_6H_{15}N^+$) to approximate amine within ET single particle measurements. Both unoxidized and oxidized amine ion fragments and ion

Table 10: Mean mass concentrations and standard deviations (μg m^{-3}) of AMS NR single particle amine fragments for marine and continental air masses in Autumn and Early Spring.

		Autumn		Early Spring	
m/z	Ion Fragment	Marine	Continental	Marine	Continental
27	CHN^+	0.0017 ± 0.0006	0.0045 ± 0.0041	0.0022 ± 0.0011	0.0021 ± 0.0006
29	CH_3N^+	0.0002 ± 0.0004	0.0001 ± 0.0001	0.0004 ± 0.0004	0.0002 ± 0.0001
30	CH_4N^+	0.0015 ± 0.0004	0.0024 ± 0.0022	0.0011 ± 0.0005	0.0008 ± 0.0003
41	$C_2H_3N^+$	0.0011 ± 0.0005	0.0029 ± 0.0027	0.0010 ± 0.0004	0.0012 ± 0.0004
42	$C_2H_4N^+$	0.0008 ± 0.0006	0.0016 ± 0.0014	0.0010 ± 0.0003	0.0009 ± 0.0002
43	$CHNO^+$ $C_2H_5N^+$	0.0012 ± 0.0004 0.0007 ± 0.0004	0.0029 ± 0.0023 0.0011 ± 0.0008	0.0014 ± 0.0009 0.0008 ± 0.0002	0.0013 ± 0.0004 0.0008 ± 0.0002
44	$C_2H_6N^+$	0.0005 ± 0.0002	0.0012 ± 0.0011	0.0010 ± 0.0005	0.0003 ± 0.0011
58	$C_2H_4NO^+$ $C_3H_8N^+$	0.0005 ± 0.0001 0.0002 ± 0.0001	0.0007 ± 0.0003 0.0004 ± 0.0003	0.0006 ± 0.0003 0.0004 ± 0.0002	0.0004 ± 0.0001 0.0003 ± 0.0001
59	$C_2H_5NO^+$ $C_3H_9N^+$	0.0004 ± 0.0001 0.0001 ± 0.0001	0.0006 ± 0.0004 0.0001 ± 0.0001	0.0004 ± 0.0002 0.0001 ± 0.0002	0.0003 ± 0.0001 0.0001 ± 0.0001
63	C_4HN^+	0.0031 ± 0.0003	0.0030 ± 0.0005	0.0010 ± 0.0004	0.0013 ± 0.0003
72	$C_3H_6NO^+$ $C_4H_{10}N^+$	0.0002 ± 0.0001 0.0001 ± 0.0001	0.0004 ± 0.0002 0.0001 ± 0.0001	0.0005 ± 0.0006 0.0002 ± 0.0001	0.0002 ± 0.0001 0.0001 ± 0.0001
73	$C_2H_3NO_2^+$ $C_2H_5N_2O^+$ $C_3H_7NO^+$ $C_4H_{11}N^+$	0.0003 ± 0.0001 0.0022 ± 0.0008 0.0019 ± 0.0005 0.0002 ± 0.0001	0.0007 ± 0.0005 0.0024 ± 0.0009 0.0019 ± 0.0003 0.0002 ± 0.0001	0.0003 ± 0.0001 0.0021 ± 0.0009 0.0019 ± 0.0010 0.0002 ± 0.0001	0.0002 ± 0.0001 0.0016 ± 0.0006 0.0016 ± 0.0005 0.0001 ± 0.0001
84	$C_4H_6NO^+$ $C_5H_{10}N^+$	0.0001 ± 0.0001 0.0001 ± 0.0001	0.0003 ± 0.0003 0.0002 ± 0.0002	0.0001 ± 0.0001 0.0003 ± 0.0003	0.0002 ± 0.0001 0.0002 ± 0.0001
85	$C_4H_7NO^+$ $C_5H_{11}N^+$	0.0003 ± 0.0003 0.0002 ± 0.0001	0.0003 ± 0.0002 0.0003 ± 0.0005	0.0002 ± 0.0001 0.0003 ± 0.0001	0.0002 ± 0.0001 0.0003 ± 0.0001
86	$C_4H_8NO^+$ $C_5H_{12}N^+$	0.0001 ± 0.0001 0.0001 ± 0.0001	0.0001 ± 0.0001 0.0001 ± 0.0001	0.0001 ± 0.0001 0.0001 ± 0.0001	0.0001 ± 0.0001 0.0001 ± 0.0001
100	$C_4H_8N_2O^+$ $C_5H_{10}NO^+$ $C_6H_{14}N^+$	0.0001 ± 0.0001 0.0001 ± 0.0001 0.0001 ± 0.0001	0.0001 ± 0.0001 0.0001 ± 0.0001 0.0001 ± 0.0001	0.0001 ± 0.0001 0.0001 ± 0.0001 0.0001 ± 0.0001	0.0001 ± 0.0001 0.0001 ± 0.0001 0.0001 ± 0.0001
101	$C_6H_{15}N^+$	0.0001 ± 0.0001	0.0001 ± 0.0001	0.0001 ± 0.0001	0.0001 ± 0.0001

fragments of parent amines are included. The average mass concentration and standard deviation of AMS NR single particle amine fragments in both marine and continental air masses during Autumn and Early Spring are shown in Table 10. Mass concentrations of AMS NR single particle amine fragments during marine periods were equivalent for both seasons but higher in Autumn than in Early Spring for continental air masses. The average mass concentration was also higher during marine periods in Early Spring but lower during marine periods in Autumn, similar to the trend in mass concentrations seen for AMS NR amine fragments estimated by $C_xH_yN_z$ ion fragments.

Figure 16 displays the differences and similarities in the selection of AMS NR single particle amine fragments compared to the selection of AMS NR amine fragments. Both AMS NR single particle amine fragments and AMS NR amine fragments have little variability when regressed against FTIR NV amine groups in Early Spring and display a nearly vertical slope with p-values of 0.26 and 0.66, respectively. During Autumn, AMS NR single particle amine fragments and AMS NR amine fragments both display a strong correlation ($R = 0.87$) to FTIR NV amine groups. The p-values of these correlations are 0.95 for the former and 0.08 for the latter. While each of the four correlations is not statistically significant ($p > 0.05$), the overall p-value is lower when using AMS NR amine fragments rather than AMS NR single particle amine fragments. This shows that the sum of AMS NR amine fragments is less variable than the sum of AMS NR single particle amine fragments. Therefore, AMS NR amine fragments likely have more similarity to FTIR NV amine groups than the AMS NR single particle amine fragments, consistent with the expectation that the single particle signals are less accurate because of their lower m/z resolution and lower fragment specificity.

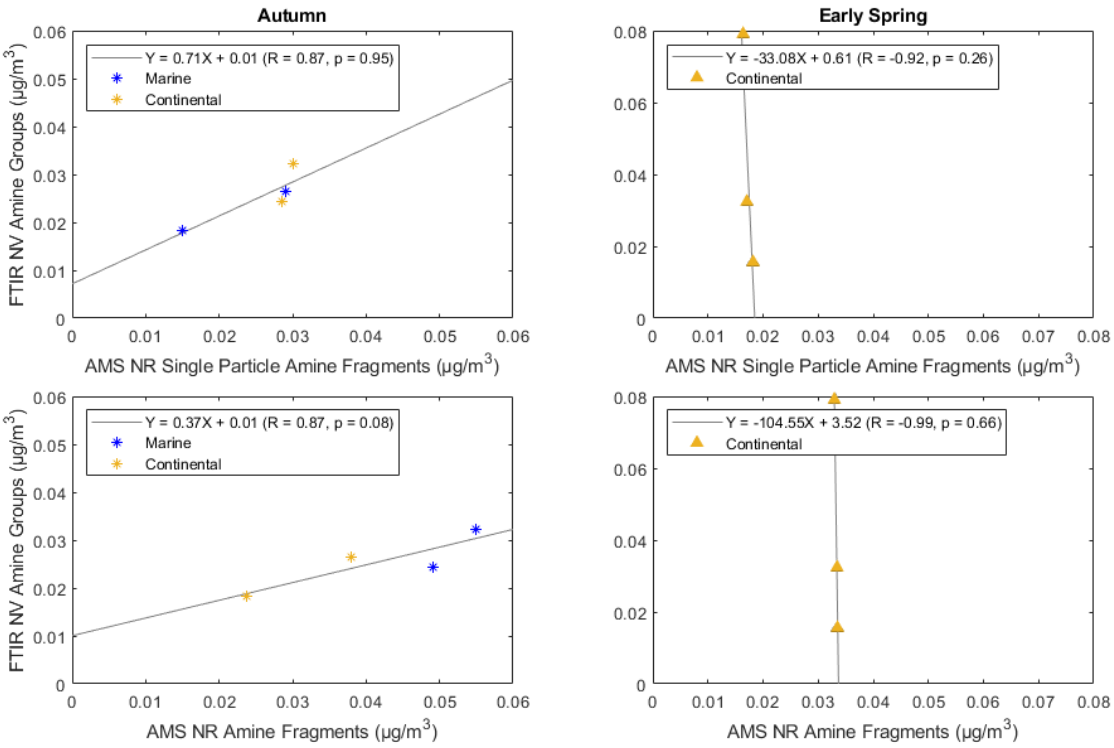

Figure 16: Scatter plot of FTIR (ADL) NV amine groups in particles with diameters <1 µm versus (top row) AMS NR single particle amine fragments and (bottom row) AMS NR amine fragments during (left column) Autumn and (right column) Early Spring. Marker colors represent air mass type (b,c): blue: marine, yellow: continental. The solid grey lines are the lines of best fit obtained using an ordinary least squares regression. A two-tailed T test is used to estimate p-values.

The ten AMS NR single particle amine fragments with the highest mass concentrations were CHN^+, CH_4N^+, $C_2H_3N^+$, $C_2H_4N^+$, $CHNO^+$, $C_2H_5N^+$, $C_2H_6N^+$, C_4HN^+, $C_2H_5N_2O^+$, $C_3H_7NO^+$. The presence of m/z 73 ($C_2H_5N_2O^+$, $C_3H_7NO^+$) in a mass spectrum is indicative of biomass burning, yet the concentration of these fragments remained largely constant across all periods. This either suggests that these fragments may come from a non-continental source or that a continental influence is present even for marine air masses. Figure 17 shows the variability of these low-molecular-weight ion fragments across marine and continental periods in Autumn and Early Spring. The average mass was highest during continental periods in Autumn for CHN^+, CH_4N^+, $C_2H_3N^+$, $C_2H_4N^+$, $CHNO^+$, $C_2H_5N^+$, $C_2H_6N^+$, $C_2H_5N_2O^+$, and $C_3H_7NO^+$. For C_4HN^+, the highest mass concentration was recorded during marine periods in Autumn. The average mass

was lowest during marine periods in Autumn for CHN^+, $C_2H_4N^+$, $CHNO^+$, $C_2H_5N^+$, and $C_2H_6N^+$, during marine periods in Early Spring for $C_2H_3N^+$ and C_4HN^+, and during continental periods in Early Spring for CH_4N^+, $C_2H_5N_2O^+$, and $C_3H_7NO^+$.

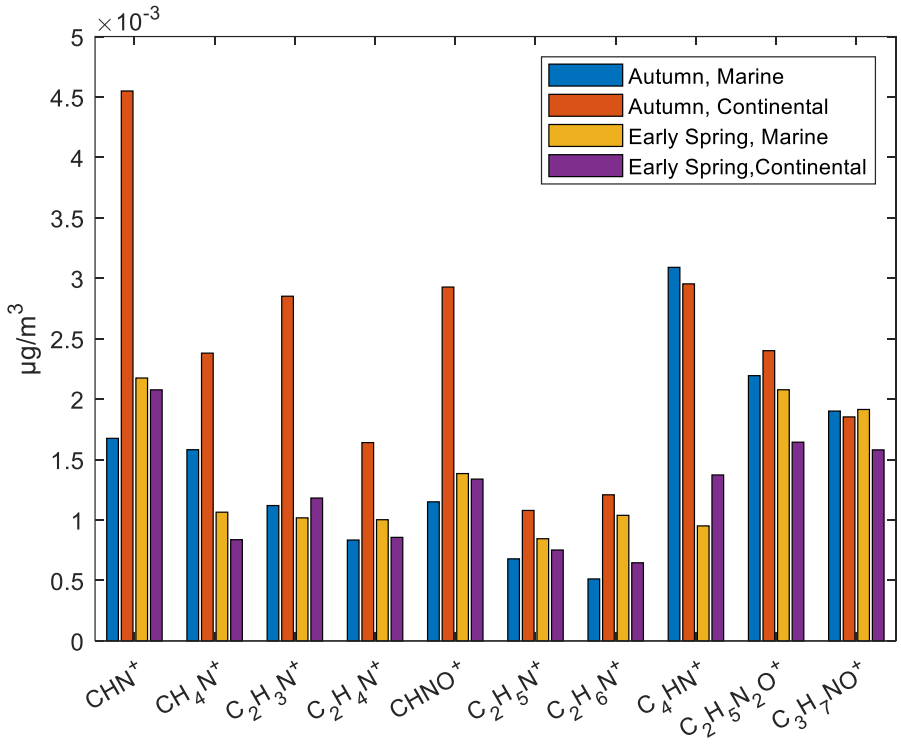

Figure 17: Bar graph of the 10 highest mass concentrations among AMS NR single particle amine fragments for marine air masses in Autumn (blue), continental air masses in Autumn (orange), marine air masses in Early Spring (yellow), and continental air masses in Early Spring (purple).

The average fraction of total ion signal that each AMS NR single particle amine fragment contributes to its respective m/z is given in Table 11. While some AMS NR single particle fragments accounted for a greater portion of the average mass concentration, additional non-AMS NR single particle amine fragments that were fitted to the same m/z had dominated the signal, leading to a smaller fraction of the signal being apportioned to AMS NR single particle amine fragments. In Autumn, the fractions of AMS NR single particle amine fragments during marine periods were greater than during continental periods. In Early Spring, 8 of the 29 AMS

NR single particle amine fragments accounted for a lower fraction of the ion signal in continental air masses than in marine air masses.

Table 11: Mean ion signal fractions and standard deviations of AMS NR single particle amine fragments for marine and continental air masses in Autumn and Early Spring.

		Autumn		Early Spring	
m/z	Ion Fragment	Marine	Continental	Marine	Continental
27	CHN^+	0.211 ± 0.064	0.160 ± 0.064	0.318 ± 0.156	0.238 ± 0.062
29	CH_3N^+	0.001 ± 0.001	0.001 ± 0.001	0.001 ± 0.001	0.001 ± 0.001
30	CH_4N^+	0.099 ± 0.088	0.074 ± 0.032	0.084 ± 0.042	0.039 ± 0.008
41	$C_2H_3N^+$	0.123 ± 0.033	0.097 ± 0.036	0.194 ± 0.076	0.196 ± 0.061
42	$C_2H_4N^+$	0.104 ± 0.049	0.076 ± 0.040	0.168 ± 0.047	0.112 ± 0.044
43	$CHNO^+$ $C_2H_5N^+$	0.090 ± 0.023 0.052 ± 0.020	0.062 ± 0.027 0.029 ± 0.017	0.139 ± 0.042 0.108 ± 0.028	0.106 ± 0.053 0.057 ± 0.021
44	$C_2H_6N^+$	0.004 ± 0.003	0.003 ± 0.001	0.008 ± 0.006	0.004 ± 0.001
58	$C_2H_4NO^+$ $C_3H_8N^+$	0.204 ± 0.042 0.110 ± 0.037	0.149 ± 0.057 0.072 ± 0.031	0.199 ± 0.041 0.136 ± 0.047	0.174 ± 0.037 0.107 ± 0.037
59	$C_2H_5NO^+$ $C_3H_9N^+$	0.126 ± 0.020 0.051 ± 0.018	0.112 ± 0.035 0.040 ± 0.018	0.118 ± 0.062 0.064 ± 0.030	0.109 ± 0.045 0.060 ± 0.019
63	C_4HN^+	0.405 ± 0.030	0.321 ± 0.097	0.217 ± 0.071	0.334 ± 0.067
72	$C_3H_6NO^+$ $C_4H_{10}N^+$	0.083 ± 0.020 0.040 ± 0.010	0.081 ± 0.019 0.034 ± 0.015	0.149 ± 0.129 0.078 ± 0.030	0.102 ± 0.038 0.062 ± 0.019
73	$C_2H_3NO_2^+$ $C_2H_5N_2O^+$ $C_3H_7NO^+$ $C_4H_{11}N^+$	0.050 ± 0.018 0.186 ± 0.042 0.160 ± 0.030 0.042 ± 0.022	0.066 ± 0.028 0.173 ± 0.051 0.141 ± 0.041 0.032 ± 0.017	0.171 ± 0.373 0.157 ± 0.049 0.152 ± 0.066 0.046 ± 0.029	0.050 ± 0.024 0.176 ± 0.063 0.164 ± 0.053 0.038 ± 0.013
84	$C_4H_6NO^+$ $C_5H_{10}N^+$	0.101 ± 0.022 0.096 ± 0.021	0.086 ± 0.025 0.080 ± 0.040	0.079 ± 0.033 0.132 ± 0.106	0.083 ± 0.023 0.116 ± 0.057
85	$C_4H_7NO^+$ $C_5H_{11}N^+$	0.146 ± 0.056 0.086 ±0.022	0.092 ± 0.050 0.059 ± 0.029	0.108 ± 0.043 0.118 ± 0.037	0.119 ± 0.045 0.099 ± 0.031
86	$C_4H_8NO^+$ $C_5H_{12}N^+$	0.105 ± 0.155 0.088 ± 0.033	0.061 ± 0.021 0.054 ± 0.026	0.108 ± 0.034 0.084 ± 0.029	0.111 ± 0.036 0.084 ± 0.024
100	$C_4H_8N_2O^+$ $C_5H_{10}NO^+$ $C_6H_{14}N^+$	0.075 ± 0.022 0.038 ± 0.016 0.061 ± 0.023	0.037 ± 0.019 0.034 ± 0.030 0.046 ± 0.027	0.032 ± 0.016 0.035 ± 0.023 0.082 ± 0.044	0.038 ± 0.015 0.034 ± 0.025 0.067 ± 0.063
101	$C_6H_{15}N^+$	0.066 ± 0.024	0.027 ± 0.021	0.092 ± 0.027	0.058 ± 0.026

6.3. ET Single Particle Analysis

The event trigger (ET) mode of the HR-ToF-AMS used three regions of interest (ROI) corresponding to a range of m/z to identify a single particle event and extract a mass spectrum. These regions were set to m/z 43 (ROI1) with an event trigger level of 3.5 ions/extraction, m/z

55–79 (ROI2) with an event trigger level of 8 ions/extraction, and m/z 48-150 (ROI3) with an event trigger level of 9 ions/extraction. ROI1 could be triggered by rBC- and organic-containing particles hydrocarbon while ROI2 and ROI3 was set to identify aerosol components including nitrate, sulfate and organic. The single particle measurements were initially pre-processed using Tofware version 2.5.10 to generate input data for Cluster Input Preparation Panel (CIPP) version 2.1b which is used to identify real particles. Cluster Analysis Panel (CAP) version 2.1a (developed by Alex Lee and Megan Willis) then uses a k-means clustering algorithm to compute an initial 10 clusters containing particles with similar spectra [85, 86].

Temporal correlations and cosine similarity for different solutions of the single particle k-means clustering analysis were determined. The number of clusters for each solution was chosen using a threshold of 10% for the average fraction of total particles for each cluster. Tables 12-13 summarizes the 2 to 10 cluster solutions and criteria of single particle analysis. A 5-cluster solution was selected for Autumn and Early Spring marine periods, a 6-cluster solution was selected for the Autumn continental period, and a 7-cluster solution was selected for the Early Spring continental period.

Table 12: Summary of criteria used for cluster analysis of single particle ET measurements taken in Autumn. Paired clusters that do not have uncentered correlation coefficients (UC) higher than 0.8 are indicated by None.

Criteria \ Cluster number (p)		2	3	4	5	6	7	8	9	10
Marine	Temporal correlation clusters strength (R > 0.8)	None	1 pair	2 pairs	4 pairs	7 pairs	11 pairs	10 pairs	12 pairs	16 pairs
	Similarity of cluster spectra (R > 0.8)	None	1 pair	2 pairs	4 pairs	7 pairs	11 pairs	10 pairs	12 pairs	15 pairs
	Clusters with less than 10% total count	None	None	None	None	2 clusters	3 clusters	4 clusters	4 clusters	6 clusters
Continental	Temporal correlation clusters strength (R > 0.8)	None	1 pair	1 pair	3 pairs	5 pairs	8 pairs	9 pairs	10 pairs	15 pairs
	Similarity of cluster spectra (R > 0.8)	None	1 pair	2 pairs	3 pairs	5 pairs	9 pairs	9 pairs	10 pairs	15 pairs
	Clusters with less than 10% total count	None	None	None	None	None	4 clusters	5 clusters	5 clusters	7 clusters

Table 13: Summary of criteria used for cluster analysis of single particle ET measurements taken in Autumn. Paired clusters that do not have uncentered correlation coefficients (UC) higher than 0.8 are indicated by None.

Criteria \ Cluster number (p)		2	3	4	5	6	7	8	9	10
Marine	Temporal correlation clusters strength (R > 0.8)	1 pair	2 pairs	4 pairs	4 pairs	8 pairs	7 pairs	12 pairs	14 pairs	20 pairs
	Similarity of cluster spectra (R > 0.8)	1 pair	2 pairs	4 pairs	4 pairs	8 pairs	7 pairs	12 pairs	14 pairs	20 pairs
	Clusters with less than 10% of total count	None	None	None	None	1 cluster	1 cluster	2 clusters	8 clusters	9 clusters
Continental	Temporal correlation clusters strength (R > 0.8)	1 pair	3 pairs	3 pairs	4 pairs	7 pairs	9 pairs	16 pairs	18 pairs	20 pairs
	Similarity of cluster spectra (R > 0.8)	1 pair	3 pairs	3 pairs	4 pairs	8 pairs	9 pairs	16 pairs	18 pairs	21 pairs
	Clusters with less than 10% of total count	None	None	None	None	None	None	1 cluster	3 clusters	3 clusters

Each cluster was categorized as oxidized organic aerosol (OOA), hydrocarbon-like organic aerosol (HOA), partially sulfate (PS), or mostly sulfate (MS) particle types. Clusters were considered organic (OOA, HOA) when 70% or more of the ion signal was organic (fORG > 70%). Organic clusters were further categorized as HOA when the highest ion signal was observed at m/z 43 ($C_3H_7^+$) and as OOA when highest ion signal was observed at m/z 44 (CO_2^+). The HOA cluster also required a larger fraction (>10%) of the ion signal from the sum of peaks in the alkane series $C_xH_{2y-1}^+$ and $C_xH_{2y+1}^+$, namely m/z 41 ($C_3H_5^+$), m/z 55 ($C_4H_7^+$), and m/z 57 ($C_4H_9^+$), than the OOA particle type (<10%). The peak at m/z 43 was not considered in this calculation since m/z 43 in OOA's mass spectrum is likely from $C_2H_3O^+$ rather than $C_3H_7^+$. Clusters were considered sulfate (PS, MS) when 40% or more of the ion signal was sulfate (fSO_4

> 40%). The MS particle type additionally required 65% of the ion signal to be sulfate ($fSO_4 \geq$ 65%). The mass spectra of PS particle type also met the criteria of attributing 30% or more of the ion signal to organics (fORG > 30%).

For each period, MS and PS clusters were further combined into a single MS cluster and a single PS cluster. One OOA cluster was resolved for all periods except during continental periods in Autumn when there were two OOA clusters (OOA-I, OOA-II). A single HOA cluster was resolved for continental air masses in Autumn. The mass spectra and time series of each particle type are found in Figures 18-22. The normalized UMR mass spectrum is used to find the signal from AMS NR single particle amine fragments by summing the product of the total ion signal fraction of each m/z in the spectrum and the average fraction of AMS NR single particle amine fragments attributed to the same m/z (estimated in Table 11). These results, along with a summary of the single particle measurements and particle types, are found in Table 14.

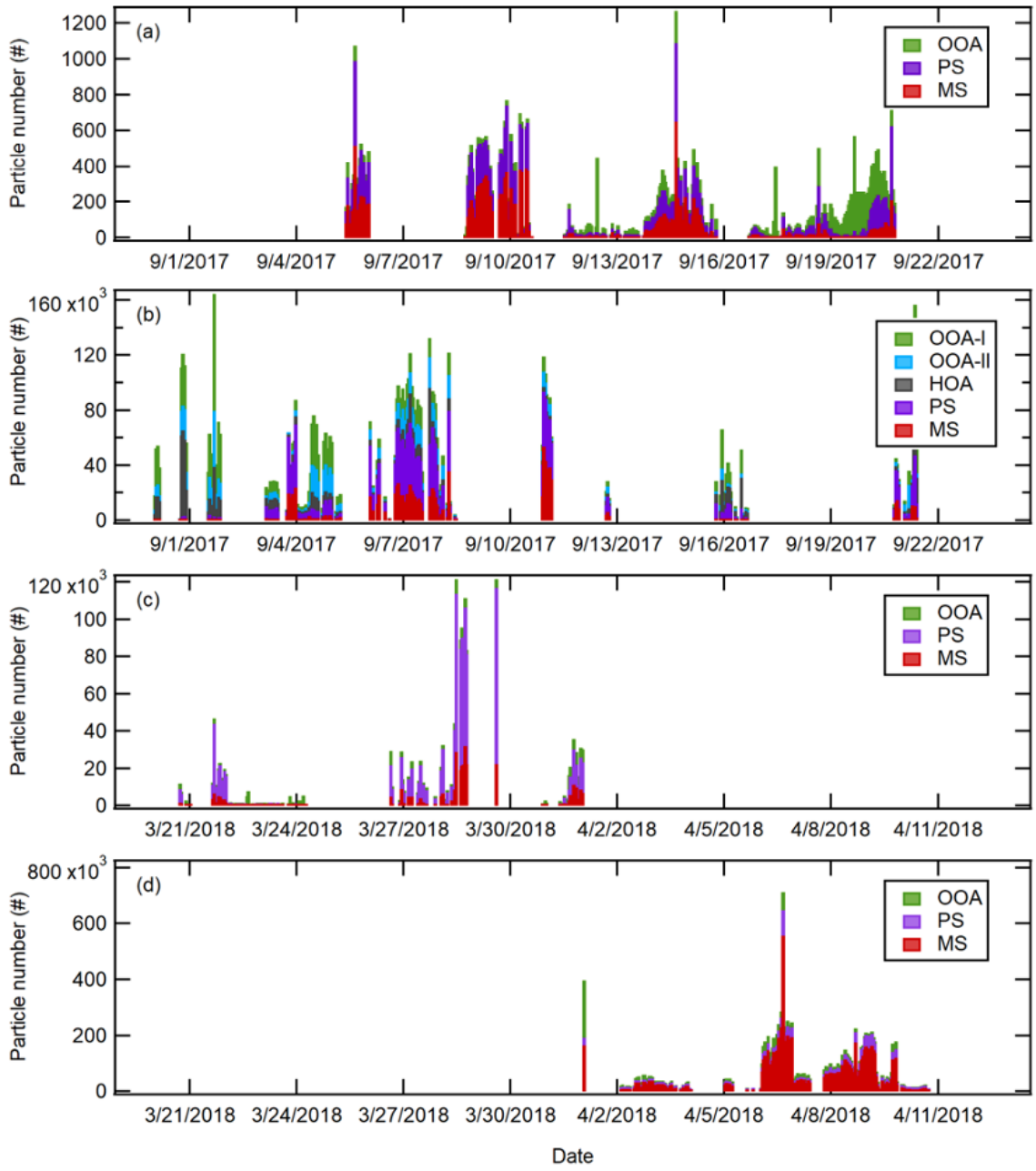

Figure 18: Time series of single particle clusters resolved from the ET mode for (a) marine air masses in Autumn, (b) continental air masses in Autumn, (c) marine air masses in Early Spring, and (d) continental air masses in Early Spring.

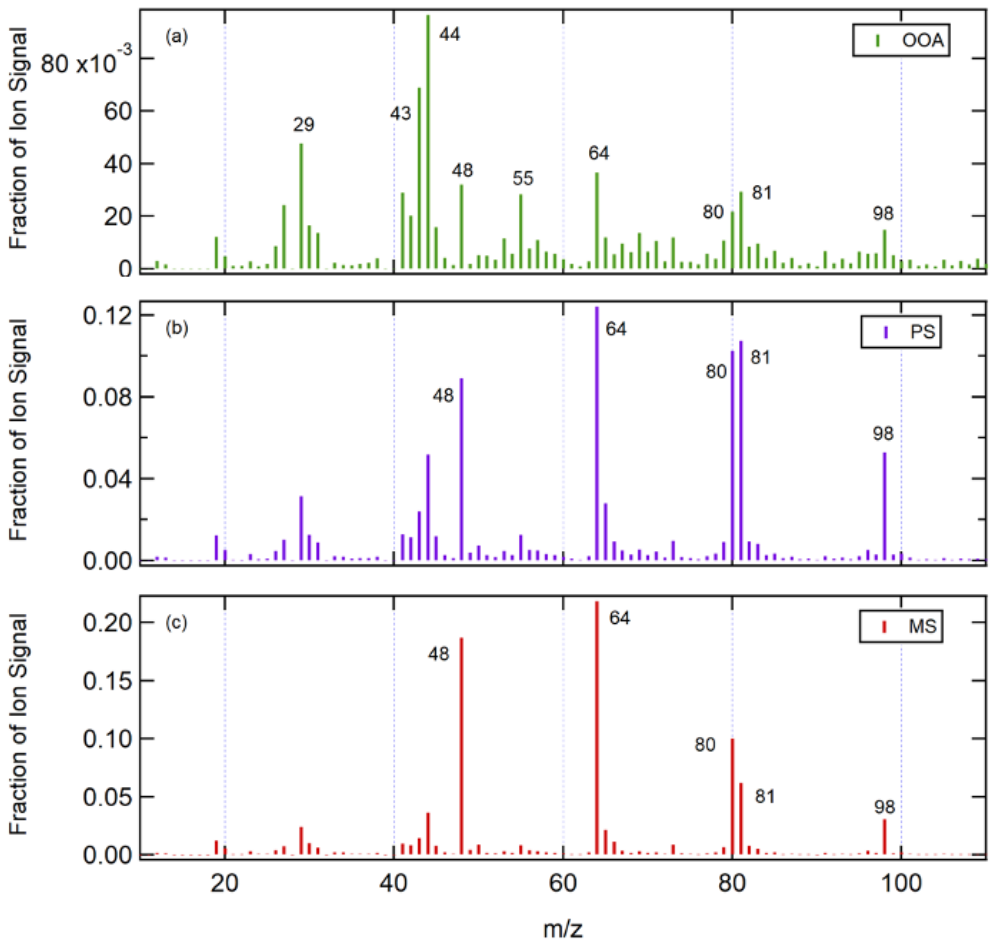

Figure 19: Mass spectra of single particle clusters resolved from the ET mode for marine air masses in Autumn. The particle types shown include (a) OOA, (b) PS, and (c) MS.

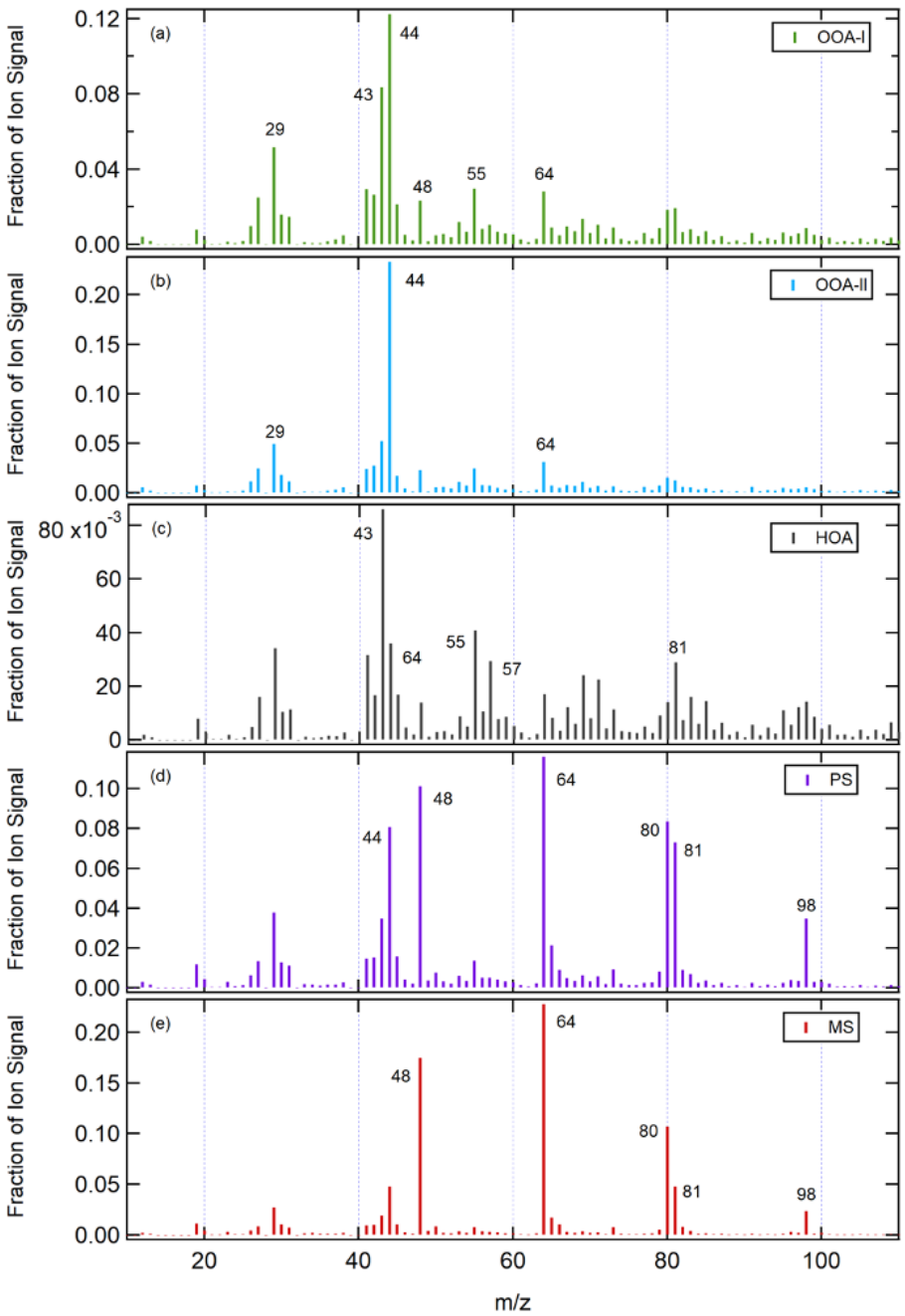

Figure 20: Mass spectra of single particle clusters resolved from the ET mode for continental air masses in Autumn. The particle types shown include (a) OOA-I, (b) OOA-II, (c) HOA, (d) PS, and (e) MS.

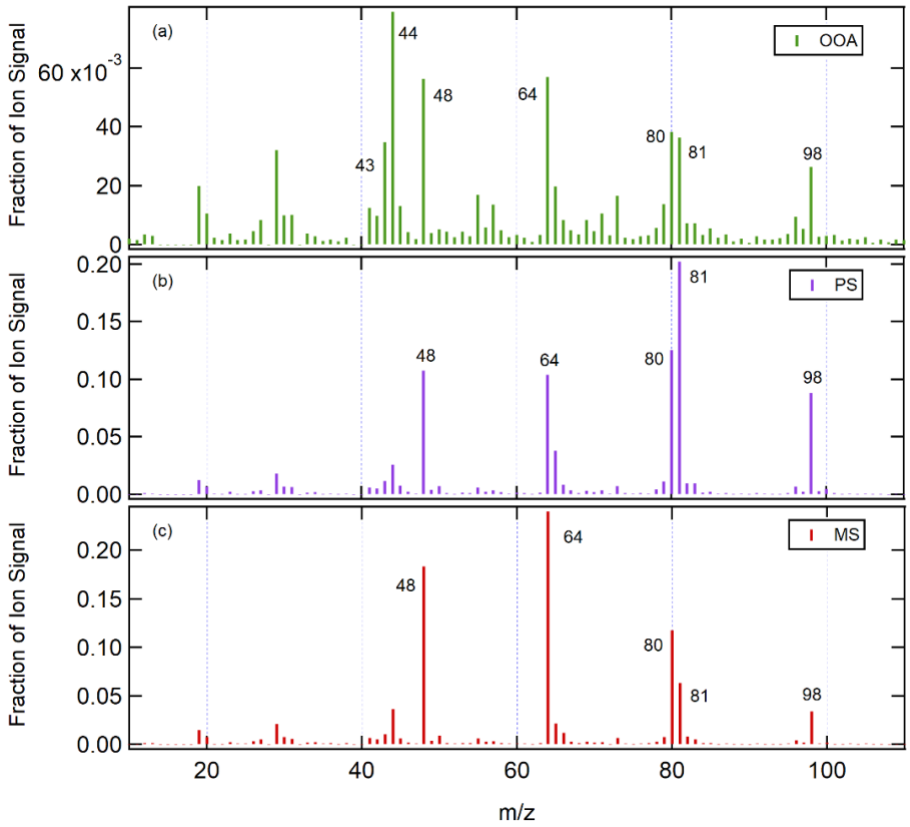

Figure 21: Mass spectra of single particle clusters resolved from the ET mode for marine air masses in Early Spring. The particle types shown include (a) OOA, (b) PS, and (c) MS.

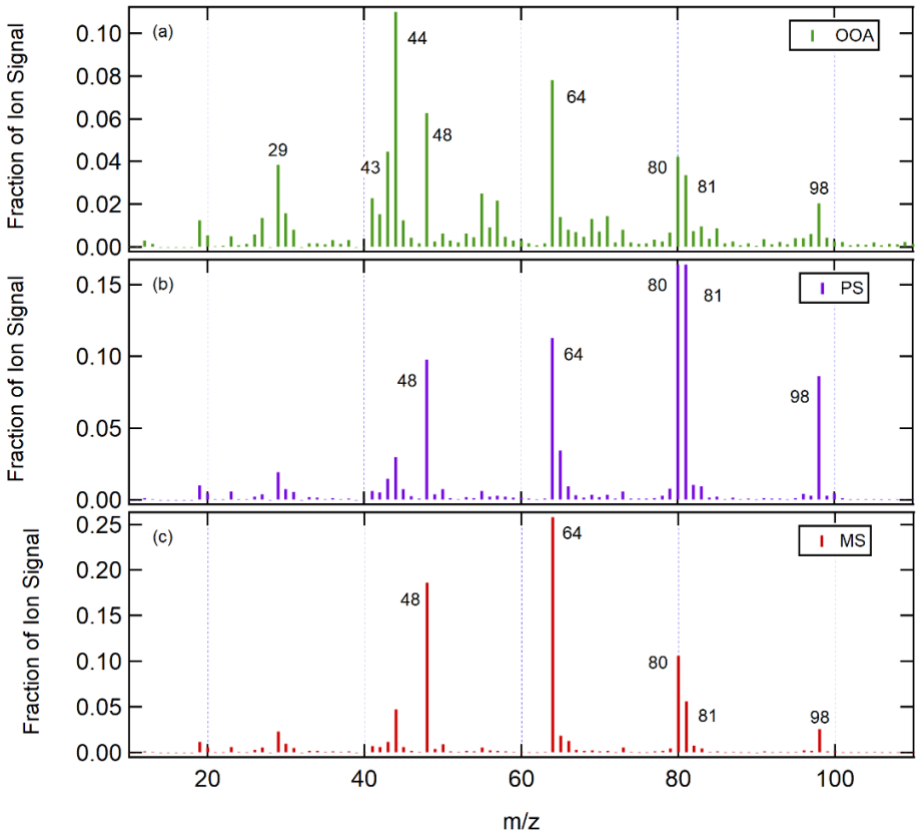

Figure 22: Mass spectra of single particle clusters resolved from the ET mode for continental air masses in Early Spring. The particle types shown include (a) OOA, (b) PS, and (c) MS.

Table 14: Summary of single particle measurements and aerosol types and identified by ET mode for marine and continental air masses in Autumn and Early Spring.

Statistic \ Particle Type		OOA	OOA-I	OOA-II	HOA	PS	MS
Marine Autumn	Particle count	15121	--	--	--	17849	19715
	Fraction of total particle count	28.7%	--	--	--	33.9%	37.4%
	Signal from AMS NR single particle amine fragments relative to the total ion signal	3.6%	--	--	--	1.9%	1.4%
	Signal from AMS NR single particle amine fragments relative to the total organic ion signal	4.6%	--	--	--	4.4%	7.5%
Marine Early Spring	Particle count	1098	--	--	--	1934	6489
	Fraction of total particle count	11.5%	--	--	--	20.3%	68.2%
	Signal from AMS NR single particle amine fragments relative to the total ion signal	3.2%	--	--	--	1.4%	1.3%
	Signal from AMS NR single particle amine fragments relative to the total organic ion signal	3.8%	--	--	--	3.7%	8.1%
Continental Autumn	Particle count	--	8522	5525	5448	10390	5709
	Fraction of total particle count	--	23.9%	15.5%	15.3%	29.2%	16.0%
	Signal from AMS NR single particle amine fragments relative to the total ion signal	--	2.8%	2.3%	2.9%	1.7%	1.1%
	Signal from AMS NR single particle amine fragments relative to the total organic ion signal	--	3.3%	2.7%	3.2%	3.8%	5.9%
Continental Early Spring	Particle count	8412	--	--	--	7851	40771
	Fraction of total particle count	14.7%	--	--	--	13.7%	71.5%
	Signal from AMS NR single particle amine fragments relative to the total ion signal	2.8%	--	--	--	1.1%	1.0%
	Signal from AMS NR single particle amine fragments relative to the total organic signal	3.9%	--	--	--	3.4%	7.1%

The mass spectra of the OOA particle type shows prominent peaks at m/z 29 (CHO^+), m/z 43 ($C_2H_3O^+$), and m/z 44 (CO_2^+). During continental Autumn periods, when two separate OOA clusters were resolved, the sum of these oxidized organic peaks was greater in the mass spectrum of OOA-II than that of OOA-I, indicating different magnitudes of particle aging. In Early Spring, OOA particles contained larger contributions from sulfate fragments identified from peaks at m/z 48 (SO^+), m/z 64 ($SO2^+$), m/z 80 (SO_3^+), m/z 81 (HSO_3^+), m/z 96 (SO_4^+), and m/z 98 ($H_2SO_4^+$). These sulfate peaks were most prominent in the mass spectrum of the OOA particle type during the continental periods in Early Spring. Additionally, the OOA particle type was more abundant relative to other particle types within continental air masses in Autumn. OOA particles made up a greater fraction of the total particle count during continental periods than during marine periods. The signal attributed to AMS NR single particle amine fragments for the OOA particle type was greater when air masses were marine. Specifically, the AMS NR single particle amine fragment fraction of the OOA mass spectrum's ion signal was 3.6% and 3.2% for marine periods and 2.3-2.8% and 2.8% for continental periods during Autumn and Early Spring, respectively. The OOA particle type had the largest contributions from AMS NR single particle amine fragments among all particle types except during continental periods in Autumn.

The HOA particle type contained substantial contributions from m/z 29 (CHO^+), m/z 43 (C_3H_7), and m/z 44 (CO_2^+) as well as m/z 55 ($C_4H_7^+$) and m/z 57 ($C_4H_9^+$) within its mass spectrum. Unlike the OOA particle type, the peaks at m/z 43 and m/z 55 are larger than the peak at m/z 44. The highest contribution from AMS NR single particle amine fragments observed in continental air masses during Autumn was for the HOA particle type with AMS NR single

particle amine fragments accounting for 2.9% of the total ion signal. However, the HOA particle type made up only 15.3% of the total particle count during this period.

The MS particle type contained large peaks at m/z 48 (SO^+), m/z 64 ($SO2^+$), m/z 80 (SO_3^+), m/z 81 (HSO_3^+), m/z 96 (SO_4^+), and m/z 98 ($H_2SO_4^+$) within its mass spectra. This particle type had the smallest contributions from AMS NR single particle amine fragments (1.0-1.4% of the ion signal) but was the most abundant across all air masses except for continental Autumn air masses. The mass spectrum of the PS particle type contained both sulfate (m/z 48, m/z 64, m/z 80, m/z 81, and m/z 96) and organic (m/z 29, m/z 43, m/z 44) contributions. In Early Spring, the oxidized organic peaks were less significant in the MS mass spectra than in Autumn. The signal apportioned to AMS NR single particle amine fragments for the PS particle type ranged from 1.1-1.9% of the total ion signal.

Correlations of particle types with various tracers are shown in Tables 15-18. The organic (OOA & HOA) particle types had a moderate to strong correlation ($0.50 < R < 0.80$) to the LVOOA factor that was resolved in Autumn. Similarly, the sulfate (PS & MS) particle types had a weak to strong correlation ($0.68 < R < 0.86$) to the Sulfate factor for both air masses and seasons. This correlation was weakest for marine air masses in Early Spring and strongest for marine air masses in Autumn. No particle type had correlated with the Amine factor during any period.

Table 15: Pearson correlation (R) coefficient values between ET single particle types and other measured properties for marine air masses in Autumn. Negative correlations are shaded blue and positive correlations are shaded red. The strength of each correlation determines the level of saturation for the corresponding shading- no correlation ($|R| < 0.25$)- gray, weak correlation ($0.25 \leq |R| < 0.50$)- light blue/red, moderate correlation ($0.50 \leq |R| < 0.80$)- medium blue/red, strong correlation ($0.80 \leq |R|$)- dark blue/red. All correlations shown are statistically significant ($p < 0.05$).

Particle Type / Tracer	OOA	PS	MS
LVOOA Factor	0.80	-0.09	-0.29
Sulfate Factor	-0.09	0.83	0.86
Amine Factor	-0.17	0.03	0.10
CCN/CN	-0.06	0.25	0.24
CCN Count	-0.18	0.08	0.04
atm. DMS	-0.10	0.38	0.32
sw. DMS	0.16	-0.14	-0.19
AMS NR OM	0.75	0.31	0.13
AMS NR Nitrate	0.38	0.16	0.05
AMS NR Sulfate	-0.07	0.83	0.85
AMS NR Ammonium	-0.04	0.37	0.45
AMS NR Chloride	-0.14	-0.09	-0.05
IC SO_4^{2-}	0.12	0.85	0.88
IC NO_3^-	0.84	0.22	0.22
IC NH_4^+	0.00	0.95	0.95
IC Na^+	0.63	-0.01	0.03
IC MSA	0.64	0.41	0.49
IC Mg^{2+}	0.65	-0.02	0.02
IC K^+	0.37	0.14	0.19
IC Cl^-	0.60	-0.12	-0.08
IC Ca^{2+}	0.67	-0.20	-0.16
IC Br^-	-0.18	-0.15	-0.24
IC Sea salt	0.62	-0.06	-0.02
Chlorophyll *a*	-0.23	-0.27	-0.17
Ozone	0.02	-0.47	-0.54
Radon	0.18	-0.37	-0.36
Sea Surface Temperature	-0.12	0.45	0.45
Photosynthetically Activated Radiation	0.13	-0.10	-0.11
Relative Humidity	-0.21	0.42	0.46
Wind Speed	0.09	-0.24	-0.37
Atmospheric Temperature	0.01	0.14	0.13

Table 16: Pearson correlation (R) coefficient values between ET single particle types and other measured properties for continental air masses in Autumn. Negative correlations are shaded blue and positive correlations are shaded red. The strength of each correlation determines the level of saturation for the corresponding shading- no correlation ($|R| < 0.25$)- gray, weak correlation ($0.25 \leq |R| < 0.50$)- light blue/red, moderate correlation ($0.50 \leq |R| < 0.80$)- medium blue/red, strong correlation ($0.80 \leq |R|$)- dark blue/red. All correlations shown are statistically significant ($p < 0.05$).

Tracer \ Particle Type	OOA-I	OOA-II	HOA	PS	MS
LVOOA Factor	0.69	0.50	0.61	-0.33	-0.31
Sulfate Factor	-0.08	0.29	-0.16	0.69	0.68
CCN Measurements	--	--	--	--	--
atm. DMS	-0.07	-0.35	-0.06	-0.46	-0.22
sw. DMS	-0.03	-0.16	-0.03	-0.16	-0.08
AMS NR OM	0.68	0.57	0.64	-0.24	-0.23
AMS NR Nitrate	0.58	0.38	0.69	-0.26	-0.24
AMS NR Sulfate	0.17	0.46	0.07	0.56	0.57
AMS NR Ammonium	0.49	0.64	0.32	0.24	0.21
AMS NR Chloride	-0.07	-0.04	-0.03	-0.04	-0.01
IC SO_4^{2-}	-0.18	0.61	-0.20	0.81	0.81*
IC NO_3^-	0.14	0.27	0.66	0.11	0.10*
IC NH_4^+	-0.21	0.56	-0.31	0.83	0.83*
IC Na^+	0.17	-0.65	0.51	-0.71	-0.71*
IC MSA	-0.65	-0.27	0.11	0.30	0.30*
IC Mg^{2+}	0.35	-0.48	0.65	-0.81	-0.81*
IC K^+	0.97	0.62	0.60	-0.60	-0.61*
IC Cl^-	-0.18	-0.87	0.21	-0.57	-0.57*
IC Ca^{2+}	0.48	-0.20	0.87	-0.79	-0.80*
IC Br^-	--	--	--	--	--
IC Sea salt	0.01	-0.78	0.39	-0.68	-0.68
Chlorophyll *a*	0.13	-0.25	0.29	-0.32	-0.34
Ozone	0.24	0.44	-0.09	0.07	-0.01
Radon	0.49	0.44	0.36	0.11	-0.03
Sea Surface Temperature	0.27	0.34	0.11	-0.05	-0.05
Photosynthetically Activated Radiation	0.18	0.16	0.35	-0.22	-0.20
Relative Humidity	-0.25	-0.16	-0.16	0.49	0.46
Wind Speed	0.07	0.05	0.05	0.03	0.00
Atmospheric Temperature	-0.07	-0.27	-0.04	-0.29	-0.15

Table 17: Pearson correlation (R) coefficient values between ET single particle types and other measured properties for marine air masses in Early Spring. Negative correlations are shaded blue and positive correlations are shaded red. The strength of each correlation determines the level of saturation for the corresponding shading- no correlation ($|R| < 0.25$)- gray, weak correlation ($0.25 \leq |R| < 0.50$)- light blue/red, moderate correlation ($0.50 \leq |R| < 0.80$)- medium blue/red, strong correlation ($0.80 \leq |R|$)- dark blue/red. All correlations shown are statistically significant ($p < 0.05$).

Particle Type / Tracer	OOA	PS	MS
Sulfate Factor	-0.20	0.29	0.28
Amine Factor	0.18	-0.05	-0.01
CCN Measurements	--	--	--
atm. DMS	-0.26	0.03	-0.04
sw. DMS	-0.04	0.41	0.38
AMS NR OM	-0.03	-0.05	-0.05
AMS NR Nitrate	0.52	0.18	0.28
AMS NR Sulfate	-0.19	0.29	0.28
AMS NR Ammonium	-0.24	0.13	0.04
AMS NR Chloride	0.37	0.28	0.29
IC Measurements	--	--	--
Chlorophyll *a*	-0.09	-0.03	0.01
Ozone	0.30	0.03	0.08
Radon	0.68	0.25	0.48
Sea Surface Temperature	-0.50	-0.25	-0.31
Photosynthetically Activated Radiation	0.29	0.39	0.36
Relative Humidity	-0.14	0.19	0.17
Wind Speed	0.04	-0.26	-0.24
Atmospheric Temperature	-0.38	-0.14	-0.19

Table 18: Pearson correlation (R) coefficient values between ET single particle types and other measured properties for marine air masses in Early Spring. Negative correlations are shaded blue and positive correlations are shaded red. The strength of each correlation determines the level of saturation for the corresponding shading- no correlation ($|R| < 0.25$)- gray, weak correlation ($0.25 \leq |R| < 0.50$)- light blue/red, moderate correlation ($0.50 \leq |R| < 0.80$)- medium blue/red, strong correlation ($0.80 \leq |R|$)- dark blue/red. All correlations shown are statistically significant ($p < 0.05$).

Tracer \ Particle Type	OOA	PS	MS
Sulfate Factor	0.14	0.69	0.79
Amine Factor	-0.05	-0.23	-0.17
CCN/CN	0.02	0.17	0.17
CCN Count	-0.07	0.09	0.10
atm. DMS	-0.42	-0.10	-0.16
sw. DMS	-0.25	-0.38	-0.35
AMS NR OM	0.16	-0.10	0.08
AMS NR Nitrate	0.07	-0.28	-0.19
AMS NR Sulfate	0.14	0.70	0.80
AMS NR Ammonium	0.18	0.15	0.38
AMS NR Chloride	-0.11	0.21	0.13
IC SO_4^{2-}	-0.31*	0.54	0.58
IC NO_3^-	-0.28*	-0.52	-0.48
IC NH_4^+	-0.30*	0.50	0.55
IC Na^+	-0.28*	0.26	0.25
IC MSA	0.34*	0.89	0.94
IC Mg^{2+}	-0.29*	0.33	0.32
IC K^+	-0.30*	0.52	0.55
IC Cl^-	-0.20*	0.12	0.09
IC Ca^{2+}	-0.40*	0.41	0.43
IC Br^-	--	--	--
IC Sea salt	-0.24	0.20	0.18
Chlorophyll *a*	-0.02	-0.01	-0.04
Ozone	0.20	-0.45	-0.23
Radon	0.02	-0.27	-0.27
Sea Surface Temperature	0.11	-0.36	-0.12
Photosynthetically Activated Radiation	0.02	0.10	0.16
Relative Humidity	-0.08	0.40	0.31
Wind Speed	0.04	0.29	0.26
Atmospheric Temperature	0.01	0.12	0.14

Non-refractory AMS species used to identify sources of single particle clusters included AMS NR OM, AMS NR nitrate, AMS NR sulfate, AMS NR ammonium, and AMS NR chloride. Moderate correlations ($0.57 < R < 0.75$) of organic particle types and AMS NR OM were observed during Autumn. However, no correlation was found during Early Spring. The PS cluster resolved for marine air masses in Autumn is the only other particle type to correlate weakly ($R = 0.38$) to AMS NR OM during both seasons. Weak to moderate correlations ($0.38 <$

R < 0.69) of the organic particle types to AMS NR nitrate were observed for all periods except during continental periods in Early Spring. The strongest correlation with AMS NR nitrate was with the HOA particle type, suggesting an anthropogenic source. A weak correlation was also observed for the MS particle type during continental periods in Early Spring. Weak to strong correlations (0.28 < R < 0.85) of the sulfate particle types to AMS NR sulfate were observed during both seasons and periods. This correlation was weakest during marine periods in Early Spring and strongest during continental periods in Autumn. Weak to moderate correlations (0.32 < R < 0.64) of all particle types and AMS NR ammonium were observed throughout different seasons and were largely inconsistent. No particle type had correlated with AMS NR chloride.

IC inorganic ions included SO_4^{2-}, NO_3^-, NH_4^+, Na^+, MSA, Mg^{2+} K^+, Cl^-, Ca^{2+}, Br^-. Correlations with IC inorganic ions were insignificant for OOA particle types during marine periods in Early Spring and for MS particle types during continental periods in Autumn. Limited marine air mass sampling resulted in too few marine IC filters to retrieve correlation coefficients for marine air masses in Early Spring. Sulfate particle types had moderate to strong correlations with IC SO_4^{2-} (0.54 < R < 0.88) and IC NH_4^+ (0.50 < R < 0.95), and weak to strong correlations (0.30 < R < 0.94) with IC MSA when IC measurements were available. Weak to strong (0.27 < R < 0.84) correlations of IC NO_3^- and organic particle types were seen in Autumn. No correlations of any particle types with IC Br^- were observed.

Additional source associated tracers included atmospheric and seawater DMS, chlorophyll *a*, ozone, and radon. No positive correlations were observed for atmospheric DMS and any of the identified particle types. Positive correlations (R = 0.38-0.41) of seawater DMS and sulfate particle types were seen for marine air masses in Early Spring. Negative correlations (-0.34 < R < -0.25) of chlorophyll *a* and the PS particle type during Autumn and the OOA-II and

MS particle types in continental air masses during Autumn were observed. The only positive correlation of chlorophyll *a* and a particle type was seen for the HOA particle type ($R = 0.29$). No particle type had correlated with chlorophyll *a* during Early Spring. A weak, positive correlation was observed for ozone and the OOA-I particle type during continental periods in Autumn and the OOA particle type in marine air masses during Early Spring. Alternatively, sulfate particle types in marine air masses in Autumn and continental air masses in Early Spring were shown to negatively correlate ($-0.54 < R < -0.45$) to ozone. Weak to moderate correlations ($0.32 < R < 0.68$) of radon and organic particle types during continental periods in Autumn and all particle types during marine periods in Early Spring were observed. However, the sulfate particle types had a negative correlation ($-0.37 < R < -0.27$) with radon within marine air masses in Autumn and continental air masses in Early Spring, indicating a local marine source.

Correlations of sea surface temperature (SST) did not display a consistent trend among particle types. Weak, positive correlations of photosynthetic activated radiation (PAR) and the HOA particle type ($R = 0.35$) and all particle types during marine periods in Early Spring ($0.29 < R < 0.39$) were found. Positive correlations ($0.31 < R < 0.49$) of sulfate particle types and relative humidity (RH) could indicate secondary organic aerosol formation in all periods except during marine periods in Early Spring. A weak, positive correlation ($0.26 < R < 0.29$) of wind speed and the sulfate particle types during continental Early Spring periods suggests a primary marine origin. Conversely, negative correlations are seen with the PS particle type during marine Early Spring periods, and the MS particle type during marine Autumn periods. No particle types had correlated with CCN number concentration but the PS particle type during marine periods in Autumn weakly correlated to CCN/CN ($R = 0.25$). No positive correlations with atmospheric temperature were observed. Only weak, negative correlations ($-0.38 < R < -0.27$) were seen for

the OOA-I and PS particle types during continental periods in Autumn and for the OOA particle type during marine periods in Early Spring.

6.4. Linear Regressions and p-values for AMS NR Amine Fragments and FTIR NV Amine Groups

Pearson correlation (R) coefficients retrieved for AMS NR amine fragments and FTIR NV amine groups during all four seasons and both air mass types are available in Table 2 and 3, respectively. The corresponding p-values for correlation coefficients pertaining to AMS NR amine fragments are shown in Table 19. Table 20 contains the p-values of correlations with FTIR NV amine groups. Correlations with black carbon and IC inorganic ions ($nssK^+$ and MSA) were typically statistically insignificant for both AMS NR amine fragments and FTIR NV amine groups. For FTIR NV Amine Groups, correlations with AMS NR chloride and AMS NR nitrate were also mostly insignificant. Linear regressions for AMS NR amine fragments and numerous tracers are displayed in Table 21. Table 22 contains the linear regressions for FTIR NV amine groups.

Table 19: p-values retrieved for correlations of AMS NR amine fragments and various tracers for marine periods (columns 1-4) and continental periods (columns 5-8). p-values that are greater than 0.05 are statistically insignificant and are shaded in red. p-values that are less than 0.05 are statistically significant and are shaded in green. A two-tailed T test is used to estimate p-values.

Air Masses	Marine				Continental			
Season	Winter	Early Spring	Late Spring	Autumn	Winter	Early Spring	Late Spring	Autumn
AMS NR OM	0.00	0.00	0.00	0.00	0.00	0.00	0.00	0.00
FTIR NV OM	0.00	0.25	0.02	0.04	0.00	0.14	0.08	0.40
AMS NR Nitrate	0.00	0.00	0.00	0.00	0.00	0.00	0.27	0.00
AMS NR Sulfate	0.00	0.00	0.00	0.00	0.00	0.00	0.00	0.00
AMS NR Chloride	0.00	0.00	0.00	0.00	0.00	0.00	0.00	0.00
AMS NR m/z 44	0.00	0.00	0.00	0.00	0.00	0.00	0.00	0.00
Black Carbon	0.06	0.45	0.16	0.00	0.00	0.00	0.00	0.00
Ozone	0.00	0.00	0.00	0.00	0.00	0.00	0.00	0.00
Radon	0.00	0.00	0.00	0.00	0.00	0.00	0.00	0.00
Wind Speed	0.00	0.00	0.00	0.00	0.00	0.00	0.00	0.00
sw. DMS	0.00	0.00	0.01	0.00	0.00	0.00	0.00	0.00
atm. DMS	0.00	0.00	0.01	0.00	0.00	0.00	0.00	0.00
Solar Radiation	0.00	0.00	0.00	0.00	0.00	0.00	0.00	0.00
Relative Humidity	0.00	0.00	0.00	0.00	0.00	0.00	0.00	0.00
Temperature	0.00	0.00	0.00	0.00	0.00	0.00	0.00	0.00
Chlorophyll *a*	0.00	0.00	0.00	0.00	0.00	0.00	0.00	0.00
SST	0.00	0.00	0.00	0.00	0.00	0.00	0.00	0.00
IC MSA	--	--	0.24	0.00	--	0.20	0.54	0.00
IC Sea Salt	0.00	--	0.05	0.00	0.03	0.00	0.61	0.17
IC nssK^+	0.05	--	0.00	0.00	0.65	0.02	0.02	0.01

Table 20: p-values retrieved for correlations of FTIR NV amine groups and various tracers for marine periods (columns 1-4) and continental periods (columns 5-8). p-values that are greater than 0.05 are statistically insignificant and are shaded in red. p-values that are less than 0.05 are statistically significant and are shaded in green. A two-tailed T test is used to estimate p-values.

Air Masses	Marine				Continental			
Season	Winter	Early Spring	Late Spring	Autumn	Winter	Early Spring	Late Spring	Autumn
AMS NR OM	0.00	--	0.00	0.00	0.00	0.00	0.03	--
FTIR NV OM	0.00	--	0.01	0.02	0.00	0.12	0.07	--
AMS NR Nitrate	0.33	--	0.30	0.98	0.18	0.93	0.32	--
AMS NR Sulfate	0.00	--	0.00	0.00	0.00	0.00	0.01	--
AMS NR Chloride	0.76	--	0.77	0.72	0.02	0.66	0.21	--
AMS NR m/z 44	0.00	--	0.00	0.00	0.00	0.00	0.00	--
Black Carbon	0.17	--	0.18	0.10	0.01	0.00	0.06	--
Ozone	0.00	--	0.00	0.00	0.00	0.00	0.00	--
Radon	0.00	--	0.00	0.00	0.00	0.00	0.00	--
Wind Speed	0.00	--	0.00	0.00	0.00	0.00	0.00	--
sw. DMS	0.00	--	0.01	0.00	0.00	0.00	--	--
atm. DMS	0.00	--	0.01	0.00	0.00	0.00	--	--
Solar Radiation	0.00	--	0.00	0.00	0.07	0.00	0.04	--
Relative Humidity	0.00	--	0.00	0.00	0.00	0.00	0.00	--
Temperature	0.00	--	0.00	0.00	0.00	0.00	0.00	--
Chlorophyll *a*	0.00	--	0.01	0.01	0.02	0.00	0.00	--
SST	0.00	--	0.00	0.00	0.00	0.00	0.00	--
IC MSA	--	--	0.09	0.36	--	0.36	0.15	--
IC Sea Salt	0.00	--	0.03	0.00	--	0.00	0.02	--
IC nssK^+	0.42	--	0.07	0.65	--	0.76	0.50	--

Table 21: Linear regressions (Y = mX + b) for various tracers versus AMS NR amine fragments for marine periods (columns 1-4) and continental periods (columns 5-8).

Air Masses	Marine				Continental			
Season	Winter	Early Spring	Late Spring	Autumn	Winter	Early Spring	Late Spring	Autumn
AMS NR OM	14X	4.8X + 0.1	28X	13X	31X	17X	34X	24X
FTIR NV OM	-21X	--	-2.4X + 0.3	19X	-17X + 1	39X -1	13X	--
AMS NR Nitrate	0.52X	-0.12X + 0.01	0.58X	0.08X + 0.01	1.1X	0.04X + 0.01	4.3X - 0.1	0.24X
AMS NR Sulfate	18X	26X	8.7X	5.0X + 0.1	22X	4.0X + 0.3	4.8X + 0.1	1.5X + 0.3
AMS NR Chloride	0.17X + 0.01	-0.04X + 0.01	-0.12X + 0.02	-0.04 + 0.01	0.16X + 0.01	-0.09X + 0.01	-0.08X + 0.02	-0.01X + 0.01
AMS NR m/z 44	3.5X	1.0X + 0.01	3.9X	2.2X + 0.1	6.5X	4.0X + 0.1	5.9X	4.6X + 0.1
Black Carbon	2.8X	-0.31X + 0.04	1.3X - 0.01	0.59X	12X	9.0X - 0.1	4.8X	3.7X
Ozone	91X + 40	-1568X + 84	-241X + 44	-142X + 33	-172X + 41	30X + 46	145X + 34	94X + 28
Radon	13811X + 60	-315X + 386	-1860X + 341	580X + 397	31344X + 34	7090X	10264X + 34	9747X
Wind Speed	-247X	-47X	-359X	14X	-0.43X	-174X	-28X	-28X
sw. DMS	15X + 1	-12X + 3	-34X + 4	3.7X + 3.2	7.1X + 1.3	27X + 4	-48X + 4	-7X + 3
atm. DMS	-1326X + 85	5945X -61	-6285X + 570	995X + 111	5049X + 14	-4689X + 226	-2971X + 331	2800X + 38
Solar Radiation	-891X + 65	163X + 3	3677X + 4	1656X + 3	-257X +1	7562X + 4	-902X + 4	1414X + 3
Relative Humidity	-2074X + 103	-2.5X + 78	-89X + 86	-46X + 83	174X + 74	-336X +79	28X + 77	-126X + 89
Temperature	-592X +18	572X + 2	-96X + 11	132X + 10	183X +9	132X +9	100X + 5	37X + 15
Chlorophyll *a*	-7.5X + 0.6	4.5X + 0.5	19X + 1	-12X + 1	16X	-3.9X + 0.7	-0.5X + 1.6	-2.0X + 0.4
SST	-265X + 17	465X + 6	-153X + 14	102X + 12	181X + 11	139X + 12	83X + 7	52X + 15
IC MSA	--	--	4.9X – 0.1	1.8X	--	13X	0.16X + 0.06	0X
IC Sea Salt	210X – 2	--	-44X + 1	60X – 1	-447X	20X + 1	-0.40X + 0.08	-0.47X + 0.48
IC nssK^+	3.3X	--	0.10X	0.33X	5.3X – 0.1	2.5X – 0.1	0.41X	0.35X -0.01

Table 22: Linear regressions (Y = mX + b) for various tracers versus FTIR NV amine groups for marine periods (columns 1-4) and continental periods (columns 5-8).

Air Masses	Marine				Continental			
Season	Winter	Early Spring	Late Spring	Autumn	Winter	Early Spring	Late Spring	Autumn
AMS NR OM	-0.36X + 0.20	--	2.0X + 0.4	-1.7X + 0.3	1.6X + 0.5	2.2X + 0.4	33X + 2	--
FTIR NV OM	8.9X + 0.2	--	10X	10X	4.6X + 0.2	11.4X	2.1X + 0.4	--
AMS NR Nitrate	-0.02X	--	0.04X	-0.04X	0X	-0.02X	-3.0X + 0.1	--
AMS NR Sulfate	-0.93X + 0.01	--	3.2X + 0.2	3.7X + 0.2	2.6X + 0.3	-3.0X + 0.5	-4.9X + 0.4	--
AMS NR Chloride	0.12X	--	0.70X	0X	0.10X	0.13X	-0.05X	--
AMS NR m/z 44	-0.10X + 0.06	--	-0.82X + 0.15	-0.66X + 0.15	0.18X + 0.11	0.76X + 0.18	-5.1X + 0.4	--
Black Carbon	-32X + 1	--	-1.1X + 0.1	0.18X + 0.02	2.5X + 0.04	0.15X + 0.19	-1.3X + 0.1	--
Ozone	41X + 41	--	57X + 37	-94X + 28	19X +33	47X + 48	71X + 40	--
Radon	-3698X + 304	--	993X + 277	-1904X + 446	-4413X + 855	-67X + 886	-3048X + 616	--
Wind Speed	-62X + 11	--	-37X + 10	14X + 10	54X + 12	70X + 10.6	1.1X + 6.1	--
sw. DMS	-6.0X + 1.2	--	97X + 0.62	-46X + 3	7.6X + 0.2	-5.6X + 1.5	--	--
atm. DMS	-405X + 79	--	21137X + 135	-1216X + 80	1532X + 47	-235X + 64	--	--
Solar Radiation	-1848X + 73	--	621X + 147	-2647X + 149	1745X + 1	105X + 181	-13163X + 642	--
Relative Humidity	-145X + 75	--	314X + 79	-12X + 82	-114X + 1	-104X + 69	-156X + 642	--
Temperature	-98X + 11	--	-216X + 12	103X + 13	16X + 9	-5.6X + 12	-21X + 10	--
Chlorophyll *a*	1.7X + 0.4	--	61X	-5.2X + 0.3	-15X + 2	0.45X + 0.50	-7.9X + 1.4	--
SST	-110X + 14	--	-252X + 14	143X + 14	-46X +16	13X + 15	2.9X + 10.7	--
IC MSA	--	--	4X	-0.13X	--	-0.95X + 0.07	-1.1X + 0.1	--
IC Sea Salt	10X + 1	--	8.4X + 0.3	14X	--	9.2X + 0.9	-0.60X + 0.10	--
IC $nssK^+$	0.08X	--	0X + 0.06	0.003X + 0.009	--	0.13X + 0.01	-0.09X + 0.01	--

6.5. CCN Activity

The extent to which amine affects CCN activity is explored by determining particle hygroscopicity using SMPS and CCNC measurements made during the Autumn and Early Spring seasons. A thermodenuder Scanning Mobility Particle Sizer (SMPS) system was used to measure the number of particles with geometric mean diameters between ~0.02 and 0.5 μm. Unheated samples produced measurements with a time resolution of 2 minutes (Quinn et al., 2019). Measurements from the SMPS system and a Cloud Condensation Nuclei Counter (CCNC, DMT, Boulder, CO) measuring ambient CCN concentrations at 0.1% supersaturation were used to determine aerosol hygroscopicity. CCN measurements were taken every 10 seconds. Data from these two instruments were synchronized into 2-minute averaged data for further analysis.

The critical diameter is found by summing the number of particles from the bin with the largest diameter down to the bin with the diameter by which the following equation is satisfied

$$\frac{N_{CCN}}{N_{CN}} = 1 \quad (1)$$

Hygroscopicity parameters (κ) are determined using SMPS and CCN counter data by the following equations

$$\kappa = \frac{4A^3}{27\, D_{crit}^3\, ln^2\, Sc} \quad (2)$$

$$A = \frac{\sigma_{s/a}\, M_w}{RT\rho_w} \quad (3)$$

where $\sigma_{s/a}$ is the surface tension of pure water (0.073 J m^{-2}), Sc is the ratio of supersaturation (for SS = 0.1%, $Sc = 1.01$), M_w is the molecular weight of water (18.016 g mol^{-1}), ρ_w is the density of water (1000 kg mol^{-1}), R is the universal gas constant (8.3145 J mol^{-1} K^{-1}), T is the ambient temperature (298.15 K) , and D_{crit} is the diameter by which 100% of particles have activated to CCN (Petters and Kreidenweis, 2007).

Measurements when CCN/CN >1 and when the CCN count was less than 100 cm^{-3} were excluded from the dataset. Table S19 contains a summary of the remaining measurements. The low duty cycle of ambient sampling coupled with low CCN concentrations resulted in only a finite number of κ estimates that limited further interpretation.

Table 23: Critical Diameters and Hygroscopicity Estimates.

Time	Cruise	Air Mass	CCN (cm^{-3})	CN (cm^{-3})	CCN/CN	D_{crit} (μm)	κ
09/09/2017 04:08	3	Marine	104	282	0.37	0.14	0.57
09/09/2017 04:16	3	Marine	109	289	0.38	0.13	0.63
09/09/2017 04:18	3	Marine	110	289	0.38	0.13	0.70
09/15/2017 01:58	3	Continental	171	342	0.50	0.11	1.21
09/15/2017 06:28	3	Continental	140	295	0.48	0.10	1.34
09/15/2017 06:34	3	Continental	132	291	0.45	0.04	22.14
09/15/2017 06:36	3	Continental	138	290	0.47	0.11	1.21
09/15/2017 06:38	3	Continental	135	291	0.46	0.11	1.21
03/23/2018 11:24	4	Marine	109	206	0.53	0.02	112.04
03/23/2018 11:26	4	Marine	109	204	0.54	0.12	0.78
03/23/2018 11:28	4	Marine	109	205	0.53	0.11	1.08
03/23/2018 11:34	4	Marine	108	203	0.53	0.03	42.45
03/23/2018 11:36	4	Marine	107	204	0.52	0.11	0.97
03/23/2018 11:38	4	Marine	111	204	0.54	0.10	1.34
04/01/2018 17:44	4	Continental	150	506	0.30	0.07	3.54
04/01/2018 17:46	4	Continental	188	507	0.37	0.10	1.50
04/01/2018 17:48	4	Continental	199	515	0.39	0.10	1.34
04/01/2018 22:14	4	Continental	157	478	0.33	0.07	3.96
04/01/2018 22:16	4	Continental	180	480	0.37	0.11	1.08
04/01/2018 22:18	4	Continental	209	474	0.44	0.10	1.50
04/01/2018 22:24	4	Continental	205	477	0.43	0.05	9.36
04/01/2018 22:26	4	Continental	195	480	0.41	0.10	1.50
04/01/2018 22:28	4	Continental	173	500	0.35	0.11	1.08
04/02/2018 02:54	4	Continental	167	567	0.29	0.07	3.54
04/02/2018 02:56	4	Continental	195	562	0.35	0.11	1.21
04/02/2018 02:58	4	Continental	191	544	0.35	0.11	1.21
04/02/2018 03:04	4	Continental	181	532	0.34	0.06	6.76
04/02/2018 03:06	4	Continental	185	534	0.35	0.11	1.21
04/02/2018 03:08	4	Continental	178	532	0.34	0.11	1.08
04/03/2018 00:08	4	Continental	180	585	0.31	0.07	3.96
04/03/2018 04:34	4	Continental	159	506	0.31	0.05	10.44
04/03/2018 04:36	4	Continental	158	505	0.31	0.12	0.78
04/03/2018 04:38	4	Continental	158	502	0.31	0.12	0.78
04/03/2018 04:44	4	Continental	152	502	0.30	0.05	11.61
04/03/2018 04:46	4	Continental	154	501	0.31	0.12	0.87
04/03/2018 04:48	4	Continental	150	498	0.30	0.13	0.70
04/03/2018 09:18	4	Continental	101	427	0.24	0.13	0.70
04/03/2018 09:28	4	Continental	100	458	0.22	0.13	0.70
04/05/2018 03:24	4	Continental	105	201	0.52	0.10	1.34

Table 24: Critical Diameters and Hygroscopicity Estimates, Continued.

Time	Cruise	Air Mass	CCN (cm^{-3})	CN (cm^{-3})	CCN/CN	D_{crit} (μm)	κ
04/05/2018 03:26	4	Continental	102	199	0.51	0.12	0.87
04/05/2018 03:28	4	Continental	101	202	0.50	0.10	1.50
04/07/2018 02:38	4	Continental	158	333	0.47	0.12	0.87
04/07/2018 02:44	4	Continental	165	336	0.49	0.11	1.08
04/07/2018 02:46	4	Continental	161	339	0.48	0.11	0.97
04/07/2018 02:48	4	Continental	163	340	0.48	0.11	1.08
04/07/2018 22:48	4	Continental	161	449	0.36	0.14	0.51
04/08/2018 03:18	4	Continental	208	423	0.49	0.11	0.97
04/08/2018 03:24	4	Continental	177	425	0.42	0.06	7.53
04/08/2018 03:26	4	Continental	221	425	0.52	0.11	1.21
04/08/2018 03:28	4	Continental	221	426	0.52	0.11	1.21
04/08/2018 07:58	4	Continental	156	285	0.55	0.09	2.07
04/08/2018 08:04	4	Continental	144	279	0.52	0.03	42.45
04/08/2018 08:06	4	Continental	150	279	0.54	0.10	1.50
04/08/2018 08:08	4	Continental	152	278	0.55	0.09	2.07
04/08/2018 12:36	4	Continental	114	282	0.41	0.11	1.21
04/08/2018 12:38	4	Continental	114	282	0.40	0.10	1.50
04/08/2018 12:44	4	Continental	111	282	0.39	0.03	38.04
04/08/2018 12:46	4	Continental	114	280	0.41	0.09	1.67
04/08/2018 12:48	4	Continental	115	281	0.41	0.10	1.50
04/09/2018 04:06	4	Continental	236	499	0.47	0.09	1.86
04/09/2018 04:08	4	Continental	241	502	0.48	0.09	1.86
04/09/2018 04:14	4	Continental	235	503	0.47	0.02	213.29
04/09/2018 04:16	4	Continental	255	517	0.49	0.09	2.30
04/09/2018 04:18	4	Continental	247	501	0.49	0.09	1.67
04/09/2018 16:34	4	Continental	203	687	0.29	0.11	1.08
04/09/2018 16:36	4	Continental	192	666	0.29	0.12	0.87
04/09/2018 16:38	4	Continental	192	666	0.29	0.05	14.47
04/10/2018 01:44	4	Continental	137	748	0.18	0.03	34.21
04/10/2018 01:46	4	Continental	157	744	0.21	0.08	2.57
04/10/2018 01:48	4	Continental	158	767	0.21	0.09	1.67
04/10/2018 01:54	4	Continental	163	752	0.22	0.02	101.25
04/10/2018 01:56	4	Continental	144	720	0.20	0.10	1.34
04/10/2018 01:58	4	Continental	137	697	0.20	0.10	1.50
04/10/2018 06:24	4	Continental	157	673	0.23	0.02	191.13
04/10/2018 06:26	4	Continental	136	678	0.20	0.11	1.21
04/10/2018 06:28	4	Continental	135	663	0.20	0.11	1.08
04/10/2018 06:34	4	Continental	156	696	0.22	0.02	112.04
04/10/2018 06:36	4	Continental	169	699	0.24	0.10	1.50
04/10/2018 06:38	4	Continental	156	714	0.22	0.11	1.21
04/10/2018 11:04	4	Continental	211	840	0.25	0.03	38.04
04/10/2018 11:06	4	Continental	215	841	0.26	0.11	1.08
04/10/2018 11:08	4	Continental	228	839	0.27	0.10	1.34
04/10/2018 11:14	4	Continental	250	885	0.28	0.02	191.13
04/10/2018 11:16	4	Continental	200	872	0.23	0.12	0.87
04/10/2018 11:18	4	Continental	217	863	0.25	0.11	1.21

6.6. Acknowledgements

The thesis, in part, is currently being prepared for submission for publication of the material. Berta, Veronica Z.; Russell, Lynn M., Price, Derek J.; Chen, Chia-Li; Lee, Alex K.Y.; Quinn, Patricia K.; Bates, Timothy S.; Bell, Thomas G.; Behrenfeld, Mike J. The thesis author was the primary researcher and author of this material.

REFERENCES

1. Tang XC, Price D, Praske E, Lee SA, Shattuck MA, Purvis-Roberts K, Silva PJ, Asa-Awuku A, Cocker DR. 2013. NO3 radical, OH radical and O-3-initiated secondary aerosol formation from aliphatic amines. *Atmospheric Environment*. 72:105-112. doi: 10.1016/j.atmosenv.2013.02.024.

2. Malloy QGJ, Qi L, Warren B, Cocker DR, Erupe ME, Silva PJ. 2009. Secondary organic aerosol formation from primary aliphatic amines with NO3 radical. *Atmospheric Chemistry and Physics*. 9(6):2051-2060. doi: 10.5194/acp-9-2051-2009.

3. Bork N, Elm J, Olenius T, Vehkamaki H. 2014. Methane sulfonic acid-enhanced formation of molecular clusters of sulfuric acid and dimethyl amine. *Atmospheric Chemistry and Physics*. 14(22):12023-12030. doi: 10.5194/acp-14-12023-2014.

4. Yao L, Garmash O, Bianchi F, Zheng J, Yan C, Kontkanen J, Junninen H, Mazon SB, Ehn M, Paasonen P, Sipila M, Wang MY, Wang XK, Xiao S, Chen HF, Lu YQ, Zhang BW, Wang DF, Fu QY, Geng FH, Li L, Wang HL, Qiao LP, Yang X, Chen JM, Kerminen VM, Petaja T, Worsnop DR, Kulmala M, Wang L. 2018. Atmospheric new particle formation from sulfuric acid and amines in a Chinese megacity. *Science*. 361(6399):278-+. doi: 10.1126/science.aao4839.

5. Tang X, Price D, Praske E, Vu DN, Purvis-Roberts K, Silva PJ, Cocker DR, Asa-Awuku A. 2014. Cloud condensation nuclei (CCN) activity of aliphatic amine secondary aerosol. *Atmospheric Chemistry and Physics*. 14(12):5959-5967. doi: 10.5194/acp-14-5959-2014.

6. Ge X, Wexler AS, Clegg SL. 2011. Atmospheric amines - Part I. A review. *Atmospheric Environment*. 45:524-546.

7. Lee C. 1988. Amino Acid and Amine Biogeochemistry in Marine Particulate Material and Sediments. *Nitrogen Cycling in Coastal Marine Environments*: Wiley.

8. King GM. 1985. DISTRIBUTION AND METABOLISM OF QUATERNARY AMINES IN SALT MARSHES. *Estuaries*. 8(2B):A6-A6.

9. Steiner M, Hartmann T. 1968. OCCURENCE AND DISTRIBUTION OF VOLATILE AMINES IN MARINE ALGAE. *Planta*. 79(2):113-&. doi: 10.1007/bf00390154.

10. Myriokefalitakis S, Vignati E, Tsigaridis K, Papadimas C, Sciare J, Mihalopoulos N, Facchini MC, Rinaldi M, Dentener FJ, Ceburnis D, Hatzianastasiou N, O'Dowd CD, van Weele M, Kanakidou M. 2010. Global Modeling of the Oceanic Source of Organic Aerosols. *Advances in Meteorology*. 2010. doi: 10.1155/2010/939171.

11. Frossard AA, Russell LM, Burrows SM, Elliott SM, Bates TS, Quinn PK. 2014. Sources and composition of submicron organic mass in marine aerosol particles. *Journal of Geophysical Research-Atmospheres*. 119(22):12977-13003. doi: 10.1002/2014jd021913.

12. Lewis S, Russell L, Saliba G, Quinn P, Bates T, Carlson C, Baetge N, Aluwihare L, Boss E, Frossard A, Bell T, Behrenfeld M. 2022. Characterization of Sea Surface Microlayer and Marine Aerosol Organic Composition Using STXM-NEXAFS Microscopy and FTIR Spectroscopy. *ACS Earth and Space Chemistry*. doi: 10.1021/acsearthspacechem.2c00119.

13. Russell LM, Bahadur R, Ziemann PJ. 2011. Identifying organic aerosol sources by comparing functional group composition in chamber and atmospheric particles. *Proceedings of the National Academy of Sciences of the United States of America*. 108(9):3516-3521. doi: 10.1073/pnas.1006461108.

14. Facchini MC, Decesari S, Rinaldi M, Carbone C, Finessi E, Mircea M, Fuzzi S, Moretti F, Tagliavini E, Ceburnis D, O'Dowd CD. 2008. Important Source of Marine Secondary Organic Aerosol from Biogenic Amines. *Environmental Science & Technology*. 42(24):9116-9121. doi: 10.1021/es8018385.

15. Muller C, Iinuma Y, Karstensen J, van Pinxteren D, Lehmann S, Gnauk T, Herrmann H. 2009. Seasonal variation of aliphatic amines in marine sub-micrometer particles at the Cape Verde islands. *Atmospheric Chemistry and Physics*. 9(24):9587-9597.

16. Hawkins LN, Russell LM, Covert DS, Quinn PK, Bates TS. 2010. Carboxylic acids, sulfates, and organosulfates in processed continental organic aerosol over the southeast Pacific Ocean during VOCALS-REx 2008. *Journal of Geophysical Research-Atmospheres*. 115:16. doi: 10.1029/2009jd013276.

17. Russell LM, Takahama S, Liu S, Hawkins LN, Covert DS, Quinn PK, Bates TS. 2009. Oxygenated fraction and mass of organic aerosol from direct emission and atmospheric processing measured on the R/V Ronald Brown during TEXAQS/GoMACCS 2006. *Journal of Geophysical Research-Atmospheres*. 114:15. doi: 10.1029/2008jd011275.

18. Frossard AA, Russell LM, Massoli P, Bates TS, Quinn PK. 2014. Side-by-Side Comparison of Four Techniques Explains the Apparent Differences in the Organic Composition of Generated and Ambient Marine Aerosol Particles. *Aerosol Science and Technology*. 48(3):V-X. doi: 10.1080/02786826.2013.879979.

19. Gilardoni S, Russell LM, Sorooshian A, Flagan RC, Seinfeld JH, Bates TS, Quinn PK, Allan JD, Williams B, Goldstein AH, Onasch TB, Worsnop DR. 2007. Regional variation of organic functional groups in aerosol particles on four US east coast platforms during the International Consortium for Atmospheric Research on Transport and Transformation 2004 campaign. *Journal of Geophysical Research-Atmospheres*. 112(D10). doi: 10.1029/2006jd007737.

20. Liu S, Day DA, Shields JE, Russell LM. 2011. Ozone-driven daytime formation of secondary organic aerosol containing carboxylic acid groups and alkane groups. *Atmospheric Chemistry and Physics*. 11(16):8321-8341. doi: 10.5194/acp-11-8321-2011.

21. Miyazaki Y, Kawamura K, Jung J, Furutani H, Uematsu M. 2011. Latitudinal distributions of organic nitrogen and organic carbon in marine aerosols over the western North Pacific. *Atmospheric Chemistry and Physics*. 11(7):3037-3049. doi: 10.5194/acp-11-3037-2011.

22. Liu ZY, Li M, Wang XF, Liang YH, Jiang YR, Chen J, Mu JS, Zhu YJ, Meng H, Yang LX, Hou KY, Wang YF, Xue LK. 2022. Large contributions of anthropogenic sources to amines in fine particles at a coastal area in northern China in winter. *Science of the Total Environment*. 839. doi: 10.1016/j.scitotenv.2022.156281.

23. Wang YL, Zhang JW, Marcotte AR, Karl M, Dye C, Herckes P. 2015. Fog chemistry at three sites in Norway. *Atmospheric Research*. 151:72-81. doi: 10.1016/j.atmosres.2014.04.016.

24. van Pinxteren M, Fomba KW, van Pinxteren D, Triesch N, Hoffmann EH, Cree CHL, Fitzsimons MF, von Tumpling W, Herrmann H. 2019. Aliphatic amines at the Cape Verde Atmospheric Observatory: Abundance, origins and sea-air fluxes. *Atmospheric Environment*. 203:183-195. doi: 10.1016/j.atmosenv.2019.02.011.

25. Youn JS, Crosbie E, Maudlin LC, Wang Z, Sorooshian A. 2015. Dimethylamine as a major alkyl amine species in particles and cloud water: Observations in semi-arid and coastal regions. *Atmospheric Environment*. 122:250-258. doi: 10.1016/j.atmosenv.2015.09.061.

26. Xie H, Feng LM, Hu QJ, Zhu YJ, Gao HW, Gao Y, Yao XH. 2018. Concentration and size distribution of water-extracted dimethylaminium and trimethylaminium in atmospheric particles during nine campaigns - Implications for sources, phase states and formation pathways. *Science of the Total Environment*. 631-632:130-141. doi: 10.1016/j.scitotenv.2018.02.303.

27. Kollner F, Schneider J, Willis MD, Klimach T, Helleis F, Bozem H, Kunkel D, Hoor P, Burkart J, Leaitch WR, Aliabadi AA, Abbatt JPD, Herber AB, Borrmann S. 2017. Particulate trimethylamine in the summertime Canadian high Arctic lower troposphere. *Atmospheric Chemistry and Physics*. 17(22):13747-13766. doi: 10.5194/acp-17-13747-2017.

28. Carpenter LJ, Fleming ZL, Read KA, Lee JD, Moller SJ, Hopkins JR, Purvis RM, Lewis AC, Muller K, Heinold B, Herrmann H, Fomba KW, van Pinxteren D, Muller C, Tegen I, Wiedensohler A, Muller T, Niedermeier N, Achterberg EP, Patey MD, Kozlova EA, Heimann M, Heard DE, Plane JMC, Mahajan A, Oetjen H, Ingham T, Stone D, Whalley LK, Evans MJ, Pilling MJ, Leigh RJ, Monks PS, Karunaharan A, Vaughan S, Arnold SR, Tschritter J, Pohler D, Friess U, Holla R, Mendes LM, Lopez H, Faria B, Manning AJ, Wallace DWR. 2010. Seasonal characteristics of tropical marine boundary layer air measured at the Cape Verde Atmospheric Observatory. *Journal of Atmospheric Chemistry*. 67(2-3):87-140. doi: 10.1007/s10874-011-9206-1.

29. Lewis SL, Saliba G, Russell LM, Quinn PK, Bates TS, Behrenfeld MJ. 2021. Seasonal Differences in Submicron Marine Aerosol Particle Organic Composition in the North Atlantic. *Frontiers in Marine Science*. 8:13. doi: 10.3389/fmars.2021.720208.

30. Bates TS, Quinn PK, Frossard AA, Russell LM, Hakala J, Petaja T, Kulmala M, Covert DS, Cappa CD, Li SM, Hayden KL, Nuaaman I, McLaren R, Massoli P, Canagaratna MR, Onasch TB, Sueper D, Worsnop DR, Keene WC. 2012. Measurements of ocean derived aerosol off the coast of California. *Journal of Geophysical Research-Atmospheres*. 117. doi: 10.1029/2012jd017588.

31. Huang XF, Kao SJ, Lin J, Qin XF, Deng CR. 2018. Development and validation of a HPLC/FLD method combined with online derivatization for the simple and simultaneous determination of trace amino acids and alkyl amines in continental and marine aerosols. *Plos One*. 13(11). doi: 10.1371/journal.pone.0206488.

32. Beale R, Airs R. 2016. Quantification of glycine betaine, choline and trimethylamine N-oxide in seawater particulates: Minimisation of seawater associated ion suppression. *Analytica Chimica Acta*. 938:114-122. doi: 10.1016/j.aca.2016.07.016.

33. Saliba G, Chen CL, Lewis S, Russell LM, Quinn PK, Bates TS, Bell TG, Lawler MJ, Saltzman ES, Sanchez KJ, Moore R, Shook M, Rivellini LH, Lee A, Baetge N, Carlson CA, Behrenfeld MJ. 2020. Seasonal Differences and Variability of Concentrations, Chemical Composition, and Cloud Condensation Nuclei of Marine Aerosol Over the North Atlantic. *Journal of Geophysical Research-Atmospheres*. 125(19):24. doi: 10.1029/2020jd033145.

34. DeCarlo PF, Kimmel JR, Trimborn A, Northway MJ, Jayne JT, Aiken AC, Gonin M, Fuhrer K, Horvath T, Docherty KS, Worsnop DR, Jimenez JL. 2006. Field-deployable, high-resolution, time-of-flight aerosol mass spectrometer. *Analytical Chemistry*. 78(24):8281-8289. doi: 10.1021/ac061249n.

35. Russell LM, Chen C-L, Betha R, Price DJ, Lewis S. 2018. Aerosol Particle Chemical and Physical Measurements on the 2015, 2016, 2017, and 2018 North Atlantic Aerosols and Marine Ecosystems Study (NAAMES) Research Cruises (Curated Collection). UC San Diego Library Digital Collections. doi: 10.6075/J04T6GJ6.

36. Schurman MI, Lee T, Desyaterik Y, Schichtel BA, Kreidenweis SM, Collett JL. 2015. Transport, biomass burning, and in-situ formation contribute to fine particle concentrations at a remote site near Grand Teton National Park. *Atmospheric Environment*. 112:257-268. doi: 10.1016/j.atmosenv.2015.04.043.

37. Thamban NM, Lalchandani V, Kumar V, Mishra S, Bhattu D, Slowik JG, Prevot ASH, Satish R, Rastogi N, Tripathi SN. 2021. Evolution of size and composition of fine particulate matter in the Delhi megacity during later winter. *Atmospheric Environment*. 267. doi: 10.1016/j.atmosenv.2021.118752.

38. Sanchez KJ, Chen CL, Russell LM, Betha R, Liu J, Price DJ, Massoli P, Ziemba LD, Crosbie EC, Moore RH, Muller M, Schiller SA, Wisthaler A, Lee AKY, Quinn PK, Bates TS, Porter J, Bell TG, Saltzman ES, Vaillancourt RD, Behrenfeld MJ. 2018. Substantial Seasonal Contribution of Observed Biogenic Sulfate Particles to Cloud Condensation Nuclei. *Scientific Reports*. 8. doi: 10.1038/s41598-018-21590-9.

39. Kamruzzaman M, Takahama S, Dillner AM. 2018. Quantification of amine functional groups and their influence on OM/OC in the IMPROVE network. *Atmospheric Environment*. 172:124-132. doi: 10.1016/j.atmosenv.2017.10.053.

40. Maria SF, Russell LM, Turpin BJ, Porcja RJ. 2002. FTIR measurements of functional groups and organic mass in aerosol samples over the Caribbean. *Atmospheric Environment*. 36(33):5185-5196. doi: 10.1016/s1352-2310(02)00654-4.

41. Takahama S, Johnson A, Russell LM. 2013. Quantification of Carboxylic and Carbonyl Functional Groups in Organic Aerosol Infrared Absorbance Spectra. *Aerosol Science and Technology*. 47(3):310-325. doi: 10.1080/02786826.2012.752065.

42. Quinn PK, Coffman DJ, Kapustin VN, Bates TS, Covert DS. 1998. Aerosol optical properties in the marine boundary layer during the First Aerosol Characterization Experiment (ACE 1) and the underlying chemical and physical aerosol properties. *Journal of Geophysical Research-Atmospheres*. 103(D13):16547-16563. doi: 10.1029/97jd02345.

43. NOAA PMELACG. 2018 [Available from: https://saga.pmel.noaa.gov/data/.

44. Quinn PK, Bates TS, Coffman DJ, Upchurch L, Johnson JE, Moore R, Ziemba L, Bell TG, Saltzman ES, Graff J, Behrenfeld MJ. 2019. Seasonal Variations in Western North Atlantic Remote Marine Aerosol Properties. *Journal of Geophysical Research-Atmospheres*. 124(24):14240-14261. doi: 10.1029/2019jd031740.

45. Pilson MEQ. 2013. *An Introduction to the Chemistry of the Sea*: Cambridge University press.

46. Bell TG, Porter JG, Wang WL, Lawler MJ, Boss E, Behrenfeld MJ, Saltzman ES. 2021. Predictability of Seawater DMS During the North Atlantic Aerosol and Marine Ecosystem Study (NAAMES). *Frontiers in Marine Science*. 7. doi: 10.3389/fmars.2020.596763.

47. Werdell PJ, Bailey S, Fargion G, Pietras C, Knobelspiesse K, Feldman G, McClain C. 2003. Unique data repository facilitates ocean color satellite validation. *Eos, Transactions American Geophysical Union*. 84(38):377-387. doi: https://doi.org/10.1029/2003EO380001.

48. Saliba G, Chen CL, Lewis S, Russell LM, Rivellini LH, Lee AKY, Quinn PK, Bates TS, Haentjens N, Boss ES, Karp-Boss L, Baetge N, Carlson CA, Behrenfeld MJ. 2019. Factors driving the seasonal and hourly variability of sea-spray aerosol number in the North Atlantic. *Proceedings of the National Academy of Sciences of the United States of America*. 116(41):20309-20314. doi: 10.1073/pnas.1907574116.

49. O'Dowd CD, Facchini MC, Cavalli F, Ceburnis D, Mircea M, Decesari S, Fuzzi S, Yoon YJ, Putaud JP. 2004. Biogenically driven organic contribution to marine aerosol. *Nature*. 431(7009):676-680. doi: 10.1038/nature02959.

50. Bates TS, Quinn PK, Coffman DJ, Johnson JE, Upchurch L, Saliba G, Lewis S, Graff J, Russell LM, Behrenfeld MJ. 2020. Variability in Marine Plankton Ecosystems Are Not

Observed in Freshly Emitted Sea Spray Aerosol Over the North Atlantic Ocean. *Geophysical Research Letters*. 47(1). doi: 10.1029/2019gl085938.

51. Russell LM, Hawkins LN, Frossard AA, Quinn PK, Bates TS. 2010. Carbohydrate-like composition of submicron atmospheric particles and their production from ocean bubble bursting. *Proceedings of the National Academy of Sciences of the United States of America*. 107(15):6652-6657. doi: 10.1073/pnas.0908905107.

52. Carlson CA, Ducklow HW, Michaels AF. 1994. ANNUAL FLUX OF DISSOLVED ORGANIC-CARBON FROM THE EUPHOTIC ZONE IN THE NORTHWESTERN SARGASSO SEA. *Nature*. 371(6496):405-408. doi: 10.1038/371405a0.

53. Keller MD. 1989. Dimethyl Sulfide Production and Marine Phytoplankton: The Importance of Species Composition and Cell Size. *Biological Oceanography*. 6(5-6):375-382. doi: 10.1080/01965581.1988.10749540.

54. Liu Q, Nishibori N, Hollibaugh JT. 2022. Sources of polyamines in coastal waters and their links to phytoplankton. *Marine Chemistry*. 242. doi: 10.1016/j.marchem.2022.104121.

55. Mausz MA, Chen Y. 2019. Microbiology and Ecology of Methylated Amine Metabolism in Marine Ecosystems. *Current Issues in Molecular Biology*. 33:133-148. doi: 10.21775/cimb.033.133.

56. Malin G, Turner S, Liss P, Holligan P, Harbour D. 1993. DIMETHYLSULFIDE AND DIMETHYLSULPHONIOPROPIONATE IN THE NORTHEAST ATLANTIC DURING THE SUMMER COCCOLITHOPHORE BLOOM. *Deep-Sea Research Part I-Oceanographic Research Papers*. 40(7):1487-1508. doi: 10.1016/0967-0637(93)90125-m.

57. Chen HH, Ezell MJ, Arquero KD, Varner ME, Dawson ML, Gerber RB, Finlayson-Pitts BJ. 2015. New particle formation and growth from methanesulfonic acid, trimethylamine and water. *Physical Chemistry Chemical Physics*. 17(20):13699-13709. doi: 10.1039/c5cp00838g.

58. Chen HH, Varner ME, Gerber RB, Finlayson-Pitts BJ. 2016. Reactions of Methanesulfonic Acid with Amines and Ammonia as a Source of New Particles in Air. *Journal of Physical Chemistry B*. 120(8):1526-1536. doi: 10.1021/acs.jpcb.5b07433.

59. Chen HH, Finlayson-Pitts BJ. 2017. New Particle Formation from Methanesulfonic Acid and Amines/Ammonia as a Function of Temperature. *Environmental Science & Technology*. 51(1):243-252. doi: 10.1021/acs.est.6b04173.

60. Perraud VP, Xu X, Gerber RB, Finlayson-Pitts BJ. 2020. Integrated experimental and theoretical approach to probe the synergistic effect of ammonia in methanesulfonic acid reactions with small alkylamines. *Environmental Science-Processes & Impacts*. 22(2):305-328. doi: 10.1039/c9em00431a.

61. Murphy SM, Sorooshian A, Kroll JH, Ng NL, Chhabra P, Tong C, Surratt JD, Knipping E, Flagan RC, Seinfeld JH. 2007. Secondary aerosol formation from atmospheric reactions of aliphatic amines. *Atmospheric Chemistry and Physics*. 7(9):2313-2337. doi: 10.5194/acp-7-2313-2007.

62. Price DJ, Kacarab M, Cocker DR, Purvis-Roberts KL, Silva PJ. 2016. Effects of temperature on the formation of secondary organic aerosol from amine precursors. *Aerosol Science and Technology*. 50(11):1216-1226. doi: 10.1080/02786826.2016.1236182.

63. Smith JN, Barsanti KC, Friedli HR, Ehn M, Kulmala M, Collins DR, Scheckman JH, Williams BJ, McMurry PH. 2010. Observations of aminium salts in atmospheric nanoparticles and possible climatic implications. *Proceedings of the National Academy of Sciences of the United States of America*. 107(15):6634-6639. doi: 10.1073/pnas.0912127107.

64. Shen WC, Ren LL, Zhao Y, Zhou LY, Dai L, Ge XL, Kong SF, Yan Q, Xu HH, Jiang YJ, He J, Chen MD, Yu HA. 2017. C1-C2 alkyl aminiums in urban aerosols: Insights from ambient and fuel combustion emission measurements in the Yangtze River Delta region of China. *Environmental Pollution*. 230:12-21. doi: 10.1016/j.envpol.2017.06.034.

65. Bottenus CLH, Massoli P, Sueper D, Canagaratna MR, VanderSchelden G, Jobson BT, VanReken TM. 2018. Identification of amines in wintertime ambient particulate material using high resolution aerosol mass spectrometry. *Atmospheric Environment*. 180:173-183. doi: 10.1016/j.atmosenv.2018.01.044.

66. Verma N, Satsangi A, Lakhani A, Kumari KM. 2017. Low Molecular Weight Monocarboxylic Acids in PM2.5 and PM10: Quantification, Seasonal Variation and Source Apportionment. *Aerosol and Air Quality Research*. 17(2):485-498. doi: 10.4209/aaqr.2016.05.0183.

67. Bahreini R, Keywood MD, Ng NL, Varutbangkul V, Gao S, Flagan RC, Seinfeld JH, Worsnop DR, Jimenez JL. 2005. Measurements of secondary organic aerosol from oxidation of cycloalkenes, terpenes, and m-xylene using an Aerodyne aerosol mass spectrometer. *Environmental Science & Technology*. 39(15):5674-5688. doi: 10.1021/es048061a.

68. Altieri KE, Fawcett SE, Peters AJ, Sigman DM, Hastings MG. 2016. Marine biogenic source of atmospheric organic nitrogen in the subtropical North Atlantic. *Proceedings of the National Academy of Sciences of the United States of America*. 113(4):925-930. doi: 10.1073/pnas.1516847113.

69. Gagosian RB, Zafiriou OC, Peltzer ET, Alford JB. 1982. LIPIDS IN AEROSOLS FROM THE TROPICAL NORTH PACIFIC - TEMPORAL VARIABILITY. *Journal of Geophysical Research-Oceans*. 87(NC13):1133-1144. doi: 10.1029/JC087iC13p11133.

70. Leck C, Bigg EK. 2005. Source and evolution of the marine aerosol - A new perspective. *Geophysical Research Letters*. 32(19). doi: 10.1029/2005gl023651.

71. Takahama S, Liu S, Russell LM. 2010. Coatings and clusters of carboxylic acids in carbon-containing atmospheric particles from spectromicroscopy and their implications for cloud-nucleating and optical properties. *Journal of Geophysical Research-Atmospheres*. 115(D01202). doi: 10.1029/2009jd012622.

72. Claflin MS, Liu J, Russell LM, Ziemann PJ. 2021. Comparison of methods of functional group analysis using results from laboratory and field aerosol measurements. *Aerosol Science and Technology*. 55(9):1042-1058. doi: 10.1080/02786826.2021.1918325.

73. Liu S, Takahama S, Russell LM, Gilardoni S, Baumgardner D. 2009. Oxygenated organic functional groups and their sources in single and submicron organic particles in MILAGRO 2006 campaign. *Atmospheric Chemistry and Physics*. 9(18):6849-6863.

74. Posner LN, Pandis SN. 2015. Sources of ultrafine particles in the Eastern United States. *Atmospheric Environment*. 111:103-112. doi: 10.1016/j.atmosenv.2015.03.033.

75. Ni HY, Huang RJ, Cao JJ, Dai WT, Zhou JM, Deng HY, Aerts-Bijma A, Meijer HAJ, Dusek U. 2019. High contributions of fossil sources to more volatile organic aerosol. *Atmospheric Chemistry and Physics*. 19(15):10405-10422. doi: 10.5194/acp-19-10405-2019.

76. Silva SJ, Ridley DA, Heald CL. 2020. Exploring the Constraints on Simulated Aerosol Sources and Transport Across the North Atlantic With Island-Based Sun Photometers. *Earth and Space Science*. 7(11). doi: 10.1029/2020ea001392.

77. Maria SF, Russell LM, Gilles MK, Myneni SCB. 2004. Organic aerosol growth mechanisms and their climate-forcing implications. *Science*. 306(5703):1921-1924. doi: 10.1126/science.1103491.

78. Seinfeld JH, Pandis SN. 2016. *Atmospheric Chemistry and Physics: From Air Pollution to Climate Change*. 3rd ed: Wiley & Sons.

79. Ulbrich IM, Canagaratna MR, Zhang Q, Worsnop DR, Jimenez JL. 2009. Interpretation of organic components from Positive Matrix Factorization of aerosol mass spectrometric data. *Atmospheric Chemistry and Physics*. 9(9):2891-2918. doi: 10.5194/acp-9-2891-2009.

80. Crippa M, El Haddad I, Slowik JG, DeCarlo PF, Mohr C, Heringa MF, Chirico R, Marchand N, Sciare J, Baltensperger U, Prevot ASH. 2013. Identification of marine and continental aerosol sources in Paris using high resolution aerosol mass spectrometry. *Journal of Geophysical Research-Atmospheres*. 118(4):1950-1963. doi: 10.1002/jgrd.50151.

81. Hu WW, Hu M, Yuan B, Jimenez JL, Tang Q, Peng JF, Hu W, Shao M, Wang M, Zeng LM, Wu YS, Gong ZH, Huang XF, He LY. 2013. Insights on organic aerosol aging and the influence of coal combustion at a regional receptor site of central eastern China. *Atmospheric Chemistry and Physics*. 13(19):10095-10112. doi: 10.5194/acp-13-10095-2013.

82. Ng NL, Canagaratna MR, Zhang Q, Jimenez JL, Tian J, Ulbrich IM, Kroll JH, Docherty KS, Chhabra PS, Bahreini R, Murphy SM, Seinfeld JH, Hildebrandt L, Donahue NM, DeCarlo PF, Lanz VA, Prevot ASH, Dinar E, Rudich Y, Worsnop DR. 2010. Organic aerosol components observed in Northern Hemispheric datasets from Aerosol Mass Spectrometry. *Atmospheric Chemistry and Physics*. 10(10):4625-4641. doi: 10.5194/acp-10-4625-2010.

83. Hayes PL, Ortega AM, Cubison MJ, Froyd KD, Zhao Y, Cliff SS, Hu WW, Toohey DW, Flynn JH, Lefer BL, Grossberg N, Alvarez S, Rappenglueck B, Taylor JW, Allan JD, Holloway JS, Gilman JB, Kuster WC, De Gouw JA, Massoli P, Zhang X, Liu J, Weber RJ, Corrigan AL, Russell LM, Isaacman G, Worton DR, Kreisberg NM, Goldstein AH, Thalman R, Waxman EM, Volkamer R, Lin YH, Surratt JD, Kleindienst TE, Offenberg JH, Dusanter S, Griffith S, Stevens PS, Brioude J, Angevine WM, Jimenez JL. 2013. Organic aerosol composition and sources in Pasadena, California, during the 2010 CalNex campaign. *Journal of Geophysical Research-Atmospheres*. 118(16):9233-9257. doi: 10.1002/jgrd.50530.

84. Qi L, Bozzetti C, Corbin JC, Daellenbach KR, El Haddad I, Zhang Q, Wang JF, Baltensperger U, Prevot ASH, Chen MD, Ge XL, Slowik JG. 2022. Source identification and characterization of organic nitrogen in atmospheric aerosols at a suburban site in China. *Science of the Total Environment*. 818. doi: 10.1016/j.scitotenv.2021.151800.

85. Lee AKY, Rivellini LH, Chen CL, Liu J, Price DJ, Betha R, Russell LM, Zhang XL, Cappa CD. 2019. Influences of Primary Emission and Secondary Coating Formation on the Particle Diversity and Mixing State of Black Carbon Particles. *Environmental Science & Technology*. 53(16):9429-9438. doi: 10.1021/acs.est.9b03064.

86. Lee AKY, Willis MD, Healy RM, Onasch TB, Abbatt JPD. 2015. Mixing state of carbonaceous aerosol in an urban environment: single particle characterization using the soot particle aerosol mass spectrometer (SP-AMS). *Atmospheric Chemistry and Physics*. 15(4):1823-1841. doi: 10.5194/acp-15-1823-2015.

87. Petters MD, Kreidenweis SM. 2007. A single parameter representation of hygroscopic growth and cloud condensation nucleus activity. *Atmospheric Chemistry and Physics*. 7(8):1961-1971. doi: 10.5194/acp-7-1961-2007.